Control of immunological synapse formation

in regulatory T cells

Von der Fakultät für Lebenswissenschaften

der Technischen Universität Carolo-Wilhelmina zu Braunschweig

zur Erlangung des Grades

einer Doktorin der Naturwissenschaften

(Dr. rer. nat.)

genehmigte

D i s s e r t a t i o n

von Jana Niemz

aus Oschatz

1. Referent: Professor Dr. Martin Korte

2. Referent: Professor Dr. Jochen Hühn

eingereicht am: 31.05.2017

mündliche Prüfung (Disputation) am: 15.08.2017

Druckjahr 2017

Vorveröffentlichungen der Dissertation

Teilergebnisse aus dieser Arbeit wurden mit Genehmigung der Fakultät für Lebenswissenschaften, vertreten durch den Mentor der Arbeit, in folgenden Beiträgen vorab veröffentlicht:

Publikationen

Jana Niemz, Stefanie Kliche, Marina C Pils, Eliot Morrison, Annika Manns, Christian Freund, Jill R Crittenden, Ann M Graybiel, Melanie Galla, Lothar Jänsch, Jochen Huehn. The guanine-nucleotide exchange factor CalDAG GEFI fine-tunes functional properties of regulatory T cells. European Journal of Microbiology and Immunology, 2017, May 22;7(2):112-126.

Tagungsbeiträge

René Teich, **Jana Zenk**, Marco van Ham, Josef Wissing, Lars Philipsen, Lothar Jänsch, Jochen Hühn. Contribution of Treg-specific phosphorylation patterns to the formation of a Treg-specific immunological synapse. 44th Annual Meeting German Society for Immunology, Bonn, Germany, September 2014.

René Teich, **Jana Zenk**, Marco van Ham, Josef Wissing, Lars Philipsen, Lothar Jänsch, Jochen Hühn. The formation of a Treg-specific immunological synapse is regulated by differential phosphorylation of TCR signaling components. 18th Joint Meeting Signal Transduction Society, Weimar, Germany, November 2014.

Jana Niemz, René Teich, Marco van Ham, Josef Wissing, Lars Philipsen, Stefanie Kliche, Eliot Morrison, Annika Manns, Christian Freund, Jill R Crittenden, Ann M Graybiel, Lothar Jänsch, Jochen Hühn. The role of CalDAG GEFI during Treg-specific immunological synapse formation. 10th German Meeting on Immune Regulation, Berlin-Schmöckwitz, Germany, June 2016.

Posterbeiträge

René Teich, **Jana Zenk**, Marco van Ham, Josef Wissing, Lars Philipsen, Lothar Jänsch, Jochen Hühn. Contribution of Treg-specific phosphorylation patterns to the formation of a Treg-specific immunological synapse. 44th Annual Meeting German Society for Immunology, Bonn, Germany, September 2014.

Jana Niemz, René Teich, Marco van Ham, Josef Wissing, Lars Philipsen, Stefanie Kliche, Lothar Jänsch, Jochen Hühn. The role of CalDAG GEFI during Treg-specific immunological synapse formation. 4th European Congress of Immunology, Vienna, Austria, September 2015.

Jana Niemz, René Teich, Marco van Ham, Josef Wissing, Lars Philipsen, Stefanie Kliche, Jill R Crittenden, Ann M Graybiel, Lothar Jänsch, Jochen Hühn. The role of CalDAG GEFI during Treg-specific immunological synapse formation. 46th Annual Meeting German Society for Immunology, Hamburg, Germany, September 2016.

Summary

Regulatory T cells (Tregs) are a $CD4^+$ T cell subset, which maintains tolerance towards self and harmless foreign antigens and is characterized by expression of the master transcription factor Foxp3. Besides this well studied Treg-specific feature, several effector molecules have been identified as preferentially but not exclusively expressed in Tregs. Activation via the T cell receptor (TCR) is crucial for T cell functionality, and there is accumulating evidence that TCR signaling is differentially organized in Tregs as compared to their counterparts, conventional T cells (Tconv). Accordingly, formation and composition of the immunological synapse (IS), built at the interface of interacting immune cells, differs between Tregs and Tconv. Quantitative phosphopeptide sequencing of Tregs and Tconv, which was recently performed in our laboratory, revealed a pre-activated phenotype of Tregs as compared to Tconv and identified differentially regulated phosphorylation sites between the two T cell subsets. Those might serve as promising candidates for targeted intervention of Treg activation.

The present study (i) addressed the functional role of Themis, which is strongly under-represented in Tregs, for their suppressive capacity. Furthermore, in order to expand current knowledge about differential TCR signaling in Tregs and Tconv, (ii) phosphorylation kinetics of selected sites were performed. (iii) The functional impact of a novel phosphorylation site at Y523 of CalDAG GEFI (Calcium and DAG regulated guanine nucleotide exchange factor I), which was identified via the aforementioned phosphoproteomic approach, and (iv) the role of the protein itself for development and function of Tregs was investigated.

In summary, selective targeting of Tregs by intervention at the signaling level might serve as promising future therapeutic strategy. Up to date, the major obstacle is the lack of specific tools, both to investigate intracellular signaling at the bench and to target selected signaling processes cell subset-specifically at the bedside.

Zusammenfassung

Regulatorische T-Zellen (Treg-Zellen) sind ein Teil der $CD4^+$ T-Zellen und dienen der immunologischen Toleranz gegenüber “Selbst” und harmlosen Fremdantigenen. Das Hauptcharakteristikum von Treg-Zellen ist die Expression des bereits eingehend untersuchten Transkriptionsfaktors Foxp3. Neben Foxp3 wurden weitere Effektormoleküle identifiziert, die zwar vorwiegend, aber nicht ausschließlich von Treg-Zellen exprimiert werden, und daher nur bedingt der Unterscheidung von Treg-Zellen und konventionellen T-Zellen (Tconv-Zellen) dienen. Die Aktivierung über den T-Zellrezeptor (TCR) ist entscheidend für die Funktion aller T-Zellen, und es wird zunehmend deutlich, dass der intrazelluläre TCR Signalweg von Treg-Zellen und Tconv-Zellen divergent reguliert ist. Dementsprechend unterscheiden sich auch Formierung und Zusammensetzung der immunologischen Synapse, der Kontaktfläche zwischen interagierenden immunologischen Zellen, zwischen Treg- und Tconv-Zellen. Eine quantitative Bestimmung phosphorylierter Proteine beider T-Zellsorten, welche kürzlich in unserem Labor durchgeführt wurde, identifizierte diverse differentiell regulierte Phosphorylierungsstellen, welche vielversprechende Kandidaten zur spezifischen Intervention der Treg-Zell-Aktivierung darstellen.

In der vorliegenden Arbeit wurde (i) die funktionelle Rolle von Themis, einem Protein mit geringerer Expression in Treg- als Tconv-Zellen, für den suppressiven Phänotyp von Treg-Zellen untersucht. Um die Identifizierung differentiell phosphorylierter Proteine voranzubringen, wurden (ii) Kinetiken ausgewählter Phosphorylierungsstellen generiert. Außerdem wurde (iii) die Funktion einer Phosphorylierung des Proteins CalDAG GEFI (Calcium and DAG regulated guanine nucleotide exchange factor I) untersucht und (iv) die generelle Rolle dieses Proteins in Treg-Zellen analysiert.

Zusammenfassend stellt ein gezieltes Eingreifen in Treg-Zell-spezifische Signalwege eine vielversprechende Möglichkeit für zukünftige Therapiestrategien dar. Bisher ist hierbei das Fehlen spezifischer Hilfsmittel zur erfolgreichen Erforschung und zielgerichteten Adressierung der T-Zell-Signaltransduktion die größte Hürde.

Table of contents

Vorveröffentlichungen der Dissertation 3

Summary 4

Zusammenfassung 5

Table of contents 6

1. Introduction 9

1.1 Innate and adaptive immunity at a glance 9

1.2 T lymphocytes 10

1.2.1 Regulatory T cells: Discovery and development 11

1.2.2 Suppression mechanisms of Tregs 13

1.3 Transcriptomics and proteomics of Tregs and Tconv 14

1.4 Dissimilar TCR signaling in Tregs and Tconv 16

1.5 Immunological synapse formation 20

1.5.1 Structure and assembly of the IS 20

1.5.2 Integrin activation: inside-out and outside-in 22

1.6 The small GTPase Rap1 23

1.7 The guanine nucleotide exchange factor CalDAG GEFI 24

1.8 Aims of the study 28

2. Results 29

2.1 Themis expression levels do not affect Treg suppressive capacity *in vitro* 29

2.2 Protein phosphorylation kinetics following TCR ligation in Tregs and Tconv 31

2.2.1 Phospho-flow cytometry establishment 31

2.2.2 Phospho-flow cytometry kinetics for selected molecules 33

2.3 CalDAG GEFI fine-tunes Treg function 35

2.3.1 CalDAG GEFI is expressed in primary murine Tregs and Tconv 35

2.3.2 Phosphorylation at Y523 is not affecting DAG binding of CalDAG GEFI 36

2.3.3 Generation of CalDAG GEFI$^{-/-}$ Jurkat T cell clones and re-expression of CalDAG GEFI 37
2.3.4 CalDAG GEFI$^{-/-}$ Jurkat T cells show deficits in adhesion but retain chemotactic behavior 40
2.3.5 T cell compartment is unaltered in CalDAG GEFI$^{-/-}$ mice 45
2.3.6 Signal transduction remains unaltered in CalDAG GEFI$^{-/-}$ T cells 48
2.3.7 CalDAG GEFI$^{-/-}$ Tregs are fully functional *in vitro* 51
2.3.8 CalDAG GEFI fine-tunes Treg suppressive ability *in vivo* 53

3. Discussion 59

3.1 The role of Themis in Treg development and function 59
3.2 TCR signaling in Tregs versus Tconv 61
3.3 The role of CalDAG GEFI in murine T cells 64
3.3.1 Y523 – A novel phosphorylation site at murine CalDAG GEFI 64
3.3.2 The role of CalDAG GEFI in adhesion and migration of Jurkat T cells 66
3.3.3 Phenotypic characterization of murine CalDAG GEFI$^{-/-}$ T cells 68
3.3.4 Signaling properties of murine CalDAG GEFI$^{-/-}$ T cells 68
3.3.5 CalDAG GEFI fine-tunes Treg function *in vivo* 69
3.4 Concluding remarks 71

4. Materials and Methods 72

4.1 Mouse strains 72
4.2 Isolation of primary cells 72
4.3 Automated magnetic-activated cell sorting (MACS) 72
4.4 Flow cytometry and fluorescence-assisted cell sorting (FACS) 73
4.5 Phospho-flow cytometry (BD Biosciences) 74
4.6 Pre-activation of Tregs 74
4.7 Transduction of Tregs 74
4.8 *In vitro* suppression assay 75
4.9 Transfer colitis 75

4.10 Isolation of small intestine lamina propria lymphocytes (siLPLs) 76
4.11 Phosphotyrosine analysis 76
4.12 Cell lines 76
4.13 Production of lentiviral and retroviral particles 77
4.14 CRISPR/Cas9-mediated gene knock-out in Jurkat T cells 77
4.15 Transduction of Jurkat T cells 78
4.16 Adhesion and migration assays 78
4.17 Western Blot 79
4.18 Protein expression, purification and lipid binding assay 80
4.19 Statistical analysis 80

Supplementary Information 82

References 85

Abbreviations 105

Acknowledgment 110

Publications (other) 111

1. Introduction

1.1 Innate and adaptive immunity at a glance

Vertebrate organisms have developed strategies to protect themselves from invading, potentially harmful, entities. As a quick but rather unspecific line of defense, innate immunity comes into play with a variety of immune cells such as macrophages and neutrophils, which recognize pathogen-associated molecular patterns (PAMPs) [1] via their pattern recognition receptors (PRRs) [2, 3]. PRR activation triggers innate immune cells to secret cytokines, which in turn kick-start an inflammatory response to directly attack the pathogen and simultaneously activate the second arm of the immune system, adaptive immunity [4]. A key linker between innate and adaptive immunity are professional antigen-presenting cells (APCs), including different subsets of dendritic cells (DCs) [5]. DCs take up proteins from their surroundings, which are processed and finally linear peptides thereof are presented with the aid of the major histocompatibility complex (MHC) expressed on the DC surface [6]. Peptide-loaded MHCs (pMHC) are indispensable for antigen recognition by T lymphocytes, which represent one part of the adaptive immune system. The T cell receptor (TCR), which is constitutively attached to the T cell membrane, is restricted to antigen recognition specifically via pMHCs [7-10]. In contrast, the B cell receptor (BCR), which is expressed by the second main players of acquired immunity, namely B cells, recognizes three dimensional antigens [11]. The BCR can be secreted and acts in soluble form as antibody [10]. Both, BCR and TCR, are characterized by constant receptor domains and highly variable parts. Latter are generated by gene rearrangement, catalyzed by the enzymes recombination activating gene 1 or 2 (Rag1 and Rag2), during lymphocyte development resulting in a unique BCR or TCR expressed on every B and T cell, respectively [12-14]. Importantly, DCs are not only presenting foreign peptides but also self-antigens. At the same time, TCRs are generated during the random TCR rearrangement, which are recognizing self-peptides. This bears the risk that self-reactive T cells encounter self-antigen presenting DCs, resulting in T cell activation and autoimmunity. To prevent this scenario, the immune system has developed several strategies: In the course of thymic T cell development, thymocytes bearing a self-reactive TCR are eliminated during a process called negative selection [15]. This process is partly mediated by

the transcription factor autoimmune regulator (Aire), which allows expression and subsequently presentation of self-peptides being specific for non-thymic tissues in the thymus to enable the development of tolerance towards peripheral tissues [16, 17]. Besides this mechanism to induce central tolerance, peripheral tolerance is generated by mature T lymphocytes in secondary lymphoid organs (SLOs) either by induction of anergy or mediated by specialized immunoregulatory cells. In case a self-peptide presenting DC encounters a self-reactive T cell that has escaped central tolerance, pMHC and TCR are matching but this cell interaction usually occurs in absence of an inflammatory environment. Due to the lack of pro-inflammatory cytokines, certain costimulatory molecules are not expressed by the APC and this absence of costimulation will drive the T cell into an anergic state [18]. Besides, up to now numerous immunoregulatory cells were identified, for example myeloid-derived suppressor cells (MDSCs), regulatory B and T cells (Bregs and Tregs, respectively), which actively suppress unwanted or overshooting immune responses by various mechanisms [19, 20]. In summary, the immune system of jawed vertebrates comprises two major branches: Fast, but rather short-lived and unspecific innate immune responses as well as long-lasting and memory-forming, very specific adaptive immunity. Both responses are complementary and need to be tightly controlled to avoid exceeding immunity and reactivity towards self and harmless antigens.

1.2 T lymphocytes

T cell precursors originate from hematopoietic stem cells (HSCs) in the bone marrow and migrate to the thymus for maturation. They enter the thymus as $CD3^-$ as well as co-receptor, $CD4^-$ and $CD8^-$ respectively, negative cells. CD3 is gradually upregulated during further developmental steps, the β chain of the TCR is rearranged, and the thymocytes express a pre-TCR consisting of a surrogate α chain and the rearranged β chain. Subsequently, both co-receptors are upregulated and Rag1/2-mediated rearrangement of the TCR α chain results in expression of a mature TCR. Now, thymocytes are first positively selected for bearing a TCR on their surface, which is capable of interacting with a MHC, and those T cells, which express a TCR that recognizes MHC-presented self-peptides with high affinity are negatively selected in a second step. Finally, double positive thymocytes will downregulate the

expression of either CD4 or CD8, and commit to one the two single positive T cell lineages [21]. $CD4^+$ and $CD8^+$ T cells that have undergone positive and negative selection leave the thymus and enter the periphery, where they constitute the naïve T cell pool. Upon encounter of their cognate antigen and costimulation provided by APCs, antigen-specific naïve T cells (Tnaive) undergo clonal expansion in order to give rise to sufficient numbers of T cells to mount an efficient immune response [22]. MHC class I-restricted $CD8^+$ T cells develop into cytotoxic T lymphocytes (CTL), which for example eliminate cancer cells or cells infected by intracellular pathogens [23-28]. $CD4^+$ T cells differentiate into helper T cells (Th), by upregulation of the subset-specific transcription factor and subsequent secretion of characteristic cytokines. Up to date, numerous T helper subsets were identified; however, the four major subsets are Th1, Th2, Th17 and Tregs. Th1 are characterized by the transcription factor T-box transcription factor (TBX21, T-bet) and secret interferon γ (IFNγ) [29, 30]. The master transcription factor of Th2 cells is Trans-acting T cell-specific transcription factor (Gata-3) and the Th2 subset produces interleukin-4 (IL-4) [31-33]. Th17 cells secret IL-17 and are under control of the transcription factor RAR-related orphan receptor γ (RORγt) [34, 35]. The lineage-defining marker for Tregs is the master transcription factor Forkhead box protein p3 (Foxp3); Tregs are thoroughly introduced in the following paragraph. However, after shutdown of the immune response only a minor fraction of differentiated Th cells will convert to memory T cells, which can be rapidly re-activated by encounter of the same antigen, whereas the majority of effector T cells will be eliminated via apoptosis [36].

1.2.1 Regulatory T cells: Discovery and development

Sakaguchi and colleagues were the first to show that depletion of $CD4^+CD5^+$ T cells leads to autoimmunity and that co-transfer of $CD4^+CD5^+$ T cells with $CD4^+CD5^-$ T cells into immunodeficient mice preserves self-tolerance [37]. Another ten years later, the same group identified that the respective T cell populations are better distinguished by constitutive expression of the IL-2 receptor α chain (CD25), with $CD4^+CD25^+$ T cells having a suppressor-like phenotype as compared to $CD4^+CD25^-$ conventional T cells (Tconv) [38]. Although CD25 expression serves as predominantly reliable Treg marker in the mouse system under homeostatic conditions, it cannot be used under inflammatory conditions as it is massively

upregulated upon T cell stimulation, especially by human T cells [39-42]. Therefore, discovery of the lineage-defining marker Foxp3 was a hallmark to the Treg field: The transcription factor Foxp3 is highly expressed in $CD4^+CD25^+$ T cells and ectopic expression of Foxp3 in $CD4^+CD25^-$ T cells renders the cells suppressive. Additionally, Foxp3 expression identifies a $CD4^+CD25^-$ T cell subset, which was also described to excert suppressive functions [43-47]. It was shown, that genetic disruption of the *Foxp3* locus in mice causes fatal autoimmunity resulting in the scurfy phenotype and mutations in the *Foxp3* gene in humans leads to development of the immunodysregulation polyendocrinopathy enteropathy X-linked syndrome (IPEX) [48, 49]. On the other hand, it was also reported that an excess of Tregs might support tumor growth and chronic infection establishment [50-54]. Foxp3 was shown to be the master transcription factor of Tregs, needed for generation of the cells, stability of the lineage and functionality [55-59]. A variety of Treg signature genes such as Glucocorticoid-induced TNFR-related protein (GITR, CD357), Cytotoxic T-lymphocyte-associated antigen 4 (CTLA-4, CD152) and CD25 are regulated by Foxp3 [38, 60-62]. The *Foxp3* locus itself is epigenetically modified in stable Tregs, manifested in the demethylation of the conserved non-coding sequence (CNS) 2, also referred to as Treg-specific demethylated region (TSDR) [63, 64].

Tregs develop both in the thymus as well as in the periphery in SLOs. $CD4^+$ T cells with a TCR having a certain threshold of self-affinity can escape negative selection in the thymus and instead upregulate the transcription factor Foxp3 and commit to the Treg lineage [65, 66]. The expression of Foxp3 is either followed or preceded by upregulation of CD25, creating two Treg precursor subsets, $CD25^+Foxp3^-$ or $CD25^-Foxp3^+$ [67, 68]. Tregs that are generated during T cell development in the thymus are referred to as thymus-derived Tregs (tTregs), and it was suggested that this cohort of Tregs is ensuring self-tissue integrity [69]. A second fraction of Tregs, peripherally-induced Tregs (pTregs), is generated from Tnaive when they recognize their cognate antigen presented by APCs in a tolerogenic environment and in presence of IL-2 and transforming growth factor β (TGF-β) [70-72]. This second cohort of Tregs allows the establishment of tolerance towards harmless foreign antigens derived for example from commensal gut bacteria and nutrition [72-75]. Although several molecules were suggested to distinguish tTregs and pTregs such as Neuropilin-1 (Nrp1) and Helios, no reliable marker has been

identified so far because suggested molecules can be upregulated also by pTregs under inflammatory conditions [76-82].

In vitro induced or expanded Tregs have been proposed for several therapeutic applications e.g. to augment allograft tolerance or treat allergy and autoimmune disorders. The major obstacle until now is the instability of transferred Tregs; the cells lose Foxp3 expression and might even turn pathogenic [83]. Therefore, considerable effort is put on the development of novel strategies to differentiate stable Tregs *in vitro*, with stability referring to methylation status of the TSDR. Several compounds have been tested for their potency to induce stable Tregs, e.g. retinoic acid and vitamin C [84-88]. Another approach is the identification of candidate genes that impact *in vivo* Treg generation, in order to manipulate *in vitro* generated Tregs on a genetic level. In contrast, as Tregs are known to be detrimental in cancer settings, molecular targets are quested to specifically interfere with Treg function *in vivo* [52].

1.2.2 Suppression mechanisms of Tregs

A substantial number of studies has addressed and at least partly unraveled mechanistic modes of how Tregs promote suppression of unwanted or overshooting immunity. The identified approaches can be grouped into four distinct modes, which are all contact-dependent or at least mediated via close distance. Up to now, it is not fully understood whether every Treg is able to employ all of these mechanisms and how the cells decide which mode to use. It was suggested, that this decision is either made hierarchically or in a context-dependent manner [89].

It was shown that Tregs secrete inhibitory cytokines such as IL-10, IL-35 or TGF-β [90-95], and at least in case of IL-10, Tregs stimulate other cells to release anti-inflammatory cytokines [96]. Besides, Tregs are also capable of Granzyme A (GzmA, human Tregs), Granzyme B (GzmB, mouse Tregs) and perforin production, which cause pore formation in target cell membranes and ultimately results in apoptosis [97-101]. Another mode that leads to target cell death is via cytokine deprivation, as especially IL-2 is abundantly consumed by Tregs, as a result of the elevated expression levels of CD25 [102-104]. Transfer of cyclic AMP (cAMP), an inhibitory second messenger, through gap junctions or secretion of the ectoenzymes CD39 and CD73, which lead to generation of immunosuppressive adenosine, are

mechanisms to disrupt the target cell's metabolism [105-107]. An indirect way to suppress effector T cells is via interference with DC function and maturation. Tregs express elevated levels of CTLA-4, which binds to APC-expressed CD80/86, removes the molecule from the DC surface via trogocytosis, and thus competes with CD28 for these shared ligands. As CTLA-4 displays higher affinity for CD80/86 as compared to CD28, ligand availability for Tconv to induce costimulatory signaling is reduced [108-111]. Additionally, interaction with Treg-expressed CTLA-4 stimulates DCs to secrete Indoleamine (2,3)-dioxygenase 1 (IDO), which in turn initiates the production of pre-apoptotic metabolites by effector T cells [61, 62, 112, 113]. Besides, Tregs are also interfering with intracellular signal transduction of immature DCs. Binding of Lymphocyte activation gene 3 protein (LAG-3), expressed by Tregs, to MHC class II on the DC surface, activates downstream signaling cascades that finally result in phosphatase activation and shutdown of immunostimulatory competence [114, 115]. This suppressive mechanism is also utilized by IL-10-secreting $CD4^{+}Foxp3^{-}$ T cells [116].

1.3 Transcriptomics and proteomics of Tregs and Tconv

Extensive effort was already made to unravel transcriptomic and proteomic signatures of Tregs and Tconv in order to uncover unique Treg features. Regarding transcriptomic information, a reasonable amount of data were collected and published in various databases (e.g. Immunological Genome Project, www.immgen.org). The very first transcriptomic comparison of Tregs versus Tconv, revealed differential expression of numerous genes in the two T cell subsets, and interestingly some of those, e.g. Helios, are Foxp3-independently regulated [117]. Foxp3-dependent transcriptional regulation was addressed by two parallel studies, and both came to the conclusion that Foxp3 can act as both activator and suppressor and that many of the Foxp3-dependent differentially regulated genes are connected to T cell activation [118, 119]. However, Hill *et al.* have challenged the view of Foxp3 as a "Master regulator", as their study found comparably little direct influence of Foxp3 on the Treg transcriptional landscape [120]. Transcriptomic approaches were intensified by the development of new sequencing methods, such as next generation sequencing, which added new insights to the existing knowledge [121]. Besides general comparisons of Tregs and Tconv, considerable effort was put to analyze

differences of Tregs from several tissues, revealing that the pool of peripheral Tregs found in SLOs is rather heterogeneous in terms of gene expression patterns [122]. Since then, numerous studies have addressed transcriptional profiles of Tregs from certain tissues or of genetically modified mice in the context of gene knockout or transgenic mice [123-126].

Proteomic approaches are not as abundant so far, which can be mainly attributed to the higher need of input material for global proteomic analysis as compared to transcriptome analysis. The protein inventory of human Tregs and Tconv was addressed and thereby novel molecular players for Treg suppressive capacity, namely Galectin-10 and CD147, were identified [127, 128]. A more recent study by Procaccini *et al*. revealed differences in the metabolism of Tregs and Tconv, which showed that Tregs are predominantly relying on glycolysis to maintain their high proliferative capacity, whereas Tconv, which are less proliferative, utilize fatty-acid oxidation for energy supply [129]. Regarding energetic pathways, combined proteomic and phosphoproteomic profiling of resting and activated murine Tconv showed signaling and bioenergetic circuits that mediate the transition from T cell quiescence to activation [130]. Barra and colleagues published an extensive study comparing the proteome of *ex vivo* isolated Tregs and Tconv from spleen, lymph nodes (LNs) and thymus. They found transcription factor 7 (TCF7) significantly underrepresented in Tregs as compared to Tconv and were able to show a crucial role for lower TCF7 expression levels during tTreg development [131]. Recently, also our department performed a comparative proteome analysis of murine *ex vivo* isolated Tregs and Tconv [132]. Amongst others, we identified several histones to be differentially expressed as well as the proteins Niban, S100A4 and Themis (thymocyte-expressed molecule involved in selection). Niban was found at elevated protein levels in Tregs but so far there is no role for Niban described in T cells. S100A4, also upregulated in Tregs, is a member of the S100 family of Ca^{2+}-binding proteins containing a characteristic EF-hand motif [133] and is mostly known for its metastasis promoting activity reported for various kinds of cancer. Besides cancer context, S100A4 was shown to be involved in directed granule release at the immunological synapse (IS) formed between natural killer (NK) cells and their target cells [134]. Additionally, a role for S100A4 in Th17-mediated rheumatoid arthritis by interference with intracellular signal transduction was described [135]. Themis was

one of the rare proteins that were underrepresented in Tregs as compared to Tconv. Themis localizes at the Linker for activation of T cells (LAT) signalosome due to interaction with Growth factor receptor-bound protein 2 (GRB2) and also interacts with Tyrosine-protein phosphatase non-receptor type 6 (PTPN6, SHP-1), and it was long time believed that thereby Themis is enhancing SHP-1 activity [136, 137]. Only recently it was shown that Themis directly interacts with SHP-1 via its "cysteine-containing all beta in Themis" (CABIT) domains and this interaction is strengthened by GRB2, but not absolutely dependent on GRB2. The CABIT domains interfere with phosphatase activity of SHP-1 through oxidation of a catalytically important cysteine residue in response to physiological reactive oxygen species (ROS) production. Thereby, Themis inhibits SHP-1 and indirectly enhances TCR signaling following low-affinity antigen binding during positive selection processes in the thymus [138]. With respect to Tregs, it was reported that *Themis* transcription is downregulated by Foxp3, which finally accounts for reduced Themis protein levels in Tregs as compared to Tconv [118, 132, 139]. Themis$^{-/-}$ mice show elevated Treg frequencies in the periphery, while absolute numbers were reduced by half as compared to wild type (WT) mice, which is explained by the generally reduced T cell compartment in Themis$^{-/-}$ mice [140]. Very recently, Duguet and colleagues found improved survival and slightly augmented *in vivo* suppressive capacity of Themis-overexpressing Tregs as compared to WT cells [139].

1.4 Dissimilar TCR signaling in Tregs and Tconv

Both Tregs and Tconv require activation via the TCR in order to exert their respective effector functions [125, 126, 141, 142]. The TCR complex is a multi-protein machinery: The TCR itself is composed of either one TCRα and TCRβ chain or one TCRγ and TCRδ chain, and therefore specifies two major T cell subsets, αβ- or γδ-T cells, respectively. The TCR heterodimer is associated with one CD3δ and one CD3γ as well as two CD3ε and two CD3ζ chains, which enable intracellular signal transduction due to phosphorylation of the Immune-receptor-Tyrosine-based-Activation-Motifs (ITAM). The TCR heterodimer recognizes pMHC on the surface of APCs, with CD4$^+$ and CD8$^+$ T cells being restricted to MHC class I and class II, respectively. Due to activation of the costimulatory molecules CD4 and CD8, Lymphocyte cell-specific protein-tyrosine kinase (Lck) is recruited to the TCR

signalosome and phosphorylates the ITAMs of CD3ζ. These serve as docking stations for 70 kDa zeta-chain associated protein (ZAP70), which is activated by phosphorylation upon binding. Subsequently, ZAP70 recruits and phosphorylates LAT, which leads to the formation of the LAT signalosome comprising PLCγ1 (Phospholipase C-gamma-1), SLP-76 (SH2 domain-containing leukocyte protein of 76 kDa), GRB2 and SOS1 (Son of sevenless homolog 1) amongst others. As described above, via GRB2, Themis is located at the LAT signalosome and directly interacts with SHP-1 [138]. PLCγ1 converts phosphatidylinositol (3,4,5)-trisphosphate (PIP3) into inositol (1,4,5)-trisphosphate (IP3) and diacylglycerol (DAG) and consequently intracellular Ca^{2+} levels are increasing and numerous signaling cascades such as Ras/Raf (Rat Sarcoma/Rat Fibrosarcoma) and MEK/ERK1/2 (Mitogen-activated protein ERK kinase/ extracellular signal-regulated kinase 1 and 2) pathways are initiated. Finally, this results in the activation and nucleus translocation of several transcription factors such as activator protein 1 (AP-1), nuclear factor of activated T cells (NFAT) and nuclear factor 'kappa-light-chain-enhancer' of activated B cells (NFκB) [143]. A nearly infinite number of costimulatory molecules have been identified, which can be broadly characterized as either activating or inhibitory. With regard to $CD4^+$ T cells, one of the major costimulators is CD28, which is involved in tolerance induction. The CD28 ligands, CD80/86 are only expressed by APC in an inflammatory setting, and binding of CD28 to its ligands will trigger the T cell to be fully activated, differentiate and proliferate. It was shown that Tregs reduce their motility upon encounter with CD80/86-expressing APCs to induce sustained interaction [144]. In case, cognate antigen is detected by a T cell in absence of CD80/86 expression, the T cell becomes anergic or apoptotic [18, 145]. This scenario is utilized by Tregs to prevent Th cell activation and differentiation as described in section 1.2.2. Besides CD28, other activating costimulatory molecules are inducible costimulator (ICOS) and GITR, while inhibition is not only mediated via CTLA-4, but also by LAG-3 and programmed death-1 (PD-1), just to name a few [146-151]. Concurrent with T cell stimulation, integrin activation at the T cell surface takes place in order to support stable contacts to the APC, which also includes cytoskeletal reorganization. The entity of this whole signaling machinery close to the APC interaction site is termed the immunological synapse (IS) **(Fig. 1)**.

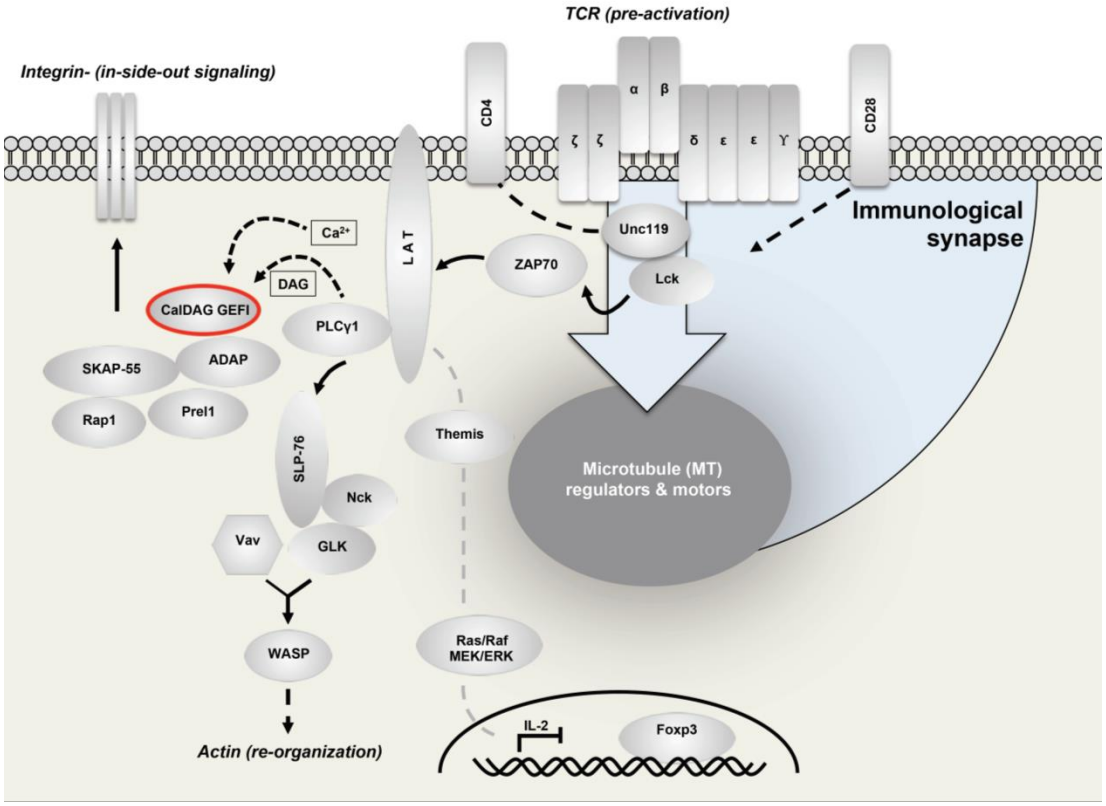

Fig. 1: Proximal TCR signaling in Tregs. Schematic picture of TCR downstream signaling cascades towards initiation/termination of gene expression, cytoskeletal reorganization and integrin activation, details can be found in the text. Arrows between molecules depict direction of signal propagation. The immunological synapse is indicated in light blue and the guanine nucleotide exchange factor CalDAG GEFI, the protein in focus of this thesis, is highlighted by a red frame. Figure is modified from a kind courtesy of Lothar Jänsch and Marco van Ham (HZI, Braunschweig).

There is growing body of evidence that TCR downstream signaling in Tregs is differentially organized as compared to Tconv [152]. Besides mere abundance of signalosome components as addressed by the above mentioned proteomic data [132], signaling processes itself differ with regards to the analyzed T cell subset. For example, Tregs exhibit reduced phosphorylation at S473 of AKT, and SHARPIN was identified to specifically control TCR signaling via ubiquitination processes in Tregs [153, 154]. Additionally, ERK1/2 activation downstream of TCR triggering as well as stimulation-induced Ca^{2+} flux are attenuated in Tregs [155-157]. Furthermore, TCR signalosome component recruitment is differentially organized in Tregs versus Tconv. It was shown by Zanin-Zhorov *et al.*, that Protein kinase C theta type (PKCΘ) is located towards the IS in Tconv, but is sequestered away in Tregs, and the scaffold protein Disc large homolog 1 (Dlgh1) is highly accumulated specifically at the Treg-IS

[158, 159]. Multi-epitope Ligand Cartography (MELC) recently performed by our department, revealed diverging recruitment kinetics for various phosphorylated signalosome components in Tregs versus Tconv [132]. Furthermore, a couple of studies addressed abundance and activation of kinases in Tregs and Tconv. It was shown that the kinome of Tregs and Tconv differs and also the activation state of certain kinases varies following TCR activation in murine and human Tregs versus Tconv [160-162], also hinting towards differentially organized TCR signaling. Besides the aforementioned proteomic comparison of *ex vivo* isolated murine Tregs and Tconv, our group also performed quantitative phosphopeptide sequencing of resting and activated Tregs and Tconv, respectively. We found numerous phosphorylation sites at various proteins to be differentially phosphorylated when comparing resting Tregs and Tconv, as well as when comparing activated cells or resting against activated cells. **Figure 2** summarizes the top 21 candidate proteins that show major regulation differences in the two examined T cell subsets. Displayed values are normalized to the phosphorylation state of resting Tconv. It is obvious that for many sites resting Tregs display a pre-activated phenotype, apparent from the elevated phosphorylation level. Whether the given phosphorylation level at the resting state is up- or downregulated upon stimulation is varying highly between the detected sites. Since a whole spectrum of signaling events was covered by this approach and taking into consideration the detected differential recruitment of phosphomolecules to the IS, it is tempting to hypothesize, that TCR ligation might lead to Treg- and Tconv-specific IS formation, respectively [132].

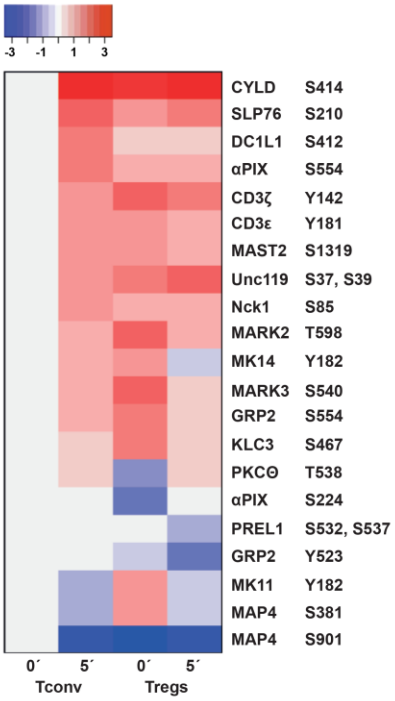

Fig. 2: Phosphoproteomic analysis reveals differential signaling dynamics in primary murine Tconv and Tregs. Tconv and Tregs were FACS-sorted from pooled spleen and LNs from BALB/c mice as $CD4^+CD25^-$ and $CD4^+CD25^+$, respectively. Cells were either left unstimulated (0´) or stimulated via streptavidin-mediated crosslinking of biotinylated anti-CD3/28 for 5 min (5´). Samples were iTRAQ-labeled, enriched for phospho-peptides and analyzed via LC-MS/MS. The heatmap displays the 21 phosphorylation sites, protein and respective site are named on the right, that were found to be most divergently regulated in Tconv (two columns on the left) versus Tregs (two columns on the right). All samples were normalized to the phosphorylation level of unstimulated Tconv (left column) and phosphorylation is depicted according to the color code given on top, with blue showing reduced phosphorylation and red depicting enhanced phosphorylation. Figure is a kind courtesy of Marco van Ham (HZI, Braunschweig).

1.5 Immunological synapse formation

1.5.1 Structure and assembly of the IS

The IS is a highly organized structure that is formed at the cell interface during interaction of T cells with APCs and was first described in 1998 by the laboratory of Abraham Kupfer [163]. It is composed of concentric rings, supramolecular activation clusters (SMACs), consisting of particular molecules implementing signal transduction and costimulation or cytoskeletal rearrangement and adhesion **(Fig. 3A)**. The inner part, the central SMAC (cSMAC) accumulates TCR/pMHC microclusters and certain costimulatory molecules such as CD28. It is surrounded by the peripheral SMAC (pSMAC), which contains CD4 and intracellular signalosome components such as Lck; furthermore, the integrin Lymphocyte function-associated antigen 1 (LFA-1) is located within the pSMAC. The most outer ring, the distal SMAC (dSMAC) consists of filamentous actin (F-actin) and the tyrosine phosphatase CD45 [163, 164]. Due to this unique structure, contrary signaling molecules are spatially separated, as for example TCR/pMHC microclusters including intracellularly phosphorylated ITAMs of CD3ζ and the phosphatase CD45. Additionally, involved molecules are organized according to size of their ectodomains to prevent steric

hindrance [163, 165] **(Fig. 3B)**. During IS assembly, recruitment processes follow a defined order and are strictly orchestrated. Upon pMHC recognition, TCR/pMHC microclusters are formed in the periphery of the contact zone aided by the actin cytoskeleton and are moved towards the center of the emerging IS via microtubule dynamics [166-169]. However, signaling from those microclusters was already reported in the periphery and is rather terminated as soon as the clusters reach the cSMAC, especially for strong agonists [167, 170, 171]. The cSMAC is depleted of F-actin and therefore enables vesicle formation and release into the synaptic cleft [172-175]. It was shown before, that B cells ingest T cell-released vesicles, which allowed for continued B cell activation [176]. Besides extracellular vesicle release, TCR/pMHC microclusters are also engulfed by the T cells at the cSMAC for termination of signaling and recycling of receptors [171, 177-179].

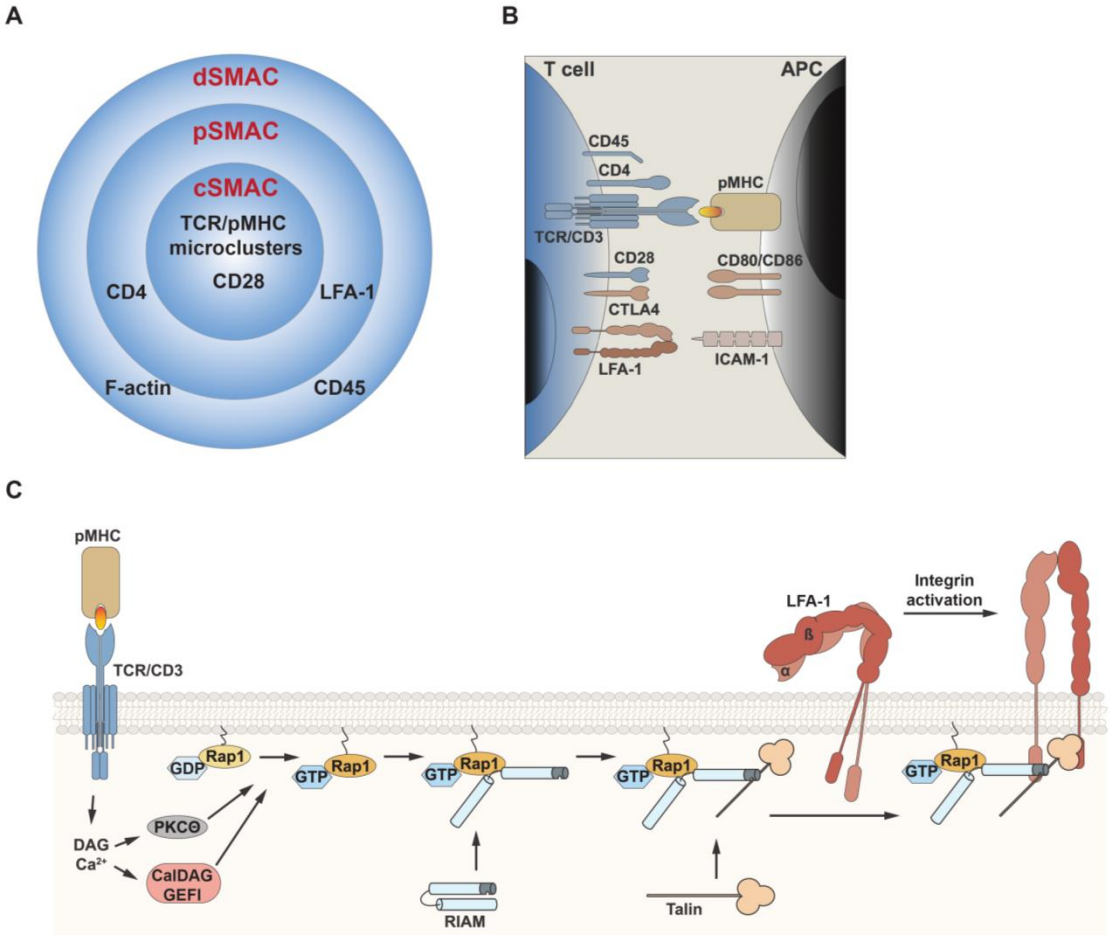

Fig. 3: Constitution of the T cell IS and integrin activation upon TCR ligation. (A) Schematic picture of the top view of a T cell IS depicting the SMACs in concentric rings with major molecules located at the respective SMAC written in black. **(B)** Side view of an IS between T cell (left side) and APC (right side) and major contributing molecules from both cell types. Receptors and respective

ligands are opposite of each other. **(C)** Schematic summary of the LFA-1 activation pathway following TCR engagement by a pMHC. Detailed information on all figure parts can be found in the text. **(A)** and **(B)** are adapted from [180], **(C)** is adapted from [181].

1.5.2 Integrin activation: inside-out and outside-in

Integrin activation is crucial for all hematopoietic cells to facilitate cell arrest and migration as well as to enable formation of sustained cell-cell interactions as for example at the IS [182]. Integrins are heterodimers composed of one out of 18 α subunits combined with one out of eight β subunits and they are found in three conformations which reflect different activation stages: One bent and two extended forms which are of low, intermediate and high affinity towards their ligand, respectively. The two extended versions differ in a shift of the headpiece of the β subunit exposing the ligand binding pocket and an additional rearrangement of the transmembrane and intracellular domains of both subunits [183, 184]. The most prominent integrin at the IS is LFA-1, which consists of CD11a (integrin α_L) and CD18 (integrin β_2) [184, 185]. During IS formation, LFA-1 is activated downstream TCR ligation via inside-out signaling. Briefly, TCR ligation causes the formation of several signaling modules, which at least partly affect integrin activation. One example is the TCR-triggered recruitment of SLP-76/ADAP/SKAP-55 (SH2 domain-containing leukocyte protein of 76 kDa/Adhesion and degranulation promoting adaptor protein/Src kinase-associated phosphoprotein of 55 kDa) to the LAT signalosome [186-189]. This module serves as docking station for RIAM (Rap1–guanosine triphosphate (GTP)-interacting adapter molecule), and RIAM in turn recruits the cytoskeletal protein Talin [190-192]. Additionally, Kindlin-3 is recruited to the intracellular integrin domains, likely through association with ADAP [193], and also binds to the β subunit albeit at a different position than Talin [194]. Another protein complex is formed after activation of the small guanosine triphosphatase (GTPase) Ras-related protein 1 (Rap1). GTP-bound Rap1 attracts its binding partner RapL (Regulator for cell adhesion and polarization enriched in lymphoid tissues) into the synapse and RapL directly binds the α subunit of LFA-1 [195, 196]. Additionally, active Rap1 also recruits RIAM, again supporting the recruitment of Talin [197, 198]. Due to the direct interaction of this adaptor protein with the subunit of LFA-1, transition from low affinity to intermediate affinity LFA-1 is mediated. The high affinity

state is reached due to the connection of the whole complex on the one side to intercellular adhesion molecule-1 (ICAM-1) and on the other side to the actin cytoskeleton via Talin, which in sum generates sufficient shear force to completely convert LFA-1 to the high affinity conformation **(Fig. 3C)** [199, 200]. However, high affinity conformation of integrins can also be induced by extracellular bivalent cations such as Mn^{2+} via outside-in signaling [201]. Certain tyrosine kinases are associated with the intracellular integrin domains and mediate outside-in signaling, thereby, submitting information regarding chemical and mechanical properties of the environment into the cell [202, 203]. Shutdown of integrin activation is less well studied and literature so far suggests that it is probably enabled through another set of small GTPases such as Cell division control protein 42 (Cdc42) and Rho-related GTP-binding protein H (RhoH) as well as proteases like calpain. Additionally, phosphorylation of certain residues within the β subunit of LFA-1 was shown to have inhibitory effects [204-208].

1.6 The small GTPase Rap1

Rap1 is the major small GTPase implementing integrin activation in T cells with regard to LFA-1 activation at the IS [195, 209, 210]. Rap1 is geranylgeranylated and therefore constitutively membrane bound [184]. It was reported to be stored in intracellular vesicles, which also allow transport of Rap1 to the cell membrane, but whether this trafficking is pervasive or a consequence of TCR stimulation remains a matter of debate [211, 212]. In the inactive state Rap1 binds guanosine diphosphate (GDP) and needs the aid of a guanine nucleotide exchange factor (GEF), which triggers release of GDP and thereby enables binding of GTP instead, in order to reach the active conformation [213]. Up to date, several Rap1 GEFs have been identified: Members of the Epac (Exchange factor directly activated by cAMP), PDZ-GEF and CalDAG GEF families, as well as C3G (CRK-SH3 domain binding GEF) and Dock4 (Dedicator of cytokinesis protein 4), which belongs to the CDM family [214-221]. Hydrolysis of GTP to GDP needs support from a Rap GTPase-activating protein (GAP), such as members of the Signal-induced proliferation-associated protein 1 (Spa-1) family [222]. As long as both Rap GEFs and Rap GAPs are present and activated, Rap1 cycles between the GDP-bound inactive and the GTP-bound active state.

Rap1 deficiency was shown to result in defective integrin activation affecting cell adhesion and migration, thereby impacting lymphocyte homing [223, 224]. Additionally, it was shown that integrin activation is indispensable for recognition of weak agonists by T cells and therefore Rap1 is involved in the generation of appropriate T cell responses [225, 226]. Besides its role in cell adhesion, Rap1 impacts ERK1/2 activation and ultimately T cell activation, but whether this impact activates or rather inhibits ERK1/2 remains controversial. It was reported that Rap1 reduces ERK1/2 activation, and that this pathway is employed by the costimulatory molecule CTLA-4 to mediate T cell inhibition and vice versa CD28 was shown to inhibit Rap1, which in turn results in activation of ERK1/2 [226-229]. On the other hand, B-Raf was identified as a direct target of Rap1 thereby promoting activation of ERK1/2 [230, 231]. Ren *et al.* had a detailed look at the molecular link between Rap1 and ERK1/2 and identified that the RapGEF CalDAG GEFI is phosphorylated by ERK1/2, which inhibits GEF activity towards Rap1, resulting in a feedback loop towards reduced ERK1/2 activation [232]. In summary, it was convincingly shown that Rap1 directly interacts with B-Raf and Raf1, which positively or negatively regulates ERK1/2, respectively [230, 233]. Therefore, Rap1 might act as both, activator and inhibitor of ERK1/2, which might be for instance cell context-dependent or an indirect effect of Rap1 [234]. Interestingly, one study also addressed the role of Rap1 specifically for Treg development and function. They could show that transgenic mice expressing constitutively active Rap1 displayed elevated frequencies of $CD4^+CD103^+$ Tregs and thus suggest a role for Rap1 in thymic and peripheral Treg development, which is at least partly independent of LFA-1 activation. However, molecular mechanisms by how Rap1 is affecting Treg development were not clarified [235, 236].

1.7 The guanine nucleotide exchange factor CalDAG GEFI

CalDAG GEFI belongs to a family of four GEFs, which were considered to be Ca^{2+} and DAG regulated [195]. CalDAG GEFI (Rasgrp2) expression is mainly reported in the nervous and hematopoietic system [237] and CalDAG GEFII (Rasgrp1) is the family member majorly abundant in T cells [238]. In B cells, preferential CalDAG GEFIII (Rasgrp3) expression was shown [239, 240], and Rasgrp4 is expressed specifically in mast cells [241]. CalDAG GEFI was identified

and first characterized as a Rap-specific GEF in the brain of rats, highly enriched in the striatum and olfactory bulb, and in the hematopoietic system of rat and human [216]. It was shown that CalDAG GEFI is massively downregulated in the brain in case of Huntington's disease and it was speculated that this downregulation serves as protective mechanism, because knockdown of CalDAG GEFI in an experimental model of Huntington's disease rescued pathology [242]. Regarding the hematopoietic system CalDAG GEFI function is best characterized in human and murine platelets and neutrophils [237, 243]. Studies regarding T cells are so far solely performed in the human system as it was reported that CalDAG GEFI is not expressed by murine T cells [184, 237]. All CalDAG GEF family members display an N-terminal Ras exchange motif (REM) domain, directly followed by RasGEF (Cdc25-like) domain **(Fig. 4A)**. Those two domains commit the guanine nucleotide exchange activity and enable the interaction with the respective GTPase. C-terminal of these catalytic domains are two EF hand motives, which render the molecule Ca^{2+} sensitive. At the C-terminal part, a C1 domain is located, which is thought to allow binding of phorbol esters such as DAG and its synthetic surrogate phorbol 12-myristate 13-acetate (PMA) [218]. Although according to literature CalDAG GEFI was considered not to be expressed in primary murine T cells [184, 237], our group detected CalDAG GEFI present in both *ex vivo* isolated murine Tregs and Tconv in the course of the aforementioned comparative proteome analysis **(Fig. 4B)** [132]. Besides the mere presence, CalDAG GEFI was also found to be phosphorylated at several amino acid residues during the performed phosphopeptide sequencing and most strikingly, a novel phosphorylation site at Y523 was detected **(Fig. 4C)** [132]. Additionally, due to the comparison of resting and activated Tregs and Tconv, our group identified a differential regulation of Y523 in resting Tregs and Tconv, with a reduced phosphorylation level in Tregs. Following 5 min stimulation via the TCR, this difference was even more pronounced due to the fact that Tconv did not alter the phosphorylation level of Y523, while the phosphorylation was massively reduced upon stimulation in Tregs **(Fig. 4D)** [132]. CalDAG GEFI Y523 is located within the C1 domain and more precisely in the loop B of the phorbol ester binding pouch **(Fig. 4E)** [244]. C1 domains are well known from protein kinase C family members to enable responsiveness towards DAG, and several studies have already addressed phorbol ester binding capacities of the CalDAG GEF family members [244-246].

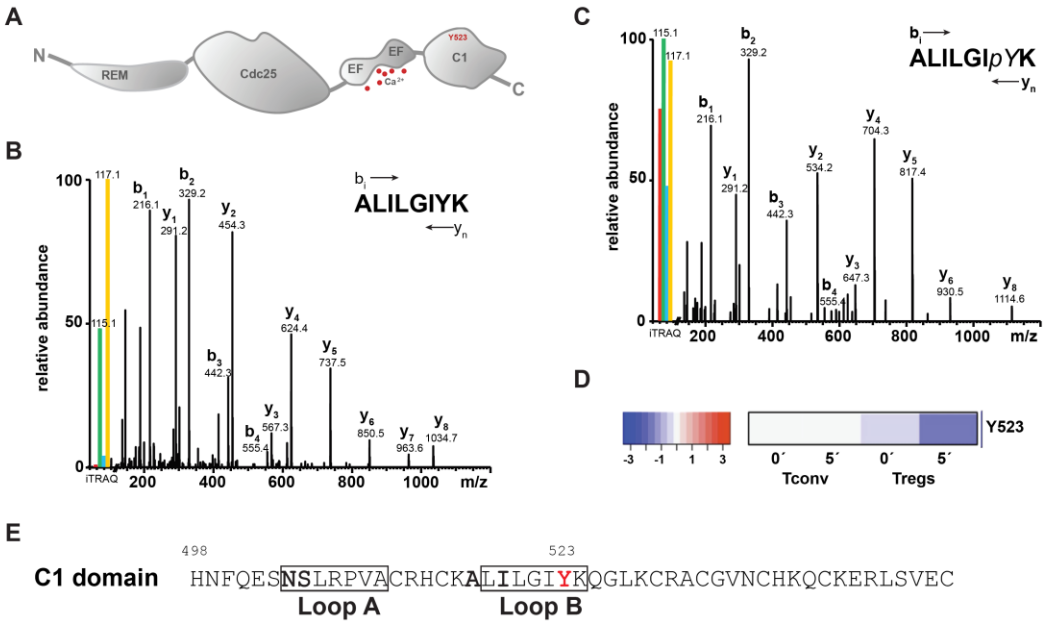

Fig. 4: The guanine nucleotide exchange factor CalDAG GEFI. CalDAG GEFI was found to be differentially phosphorylated at the so far undescribed site Y523 in primary murine Tregs versus Tconv. **(A)** Schematic overview of the protein domain structure of CalDAG GEFI. The newly identified phosphorylation site at Y523 is located within the C-terminal C1 domain (right side) and is highlighted in red. Details can be found in the text. **(B)** Tconv and Tregs were sorted from pooled spleen and LNs from BALB/c mice as $CD4^+CD25^-$ and $CD4^+CD25^+$ cells, respectively, for comparative proteomic analysis performed recently by our group. Samples were iTRAQ-labeled and analyzed via LC-MS/MS. Representative MS spectrum of one of the identifier peptides of CalDAG GEFI is shown with the peptide sequence written on the top right. A summary of the iTRAQ ion signal is depicted at the very left side of the plot, with Tregs represented by the 115.1 ion displayed in green and Tconv represented by the 117.1 ion depicted in yellow. Each peak represents part of the peptide, either starting from the N-terminus (b_i) or from the C-terminus (y_n) of the displayed peptide. **(C)** Sorted Tconv and Tregs, as described above, were either left unstimulated or stimulated via streptavidin-mediated crosslinking of biotinylated anti-CD3/28 for 5 min. Cells were lysed and lysates were enriched for phospho-peptides in order to perform quantitative phosphoproteomics. Representative MS spectrum of one of the detected phospho-peptides of CalDAG GEFI is shown with the peptide sequence written on the top right. A summary of the iTRAQ ion signals is depicted at the very left side of the plot, with resting Tregs represented by the 115.1 ion displayed in red, resting Tconv represented by the 115.1 ion displayed in green, activated Tregs represented by the 116.1 ion displayed in blue and activated Tconv represented by the 117.1 ion displayed in yellow. Each peak represents part of the phospho-peptide, either starting from the N-terminus (b_i) or from the C-terminus (y_n) of the detected peptide and the phosphorylation of the tyrosine residue becomes apparent from the mass difference of 80 Dalton between the peptide y2 in this plot and the peptide y_2 from the MS plot displayed in **(B)**, which is representing the unphosphorylated state. **(D)** Excerpt from Figure 2, displaying the phosphorylation dynamics at Y523 of CalDAG GEFI in unstimulated (0') und stimulated (5'), as described above, Tconv (two columns on the left) and Tregs (two columns on the right). The respective color code of the heatmap is displayed on the left with blue indicating reduced phosphorylation and red displaying enhanced phosphorylation. All samples were normalized to the phosphorylation level of unstimulated Tconv (left column). **(E)** Amino acid sequence of the C1 domain of CalDAG GEFI starting from amino acid 498 and including the phosphorylated tyrosine residue Y523, highlighted in red. C1 domains were shown to bind phorbol esters in a binding pouch and the amino acids contributing to the pouches

loops are enframed. **(B)** and **(C)** are a kind courtesy of Marco van Ham (HZI, Braunschweig). Proteomics and phosphoproteomics were performed by Marco van Ham and colleagues.

So far, it was shown that CalDAG GEFII and CalDAG GEFIII are responsive to DAG, while this is not the case for CalDAG GEFI. Regarding Rasgrp4, two splice variants exist from which Rasgrp4α binds DAG whereas Rasgrp4β does not. It was clearly demonstrated that unresponsiveness of CalDAG GEFI towards DAG and analogues thereof is due to amino acid differences within the phorbol ester binding pocket of the family members. The residue S506 was proven to be extraordinarily important by two independent studies [244, 246], and the latter conducted by Czikora and colleagues expanded this to the amino acids N505, A517 and I519. Interestingly, although CalDAG GEFI is not binding DAG, it is localized towards the membrane following cell stimulation and was also reported to be part of the IS, localizing within the pSMAC [247, 248]. Caloca *et al.* demonstrated that CalDAG GEFI can directly interact with F-actin and therefore it is believed that membrane recruitment is facilitated via this cytoskeletal interaction [248]. Interestingly, although CalDAG GEFI was convincingly shown not to bind DAG or PMA, still a number of studies reported PMA-induced CalDAG GEFI activity and subcellular translocation [237, 243, 249, 250]. CalDAG GEFI is a Rap1-specific GEF and therefore implements integrin activation pathways [216]. It was shown before that deficiency in CalDAG GEFI leads to impaired cell adhesion and that also cell migration is impaired in absence of CalDAG GEFI [237, 243, 249]. CalDAG GEFI$^{-/-}$ mice are healthy and fertile and do not show any obvious phenotype [237]. However, closer examination revealed that thrombus formation in those mice is impaired due to delayed integrin activation in platelets which results in slightly elevated bleeding times following injury [237]. CalDAG GEFI$^{-/-}$ neutrophils displayed an aberrant cell adhesion behavior and migration towards the site of inflammation was strongly impaired. Therefore, it was assumed that defective CalDAG GEFI is the cause for leukocyte adhesion deficiency type III (LADIII) and that CalDAG GEFI$^{-/-}$ mice serve as appropriate experimental model [243]. However, it was shown in the meantime that LADIII is caused by a mutation of Kindlin-3 rather than CalDAG GEFI [251]. Under homeostatic conditions, white blood cell count appeared at expected numbers, and as CalDAG GEFI was believed to be absent from T cells, no thorough examination of the T cell

compartment was performed so far. Published data on CalDAG GEFI's role in various cells of the hematopoietic compartment and especially the reported functional impact on human T cells make CalDAG GEFI an interesting target for the T cell field. In addition, identification of the differentially regulated novel phosphorylation site in Tregs as compared to Tconv allows speculation about T cell subset-specific function of CalDAG GEFI.

1.8 Aims of the study

It is well established that Tregs maintain immune tolerance by active suppression of effector T cell proliferation and that all T cell subsets require stimulation via the TCR in order to fulfill their designated effector functions. Moreover, there is accumulating evidence that TCR signaling is differentially organized in Tregs and Tconv, but the responsible molecular players remain to be elucidated. Using comparative proteomics and quantitative phosphopeptide sequencing as well as toponome analyzes by MELC, our department identified diverging phosphorylation dynamics and recruitment kinetics of phosphorylated components during IS formation of Tregs and Tconv [132]. Therefore, we hypothesized that the detected differences result in the formation of a Treg-specific IS, and one aim of this study was to gain more detailed insight into differentially regulated phosphorylation dynamics following TCR ligation in Tregs and Tconv. Besides this general approach to decipher Treg-specific IS formation, the role of the candidate molecule CalDAG GEFI was analyzed in more detail. The aforementioned phosphoproteomic study identified a novel phosphorylation-site of CalDAG GEFI, which we hypothesized to affect IS formation and thereby Treg functionality in general. Gathering detailed knowledge on Treg-specific characteristics during IS formation might allow for identification of targets susceptible to manipulation in order to abrogate or support Treg-IS formation.

2. Results

2.1 Themis expression levels do not affect Treg suppressive capacity *in vitro*

Employing proteomic analysis of FACS-sorted *ex vivo* isolated murine Tconv and Tregs, our group could recently identify a number of proteins that are differentially expressed in the two examined T cell subsets. Themis is one of the top candidates with a significantly reduced expression level in Tregs as compared to Tconv [132]. As shown before in other studies, Themis is a component of the TCR signalosome and plays an important role during thymocyte positive selection [138, 252]. Therefore, it was tempting to speculate that overexpression of Themis in primary murine Tregs would impair their suppressive capacity. Thus, retroviral transduction was employed, which allowed overexpression of murine Themis along with Thy1.1, serving as a reporter, in anti-CD3/28 activated $CD4^+$ T cells from $Foxp3^{hCD2}$ reporter mice. $Thy1.1^+$ Tregs were re-sorted and co-cultured with freshly FACS-sorted and Cell Trace™ Violet (CTV)-labeled Tnaive at titrated ratios in presence of T activator beads. Empty vector transduced Tregs served as control. After four days, flow cytometric analysis of the co-culture revealed the dilution of CTV in the total Tnaive population quantified by the geometric mean fluorescence intensity (Geomean) of CTV **(Fig. 5A)**. Both, Themis-overexpressing and empty vector-transduced Tregs were equally able to restrict the proliferation of Tnaive cells **(Fig. 5B and C)**. Therefore, in the used experimental setting, elevated Themis expression in Tregs has no impact on their suppressive capacity.

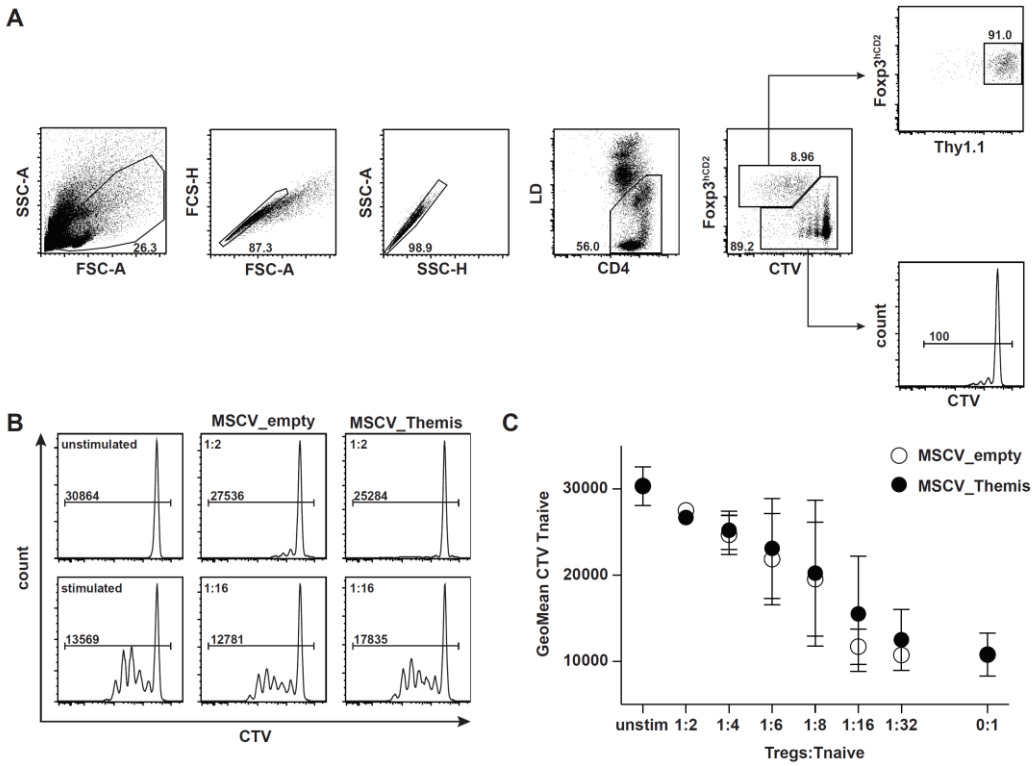

Fig. 5: *In vitro* suppression assays using Themis overexpressing Tregs. $CD4^+$ T cells were MACS-enriched from pooled spleen and LNs of $Foxp3^{hCD2}$ mice and lentivirally transduced with either empty vector (MSCV_empty) or vector containing Themis (MSCV_Themis). Transduced Tregs were resorted as $CD4^+Foxp3^{hCD2+}Thy1.1^+$ cells and co-cultured with freshly FACS-sorted CTV-labeled Tnaive at indicated ratios in presence of T activator beads. On day 4, proliferation-dependent CTV-dilution in Tnaive was assessed via flow cytometry. **(A)** Exemplary gating strategy is depicted: First gate was set on lymphocytes and doublets were excluded according to scatter properties of the cells. Further gating included living $CD4^+$ cells (LD) and separation of Tregs and Tnaive according to $Foxp3^{hCD2}$ expression as well as CTV signal. Expression of Thy1.1 as marker for transduced cells was verified on Tregs and the Geomean of CTV of the total Tnaive population was determined. Numbers in plots represent frequencies in the respective gates. **(B)** Exemplary histogram plots are shown of unstimulated (top left) and bead-stimulated Tnaive (lower left) as controls and Treg:Tnaive co-cultures at a ratio of 1:2 (upper panel) and 1:16 (lower panel) using empty vector transduced Tregs (MSCV_empty, middle) or Themis overexpressing Tregs (MSCV_Themis, right). Numbers in gates represent Geomean of the CTV signal of the Tnaive population. **(C)** Scatter plot depicts the Geomean of CTV of Tnaive cells at indicated Tregs:Tnaive ratios for empty vector (MSCV_empty) and Themis-containing vector (MSCV_Themis) transduced Tregs. Mean±SD is depicted from pooled data of three independent experiments.

2.2 Protein phosphorylation kinetics following TCR ligation in Tregs and Tconv

A phosphoproteome analysis recently performed by our group revealed differential phosphorylation dynamics comparing primary murine Tregs and Tconv, either in the resting state or after 5 min TCR stimulation **(Fig. 2)** [132]. Due to high requirements of cells and hence mice to purify sufficient numbers of Tregs and Tconv for quantitative phosphopeptide sequencing, it was experimentally not feasible to generate additional datasets for confirmation of the initial results or for inclusion of further stimulation time points. Thus in this study, phosphorylation kinetics in Tregs and Tconv following TCR ligation were addressed via flow cytometry using selected available antibodies, which allows for analysis at the single cell level and performance of kinetics to follow differential phosphorylation events in the two T cell subsets over time.

2.2.1 Phospho-flow cytometry establishment

To analyze differential phosphorylation in primary murine Tregs and Tconv at the single cell level, bulk $CD4^+$ T cells were isolated from pooled spleen and LNs of $Foxp3^{hCD2}$ reporter mice via MACS-enrichment. Cells were stained for CD4 and $Foxp3^{hCD2}$ to enable discrimination of Tregs and Tconv. Subsequently, cells were decorated with biotinylated anti-CD3 as well as anti-CD28, pre-warmed at 37 °C and stimulated by addition of streptavidin to initiate crosslinking of the biotinylated antibodies. In order to determine the optimal stimulation time span a fraction of cells was fixed to abrogate all ongoing signaling events over a time course of 30 minutes. Subsequently, T cells were permeabilized and intracellular staining for phosphorylated ERK1/2 (pERK1/2) was performed. By flow cytometric analysis, doublets and dead cells were excluded, and Tregs and Tconv were gated subsequently as $CD4^+Foxp3^{hCD2+}$ and $CD4^+Foxp3^{hCD2-}$, respectively **(Fig. 6A)**. The isotype control confirmed no unspecific background staining at all analyzed time points **(Fig. 6A, B and C)**, and stimulation via PMA/iono served as positive control **(Fig. 6A)**. Evaluation of the recorded kinetic revealed the highest frequency of $pERK1/2^+$ Tregs and Tconv within the first 5 min of stimulation, followed by a steady decrease back to basal phosphorylation levels **(Fig. 6B)**. Obviously, the phosphorylation of ERK1/2 is reduced in Tregs as compared to Tconv, which is one

of the hallmark differences in TCR signaling of the two T cell subsets **(Fig. 6B, C and D)**. Consequently, a second kinetic was performed, focusing on the first 5 min after TCR ligation and narrowing the time intervals to 30 sec each. As expected, the kinetic confirmed the occurrence of major phosphorylation events within the first 5 min after TCR triggering with an apex for pERK1/2$^+$ Tregs and Tconv after 3 min of antibody crosslinking **(Fig. 6C)**. Subsequently, stimulation conditions were optimized in order to retrieve the maximum frequency of pERK1/2$^+$ Tregs and Tconv. Therefore, several concentrations were tested ranging from 1/0.5 µg/ml to 80/40 µg/ml of anti-CD3/28, respectively. Cells were fixed after 3 min of stimulation and frequency of pERK1/2$^+$ cells was analyzed for Tregs and Tconv. The concentrations of 10/5 µg/ml anti-CD3/28 resulted in the maximum frequency of pERK1/2$^+$ Tregs and Tconv **(Fig. 6D)** and therefore this stimulation condition was chosen for the following phosphorylation kinetics.

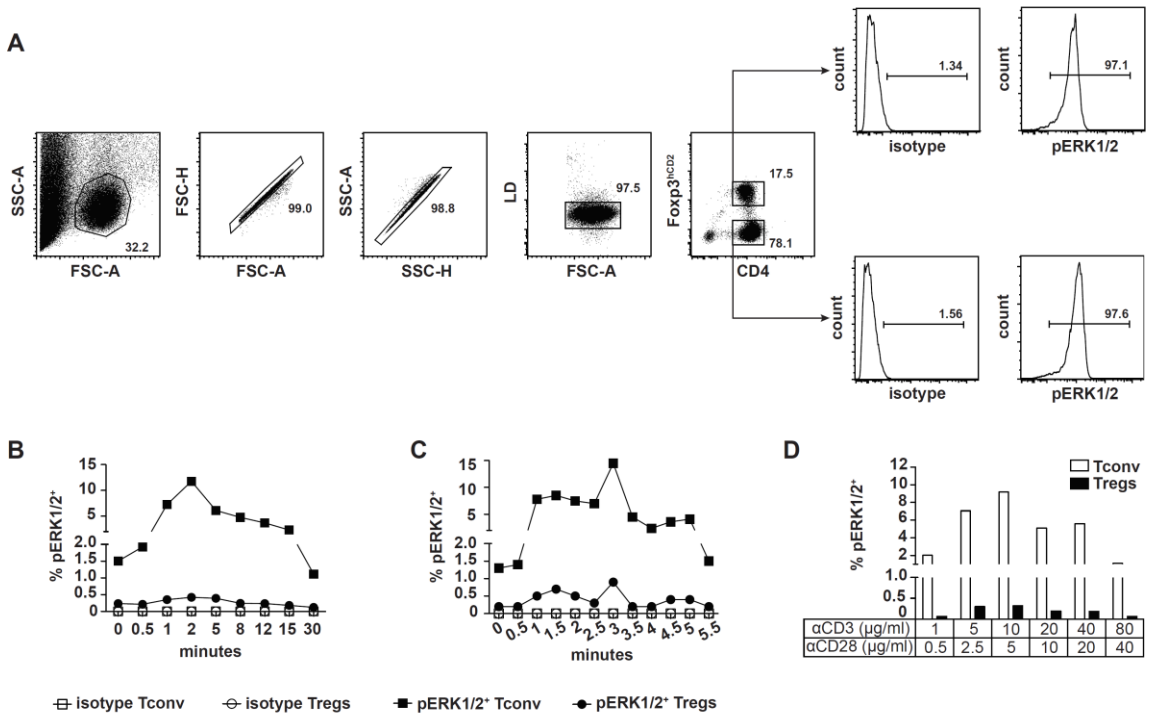

Fig. 6: Determination of appropriate time frame and optimal stimulation conditions for phospho-flow cytometry. CD4$^+$ T cells from pooled spleen and LNs of Foxp3^{hCD2} reporter mice were MACS-enriched and stimulated via streptavidin-mediated crosslinking of biotinylated anti-CD3/28. At indicated time points, a fraction of the cells was fixed and stained for pERK1/2 or isotype control. **(A)** Exemplary gating strategy depicts gating on living singlet lymphocytes. CD4$^+$Foxp3^{hCD2+} Tregs and CD4$^+$Foxp3^{hCD2-} Tconv were analyzed for pERK1/2$^+$ cells following PMA/iono stimulation with gates set according to 0 min stimulation control. The isotype control was included in all experiments to evaluate unspecific background staining. Numbers indicated in dot plots represent cell frequencies in

the respective gates. **(B)** Kinetic of the frequency of pERK1/2$^+$ Tregs (closed circles) and Tconv (closed squares) as well as isotype controls for both T cell subsets (open circles and open squares, respectively) over 30 min following addition of streptavidin to induce crosslinking of biotinylated stimulation antibodies. **(C)** Kinetic of the frequency of pERK1/2$^+$ Tregs (closed circles) and Tconv (closed squares) as well as isotype controls for both T cell subsets (open circles and open squares, respectively). **(D)** Bar graph summarizes the frequencies of pERK1/2$^+$ Tregs (closed bars) and Tconv (open bars) following 3 min stimulation via crosslinked anti-CD3/28 at indicated concentrations of biotinylated stimulation antibodies. Isotype control is not depicted as values were constantly close to zero (see **(B)** and **(C)**). All experiments were performed once.

2.2.2 Phospho-flow cytometry kinetics for selected molecules

The major limitation of phospho-flow cytometry is the availability of phospho-specific antibodies, which are suitable for flow cytometry. Therefore, verification and extension of identified candidates from the phosphoproteomic analyses was only possible for CD3ζ pY142, and additionally the present study extended to Lck pY505 and ZAP70 pY319, with ERK1/2 pT202/pY204 serving as a control [132]. Cells were stimulated and stained as described above and gated according to Foxp3^{hCD2} expression to discriminate Tregs and Tconv. Frequencies of pLck$^+$, pCD3ζ$^+$ and pZAP70$^+$ Tregs and Tconv were far below the observed frequency for pERK1/2$^+$ cells, which precluded a comparison on the frequency level for the two T cell subsets **(Fig. 7A)**. Consequently, the Geomean of the whole Treg and Tconv subset for the respective phosphorylation-site was analyzed. In line with literature, ERK1/2 phosphorylation is attenuated in Tregs as compared to Tconv, palpable from the ascent of the ratio of the Geomean for pERK1/2 (Tconv/Tregs), which was not observed for the isotype control **(Fig. 7C-E)**. However, no obvious differences in phosphorylation levels and dynamics were detected for Lck pY505, CD3ζ pY142 and ZAP70 pY319 in Tregs as compared to Tconv **(Fig. 7C-E)**. For CD3ζ pY142 the phosphoproteome detected an elevated phosphorylation state of this site in unstimulated Tregs as compared to Tconv, which was not detectable via phospho-flow cytometry **(Fig. 2 and Fig. 7D)**, indicating that variations in phosphorylation might be beyond the detection limit of phospho-flow cytometry.

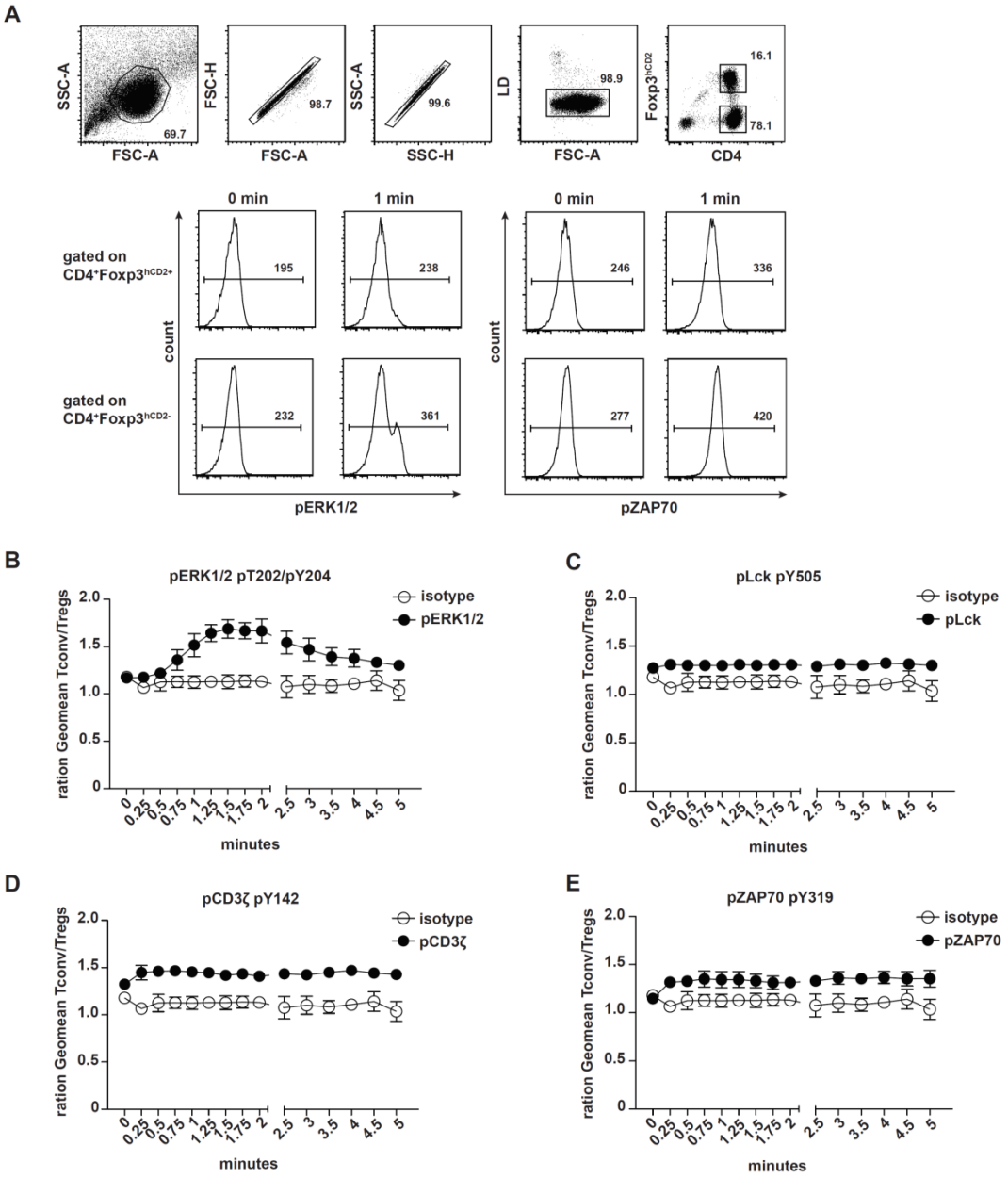

Fig. 7: Phospho-flow cytometry for pLck pY505, pCD3ζ pY142, pZAP70 pY319 and pERK1/2 pT202/pY204. $CD4^+$ T cells from pooled spleen and LNs of $Foxp3^{hCD2}$ reporter mice were MACS-enriched and stimulated via streptavidin-mediated crosslinking of biotinylated anti-CD3/28. At indicated time points, a fraction of the cells was fixed and stained intracellularly for the indicated phosphorylated protein or isotype control. **(A)** Exemplary gating strategy on singlet lymphocytes depicts: Alive Tregs and Tconv were gated as $CD4^+Foxp3^{hCD2+}$ and $CD4^+Foxp3^{hCD2-}$ cells, respectively (upper panel), and subsequently the Geomean for the respective phospho-protein for Tregs and Tconv was determined as exemplary depicted for pERK1/2 (lower panel, left) and pZAP70 (lower panel, right). Numbers in dot plots represent cell frequencies in the respective gates and numbers in histogram plots represent the Geomean of the respective population. **(B-E)** In order to analyze diverging phosphorylation kinetics and signal strength, the ratio of the Geomean for Tconv/Tregs was determined for each analyzed phospho-protein. An isotype control for the intracellular antibody was included in all experiments to evaluate unspecific background staining. Plots depict mean±SD of three independent experiments. **(B)** Kinetic of the Geomean ratio of Tconv/Tregs for pERK1/2 pT202/pY204 (closed circles) and isotype control (open circles) over 5 min. The increasing ratio indicates reduced

Geomean for Tregs as compared to Tconv. **(C)** Kinetic of the Geomean ratio of Tconv/Tregs for pLck pY505 (closed circles) and isotype control (open circles) over 5 min. **(D)** Kinetic of the Geomean ratio of Tconv/Tregs for pCD3ζ pY142 (closed circles) and isotype control (open circles) over 5 min. **(E)** Kinetic of the Geomean ratio of Tconv/Tregs for pZAP70 pY319 (closed circles) and isotype control (open circles) over 5 min.

2.3 CalDAG GEFI fine-tunes Treg function

CalDAG GEFI was detected in murine Tregs and Tconv in both, the proteomic study and the phosphopeptide sequencing recently performed in our group **(Fig. 2 and Fig. 4)** [132]. The latter study also enabled the identification of a novel phosphorylation-site within the C-terminal C1 domain of CalDAG GEFI at Y523. Since previous studies did report CalDAG GEFI as being not expressed in murine T cells [184, 237], the functional role of CalDAG GEFI in murine T cells has not been addressed yet.

2.3.1 CalDAG GEFI is expressed in primary murine Tregs and Tconv

To confirm expression of CalDAG GEFI in primary murine Tregs and Tconv, both T cell subsets were FACS-sorted as $CD4^{+}Foxp3^{hCD2+}$ and $CD4^{+}Foxp3^{hCD2-}$, respectively, from pooled spleen and LNs of $Foxp3^{hCD2}$ reporter mice. Cells were lysed and subsequently applied for Western Blot analysis. As expected from the proteomic and phosphoproteomic analysis, CalDAG GEFI was clearly detectable in both murine T cell subsets with a slightly higher expression level in Tconv as compared to Tregs **(Fig. 8)**.

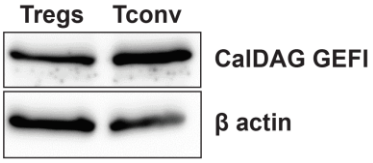

Fig. 8: CalDAG GEFI detection in murine Tregs and Tconv via Western Blotting. Tregs and Tconv were FACS-sorted from pooled spleen and LNs from $Foxp3^{hCD2}$ reporter mice as $CD4^{+}Foxp3^{hCD2+}$ and $CD4^{+}Foxp3^{hCD2-}$, respectively. Cells were lysed and equal amounts of protein, as determined via BCA assay, were separated by SDS gel electrophoresis. Proteins were blotted on PVDF membrane and CalDAG GEFI was detected at the expected molecular weight of 69 kDa via anti-Rasgrp2 antibody. Detection of β-actin served as loading control. Data are representative of five independent experiments.

2.3.2 Phosphorylation at Y523 is not affecting DAG binding of CalDAG GEFI

The recently identified phosphorylation-site at Y523 of CalDAG GEFI is located within the C1 domain of the protein [132], and it is well established that C1 domains bind the second messenger lipid DAG as well as other phorbol esters such as the DAG analogue PMA [253]. However, it remains controversially discussed whether this is also applicable for the C1 domain of CalDAG GEFI [216, 220, 244-246, 248, 249]. Presence or absence of a negatively charged phosphogroup is influencing the local charge of a protein domain and the novel phosphorylation site at Y523 locates into the B loop of CalDAG GEFI's C1 domain **(Fig. 4)**. Therefore, differential phosphorylation might result in diverging DAG binding ability of CalDAG GEFI in Tregs and Tconv. Thus, the murine C1 domain of CalDAG GEFI was cloned into an expression vector and thereby fused to a GST-tag (see section 4.18 for details). In collaboration with the group of Prof. Christian Freund from the Free University of Berlin, recombinant protein was expressed in *E. coli* and extracted to high purity. To mimic the phosphorylated and dephosphorylated state, Y523 was mutated to Y523D and Y523F, respectively. Purified proteins were subjected to membrane lipid PIP strip assays and binding to the membrane-spotted lipids was detected via the proteins GST-tag. As expected, the GST-tag alone did not show binding to any of the provided lipid spots, whereas the manufacturer's positive control, Pleckstrin homology domain of phospholipase δ1 recognizing phosphatidylinositol (4,5)-bisphosphate, developed an intense signal. However, none of the tested CalDAG GEFI C1 domain versions displayed detectable binding to DAG or any other provided lipid **(Fig. 9A)**. To allow for physiological protein folding after recombinant expression, the proteins were dialyzed against $ZnCl_2$-containing buffer **(Fig. 9B)**, and to rule out adverse effects by glycerol, it was removed from the buffer in an additional set of experiments **(Fig. 9C)**. For both preparations of recombinant protein, CalDAG GEFI's C1 domain did not allow for binding to DAG, irrespective of the phosphorylation status of Y523. Therefore, differential phosphorylation at Y523 of CalDAG GEFI does not lead to diverging DAG-mediated membrane recruitment of the protein in Tregs as compared to Tconv, and the functional role of this phosphorylation-site remains to be elucidated.

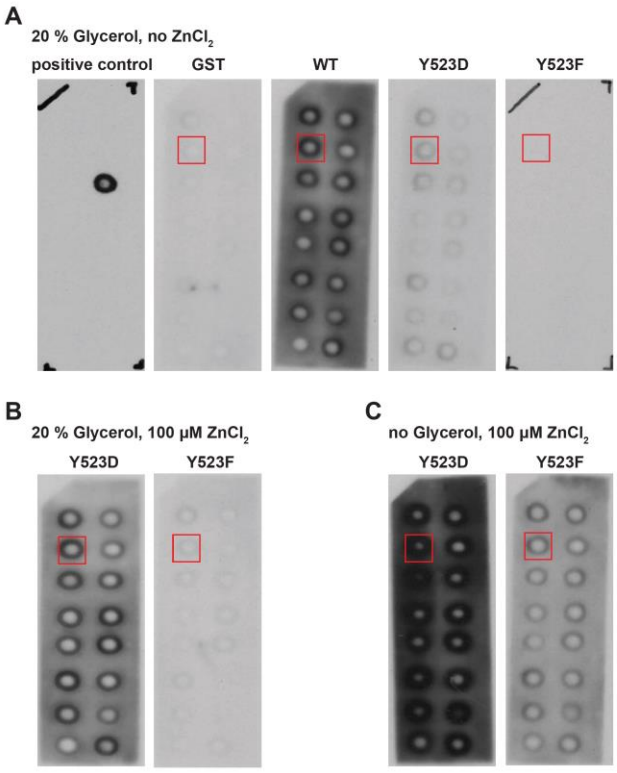

Fig. 9: Membrane lipid PIP strips using wild type and Y523D/F phosphomutant CalDAG GEFI. The murine CalDAG GEFI C1 domain, either wild type sequence (WT), phosphomimetic version (Y523D) and non-phosphorylated version (Y523F), was subcloned into pGEX-4T-1 and thereby fused to a GST-tag. Proteins were recombinantly expressed and purified via the GST-tag. Equal amounts of protein, as determined by BCA assay, were applied for membrane lipid PIP strips to test lipid binding capacity for example to DAG (red frame). Bound proteins were detected via anti-GST antibody. **(A)** Purified proteins were suspended in PBS supplemented with 20 % glycerol and applied to membrane lipid PIP strips. The manufacturer's positive control was included as well as purified GST-tag serving as negative control (GST). **(B)** Recombinant proteins were suspended in PBS supplemented with 20 % glycerol and 100 µm $ZnCl_2$. Membrane lipid PIP strips for Y523D and Y523F are depicted. **(C)** Recombinant proteins were suspended in PBS 100 µm $ZnCl_2$. Membrane lipid PIP strips for Y523D and Y523F are depicted. **(A-C)** Background staining is in accordance with the method, specific lipid binding is detected by a strong signal at the respective lipid spot. Protein expression and purification was performed by Eliot Morrison and Annika Manns from the group of Prof. Christian Freund at the Free University of Berlin. Results from one out of two to three independent experiments are depicted.

2.3.3 Generation of CalDAG GEFI$^{-/-}$ Jurkat T cell clones and re-expression of CalDAG GEFI

Although the function of the differential phosphorylation of CalDAG GEFI at Y523 in Tregs and Tconv remains to be clarified, the general role of this GEF in T cells is of interest. CRISPR/Cas9 technology was utilized to generate CalDAG GEFI$^{-/-}$ Jurkat T cells in order to address the functional implementation of

CalDAG GEFI in T cells. Single guide RNAs (sgRNAs) to target the first exon of human CalDAG GEFI were generated employing the online tool http://crispr.mit.edu/ (Zhang Lab, MIT, 2015), and oligo nucleotides were cloned into the expression vector pX458, which additionally drives transient expression of Cas9 protein and green fluorescent protein (GFP) as reporter. Jurkat wild type cells of the clone JE6 were transfected and single cells were sorted according to GFP expression 48 h after nucleofection into 96-well plates **(Fig. 10A)**. All growing clones were expanded and tested for expression of CalDAG GEFI via Western Blot approximately four weeks after single cell sorting. Importantly, CalDAG GEFI expression was massively reduced in cells from clone 1E8 as compared to wild type cells and was completely absent three weeks later. However, 15 weeks after single cell sorting, CalDAG GEFI expression recurred, which was either due to inappropriate single cell sorting or spontaneous mutation **(Fig. 10B, upper panel)**. Therefore, a second round of single cell sorting was applied to “clone” 1E8 and two descendants, referred to as clone #1 and #2, were expanded and proved to have no detectable expression of CalDAG GEFI even 24 weeks after single cell sorting. Sequencing of the genomic DNA adjacent to the binding site of the employed sgRNA confirmed a partial deletion within exon 1 of CalDAG GEFI for clone #1 and #2. All following experiments employing Jurkat T cells were performed with JE6 as wild type control and the two CalDAG GEFI$^{-/-}$ clones #1 and #2.

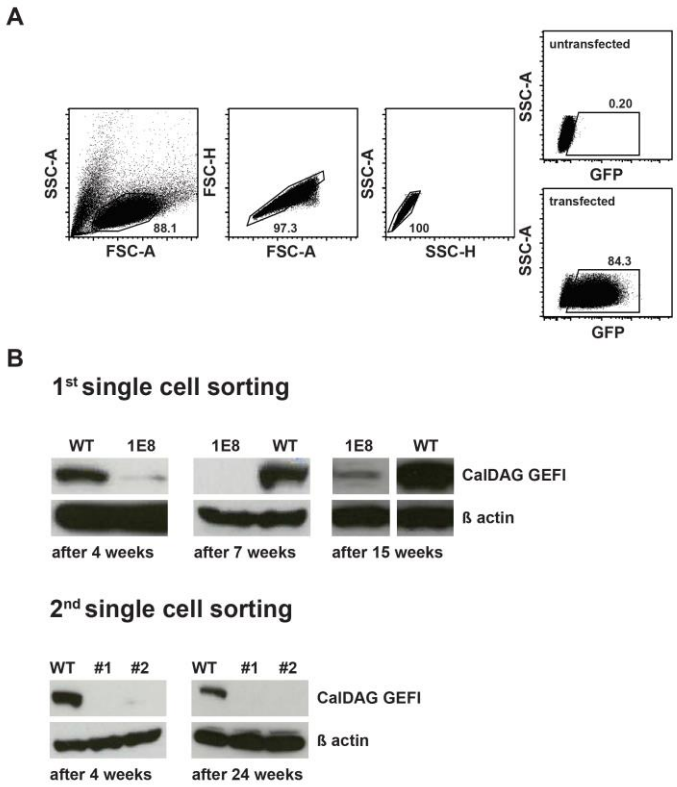

Fig. 10: Generation of CalDAG GEFI$^{-/-}$ Jurkat T cell clones by CRISPR/Cas9 technology. Wild type Jurkat T cells were transiently electroporated with an expression vector containing a human CalDAG GEFI-targeting sgRNA, and coding sequence for Cas9 protein and a GFP reporter. 48 h after transfection, single cells were sorted into 96-well round bottom plates. Expression of CalDAG GEFI was tested via Western Blotting. **(A)** Gating strategy for the single cell sorting of transfected Jurkat T cells. Cell debris and doublets were excluded according to scatter properties of the cells and GFP$^+$ cells were sorted. Untransfected cells (upper histogram) were used to set the GFP gate. Numbers in plots represent cell frequencies in respective gates. **(B)** Western Blot analysis of the clone 1E8 after the first round of single cell sorting (upper panel). First analysis was performed four weeks after single cell sorting and repeated seven and 15 weeks after single cell sorting. Second round of single cell sorting and analysis of CalDAD GEFI expression via Western Blot for clone #1 and clone #2. Expression analyses four weeks and 24 weeks after single cell sorting are depicted (lower panel). Wild type (WT) cells served as positive control and β-actin was used as loading control.

As a proof of principle, wild type CalDAG GEFI was re-expressed in both CalDAG GEFI$^{-/-}$ Jurkat T cell clones by lentiviral transduction. The employed lentiviral vector enabled tracking of transduction efficiency by expression of a GFP reporter. Approximately 80 % of the transduced cells were GFP$^+$ 72 h after transduction **(Fig. 11A)**, and effective re-expression of the CalDAG GEFI protein was confirmed by Western Blot analysis of empty vector control and CalDAG GEFI transduced Jurkat T cells as well as untransduced control cells. Expectedly, CalDAG GEFI

expression driven by the SFFV promoter provided by the lentiviral expression vector was strongly elevated in transduced cells as compared to WT **(Fig. 11B)**.

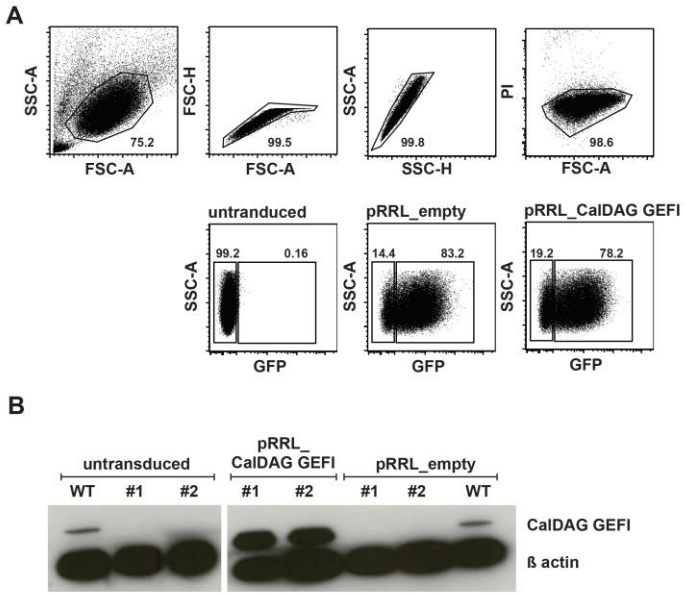

Fig. 11: Re-expression of CalDAG GEFI in CalDAG GEFI$^{-/-}$ Jurkat T cell clones. CalDAG GEFI was re-expressed in CalDAG GEFI$^{-/-}$ Jurkat T cell clones by lentiviral transduction using a vector providing a GFP reporter for the determination of transduction efficiency. **(A)** Exemplary gating strategy for the analysis of transduction efficiency via flow cytometry. Cell debris and doublets were excluded according to scatter properties of the cells and dead cells were identified by propidium iodide (PI) staining (upper panel). GFP^{+} cells were gated according to the signal of GFP^{-} untransduced cells (lower panel). **(B)** Western Blot analysis for CalDAG GEFI expression of untransduced and transduced WT Jurkat T cells, as well as clone #1 and #2. Equal amounts of loaded protein were determined by β-actin detection. Data are representative of three independent experiments.

2.3.4 CalDAG GEFI$^{-/-}$ Jurkat T cells show deficits in adhesion but retain chemotactic behavior

It was reported before that overexpression of CalDAG GEFI in Jurkat T cells results in enhanced adhesion, whereas chemokine-activated Jurkat T cells show deficits in adhesion to ICAM-1 following siRNA-mediated silencing of CalDAG GEFI expression [249]. Hence, β_1 integrin-mediated adhesion to fibronectin and β_2 integrin-dependent adhesion to ICAM-1 of CalDAG GEFI$^{-/-}$ Jurkat T cell clones was analyzed in collaboration with Dr. Stefanie Kliche from Otto-von-Guericke University of Magdeburg. Untransduced WT Jurkat T cells and CalDAG GEFI$^{-/-}$ clones #1 and #2 were tested, as well as empty or CalDAG GEFI-containing vector transduced

cells. In adhesion assays, cells were kept unstimulated or were treated with $MnCl_2$ to induce high-affinity conformation of integrins serving as positive control [201]. Expectedly, all tested cells show comparable levels of basic adhesion without any stimulation and strong adhesion to fibronectin and ICAM-1 upon $MnCl_2$ treatment **(Fig. 12A and B, left and second from left)**. TCR stimulation leads to activation of integrins by conformational changes resulting in high ligand affinity, whereas PMA induces clustering of integrins with low and intermediate ligand affinity and promotes cell adhesion by increased avidity [254]. Subsequent to TCR triggering via anti-CD3, both CalDAG GEFI$^{-/-}$ clones displayed significantly reduced adhesion to both fibronectin and ICAM-1. Binding was not affected by transduction with empty vector control but could be completely rescued by re-expression of CalDAG GEFI **(Fig. 12A and B, second from right)**. Therefore, CalDAG GEFI is needed for affinity regulation of β_1 as well as β_2 integrins. Interestingly, also PMA-induced adhesion was affected by CalDAG GEFI deficiency, although CalDAG GEFI itself is most likely not responsive to PMA, as was shown by the membrane lipid PIP strips. However, after PMA treatment both CalDAG GEFI$^{-/-}$ clones displayed significantly reduced adhesion to fibronectin as well as to ICAM-1, which was not affected by lentiviral transduction with empty vector control **(Fig. 12A and B, right)**. While β_1 integrin-dependent adhesion to fibronectin could be fully restored by CalDAG GEFI re-expression, this was not the case for cell adhesion to ICAM-1. In conclusion, CalDAG GEFI plays a role in avidity-induced cell adhesion to β_1 integrins, but whether this also applies to β_2 integrin-dependent cell adhesion remains unclear. In general, CalDAG GEFI is required in Jurkat T cells to induced cell adhesion, however, other molecules can partly rescue CalDAG GEFI deficiency as CalDAG GEFI$^{-/-}$ clones did not fully abrogate adhesion to fibronectin and ICAM-1.

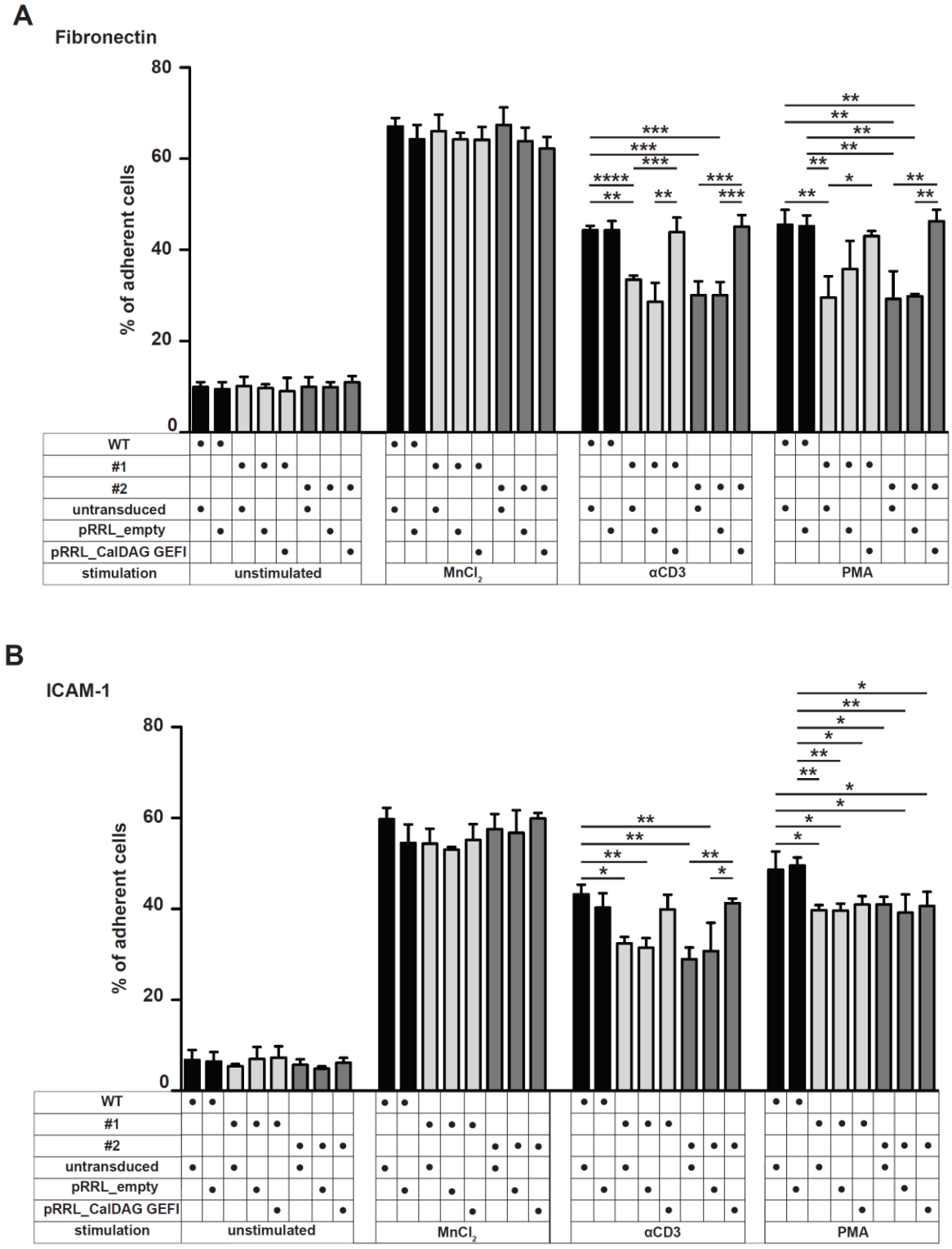

Fig. 12: Cell adhesion to fibronectin and ICAM-1 of wild type and CalDAG GEFI$^{-/-}$ Jurkat T cell clones. Adhesion properties of wild type Jurkat T cells (WT) and CalDAG GEFI$^{-/-}$ Jurkat T cell clones (#1 and #2) to **(A)** fibronectin or **(B)** ICAM-1 coated cell culture dishes were tested without stimulation (left) and following stimulation via divalent cations ($MnCl_2$, second from left), TCR ligation (αCD3, second from right) or phorbol ester treatment (PMA, right). Cells were untransduced, empty vector (pRRL_empty) or CalDAG GEFI-containing vector (pRRL_CalDAG GEFI) transduced. Frequency of

adherent cells was determined by counting after removal of unbound cells and calculated as % of input cells. Mean±SD of three independent experiments is shown. Adhesion experiments were performed by Dr. Stefanie Kliche (OvGU, Magdeburg).

Deficiency in CalDAG GEFI was shown to cause reduced migration of neutrophils [243]. As adhesion properties of the CalDAG GEFI$^{-/-}$ Jurkat T cell clones were impaired, also chemotactic functionality could be altered by CalDAG GEFI deficiency. As expected, all examined Jurkat T cells, WT and CalDAG GEFI$^{-/-}$ clones, either untransduced or transduced, showed random migration in the absence of a chemoattractant **(Fig. 13, left part)**. Upon addition of stroma-cell-derived factor-1 (SDF-1α), both WT cells and CalDAG GEFI$^{-/-}$ clones migrated towards the chemoattractant. In line, transduction and re-expression of CalDAG GEFI had no significant influence on chemotaxis of the cells. Although for clone #1, the number of migrated cells tended to result in reduced chemotaxis, this slight difference did not reach significance and was not affected by CalDAG GEFI re-expression **(Fig. 13)**. Thus, in the tested experimental setup, which was done in close cooperation with Dr. Stefanie Kliche from Otto-von-Guericke University of Magdeburg, CalDAG GEFI deficiency had no impact on migration of Jurkat T cells towards the chemoattractant SDF-1α.

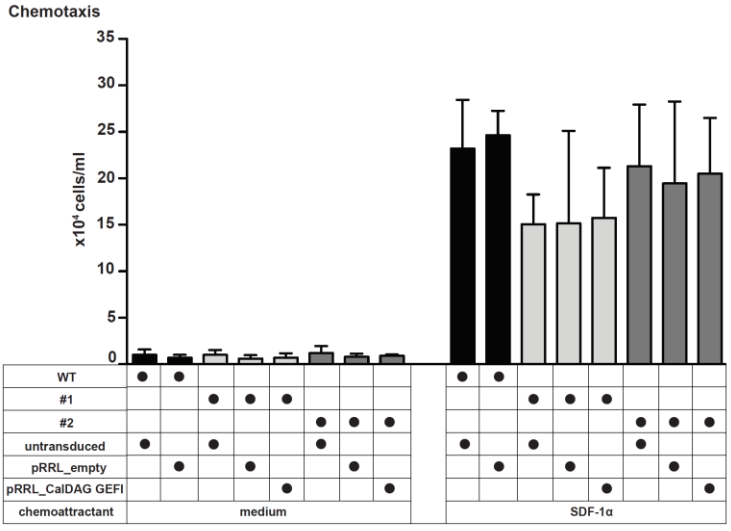

Fig. 13: Chemotactic behavior of wild type and CalDAG GEFI$^{-/-}$ Jurkat T cells. Wild type Jurkat T cells (WT) and CalDAG GEFI$^{-/-}$ Jurkat T cell clones (#1 and #2), untransduced, empty vector (pRRL_empty) or CalDAG GEFI-containing vector (pRRL_CalDAG GEFI) transduced, were tested for migration without chemoattractant (medium, left) or towards SDF-1α (right) using fibronectin-coated

transwells. The number of migrated cells was determined by counting. Mean±SD of five independent experiments is shown. Migration experiments were performed by Dr. Stefanie Kliche (OvGU, Magdeburg).

In order to exclude that the reported variations in adhesion of the CalDAG GEFI$^{-/-}$ clones were based on altered expression of important surface molecules, clones #1 and #2 were characterized for expression levels of CD3, CD11a and CXCR4 via flow cytometry. Untransduced WT and CalDAG GEFI$^{-/-}$ clones #1 and #2 were tested, as well as empty vector or CalDAG GEFI-containing vector transduced cells. In terms of frequencies, no major differences were observed regarding the expression of all three examined markers **(Fig. 14A and B)**. Therefore, the fold change of the Geomean was assessed to compare expression levels of CD3, CD11a and CXCR4. For CD3 and CXCR4 the Geomean confirmed equal expression levels on untransduced and transduced cells **(Fig. 14C and E)**. However, CD11a expression was significantly reduced on clone #1 and, the phenotype of reduced CD11a expression was not influenced by re-expression of CalDAG GEFI, indicating a clone-specific feature **(Fig. 14D)**.

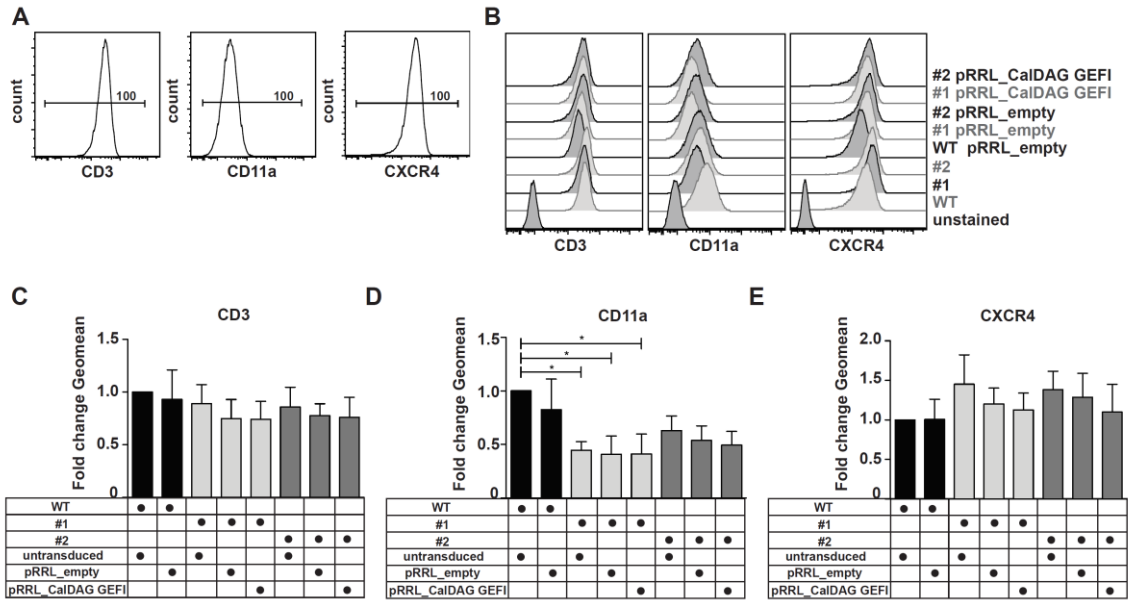

Fig. 14: Surface expression of CD3, CD11a and CXCR4 by wild type and CalDAG GEFI$^{-/-}$ Jurkat T cells. Surface expression of CD3, CD11a and CXCR4 on wild type Jurkat T cells (WT) as compared to CalDAG GEFI$^{-/-}$ Jurkat T cell clones was analyzed via flow cytometry. Empty vector (pRRL_empty), CalDAG GEFI-containing vector (pRRL_CalDAG GEFI) or untransduced cells were subjected to extracellular staining. **(A)** Cells were gated as depicted in Fig. 11A and subsequently untransduced cells and transduced GFP^{+} were analyzed. Exemplary histogram plots for pRRL_CalDAG GEFI

transduced Jurkat T cells of clone #1 are depicted. The Geomean of the signal of the respective marker was determined for the whole GFP^- (if untransduced) or GFP^+ (if transduced) cell population. Numbers in exemplary histogram plots represent population frequencies of the respective gates. **(B)** Exemplary histogram overlays of the indicated Jurkat T cells for CD3 (left), CD11a (middle) and CXCR4 (right). **(C-E)** Fold change of the Geomean of **(C)** CD3, **(D)** CD11a and **(E)** CXCR4 normalized to Geomean of untransduced WT Jurkat T cells is depicted for WT and CalDAG GEFI$^{-/-}$ Jurkat T cell clones (#1 and #2), untransduced, empty vector (pRRL_empty) or CalDAG GEFI-containing vector (pRRL_CalDAG GEFI) transduced. Mean±SD is depicted and data are pooled from, respectively representative of, five independent experiments.

2.3.5 T cell compartment is unaltered in CalDAG GEFI$^{-/-}$ mice

As CalDAG GEFI expression was not reported in murine T cells until now, the T cell compartment of CalDAG GEFI$^{-/-}$ mice was not yet characterized in detail [237]. To examine T cell development, thymi from CalDAG GEFI$^{+/+}$, CalDAG GEFI$^{+/-}$ and CalDAG GEFI$^{-/-}$ mice were isolated and single cell suspensions were analyzed by flow cytometry. Alive, single lymphocytes were gated and frequencies of $CD4^-CD8^-$ double negative (DN), $CD4^+CD8^+$ double positive (DP) as well as $CD4^+$ and $CD8^+$ single positive (CD4SP and CD8SP, respectively) cell populations appeared unaltered in CalDAG GEFI$^{+/+}$, CalDAG GEFI$^{+/-}$ and CalDAG GEFI$^{-/-}$ mice, and this also applied for $Foxp3^-$ and $Foxp3^+$ cells among CD4SP thymocytes **(Fig. 15A and B)**. Similarly, Treg precursors defined as $CD4^+CD25^+Foxp3^-$ or $CD4^+CD25^-Foxp3^+$ as well as $CD4^+CD25^+Foxp3^+$ Tregs and $CD4^+CD25^-Foxp3^-$ Tconv were found at expected frequencies **(Fig. 15A and C)**. Maturation of $Foxp3^-$ and $Foxp3^+$ CD4SP thymocytes was assessed through expression of the surface marker CD24, and no differences in maturation of the examined T cells subsets depending on CalDAG GEFI expression were observed **(Fig. 15A and D)**. Furthermore, absolute numbers of different thymic T cells populations were unaffected by CalDAG GEFI deficiency **(Suppl. Fig. 1)**, indicating that CalDAG GEFI is not affecting thymic T cell development.

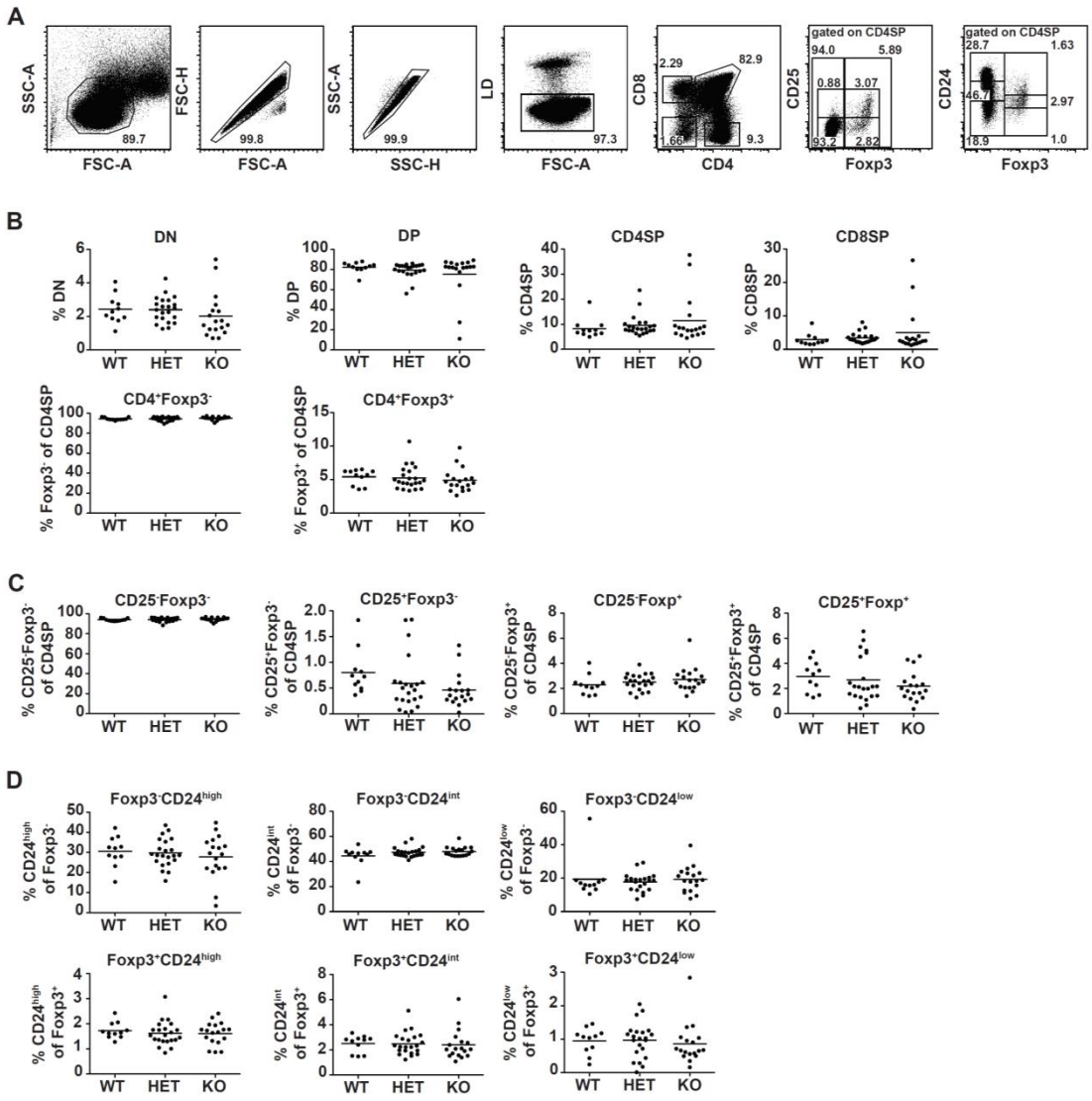

Fig. 15: Flow cytometric analysis of the thymic T cell compartment from CalDAG GEFI$^{+/+}$, CalDAG GEFI$^{+/-}$and CalDAG GEFI$^{-/-}$ mice. Single cell suspension from thymi from CalDAG GEFI$^{+/+}$ (WT) CalDAG GEFI$^{+/-}$ (HET) and CalDAG GEFI$^{-/-}$ (KO) mice were analyzed for the indicated markers. **(A)** Exemplary gating strategy is depicted. Alive, single lymphocytes were gated on CD4^{-}CD8^{-} (DN), CD4^{+}CD8^{+} (DP), CD4^{+}CD8^{-} (CD4SP) and CD4^{-}CD8^{+} (CD8SP). Amongst CD4SP it was further gated on CD25^{-}Foxp3^{-}, CD25^{-}Foxp3^{+}, CD25^{+}Foxp3^{-} and CD25^{+}Foxp3^{+} cells. Furthermore, CD24^{high}, CD24^{int} and CD24^{low} subsets amongst CD4^{+}Foxp3^{-} and CD4^{+}Foxp3^{+} cells were gated. Numbers in dot plots represent cell frequencies in respective gates. **(B-D)** Scatter plots summarize frequencies of the indicated cell population from WT, HET and KO mice: For **(B)** general T cell development including CD4 and CD8 (upper panel) and Foxp3^{-} and Foxp3^{+} amongst CD4SP thymocytes (lower panel), **(C)** CD25^{-}Foxp3^{-} Tconv, two Treg precursor subsets (CD25^{+}Foxp3^{-} and CD25^{-}Foxp3^{+}) and double positive Tregs (CD25^{+}Foxp3^{+}), as well as **(D)** maturation stages according to CD24 expression (CD24^{high}, CD24^{int} and CD24^{low}) amongst Foxp3^{-} (upper panel) and Foxp3^{+} CD4SP thymocytes (lower panel). Mean of each group is depicted and each data point in scatter plots represents an individual mouse (n=11-22 per group). Data are pooled from ten independently performed experiments.

Peripheral T cell homeostasis was assessed in single cell suspensions from pooled spleen and LNs. No alterations between CalDAG GEFI$^{+/+}$, CalDAG GEFI$^{+/-}$ and CalDAG GEFI$^{-/-}$ mice regarding population frequency and absolute numbers of total CD3$^+$ as well as CD4$^+$ and CD8$^+$ subsets amongst CD3$^+$ cells were detected. In line with these findings, amongst CD3$^+$CD4$^+$ cells, CD62L^{high} Tnaive, Foxp3$^-$ Tconv and Foxp3$^+$ Tregs, as well as Nrp1$^+$ cells amongst Tregs were observed at equal frequencies and absolute numbers in all genotypes tested **(Fig. 16A, B and Suppl. Fig. 2)**. As expected for homeostatic conditions, CD25 was nearly exclusively detectable on CD3$^+$CD4$^+$Foxp3$^+$ cells **(Fig. 16A)**. In conclusion, CalDAG GEFI$^{-/-}$ mice do not show any aberrations within the T cell compartment in SLOs under steady state conditions.

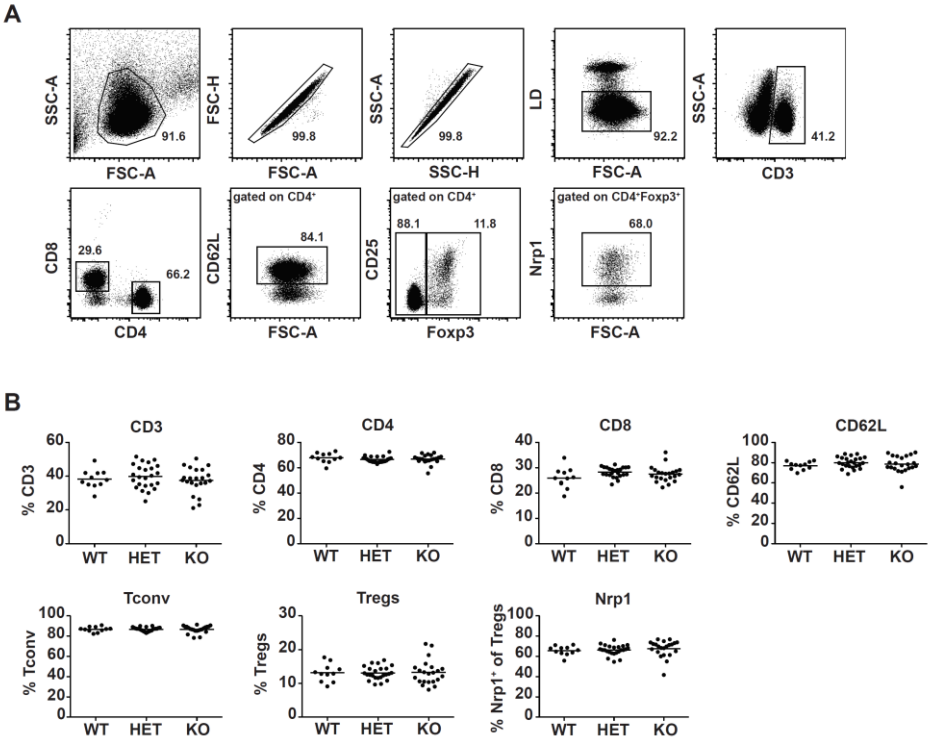

Fig. 16: Flow cytometric analysis of the T cell compartment from SLOs from CalDAG GEFI$^{+/+}$, CalDAG GEFI$^{+/-}$and CalDAG GEFI$^{-/-}$ mice. Single cell suspension from pooled spleen and LNs from CalDAG GEFI$^{+/+}$ (WT) CalDAG GEFI$^{+/-}$ (HET) and CalDAG GEFI$^{-/-}$ (KO) mice were analyzed. **(A)** Exemplary gating strategy is depicted. Alive, single lymphocytes were gated on CD3$^+$ and CD4$^+$ cells and subsequently on CD62L$^+$ as well as Foxp3$^-$ Tconv and Foxp3$^+$ Tregs amongst CD3$^+$CD4$^+$, and Nrp1$^+$ cells amongst Tregs. Numbers in dot plots represent cell frequencies in respective gates. **(B)** Summarizing scatter plots of frequencies of the indicated cell population from WT, HET and KO mice. Mean of each group is depicted and each data point in scatter plots represents an individual mouse (n=11-24 per group). Data are pooled from ten independently performed experiments.

2.3.6 Signal transduction remains unaltered in CalDAG GEFI$^{-/-}$ T cells

Previous studies reported that over-expression of CalDAG GEFI in HEK293T cells results in reduced activation of Elk1 [216]. Thus, ERK1/2 phosphorylation might be altered in T cells from CalDAG GEFI$^{-/-}$ mice. To test this hypothesis, lymphocytes from pooled spleen and LNs from CalDAG GEFI$^{+/+}$ and CalDAG GEFI$^{-/-}$ mice were stained for CD4 and CD25 and stimulated via streptavidin-mediated crosslinking of biotinylated anti-CD3/28 as described above, to determine phosphorylation of ERK1/2 over time. First, expression levels of total ERK1/2 in Tconv and Tregs from CalDAG GEFI$^{+/+}$, CalDAG GEFI$^{+/-}$ and CalDAG GEFI$^{-/-}$ mice were determined via intracellular flow cytometry. As depicted in Figure 17A, 100 % of Tconv and Tregs were ERK1/2^{+} and also in terms of Geomean, no variations were detectable. For pERK1/2 kinetics, pERK1/2^{+} cells were set according to the basal pERK1/2^{+} frequency at 0 min of stimulation before addition of streptavidin for Foxp3^{-} Tconv and Foxp3^{+} Tregs. Staining with the appropriate isotype control did not result in detectable background signals at any analyzed time point **(Fig. 17B)**. Consistent with literature, generally lower frequencies of pERK1/2^{+} Tregs were observed as compared to Tconv **(Fig. 17C)** [156]. In contrast to the aforementioned hypothesis, no differences were observed regarding pERK1/2^{+} Tregs or Tconv from CalDAG GEFI$^{+/+}$ versus CalDAG GEFI$^{-/-}$ mice. Although for Tconv a trend for elevated frequencies of pERK1/2^{+} cells from CalDAG GEFI$^{+/+}$ mice was detected, this difference did not reach statistical significance and additionally was not applicable for Tregs **(Fig. 17C)**. In conclusion, ERK1/2 activation in primary murine T cells is not affected by CalDAG GEFI deficiency.

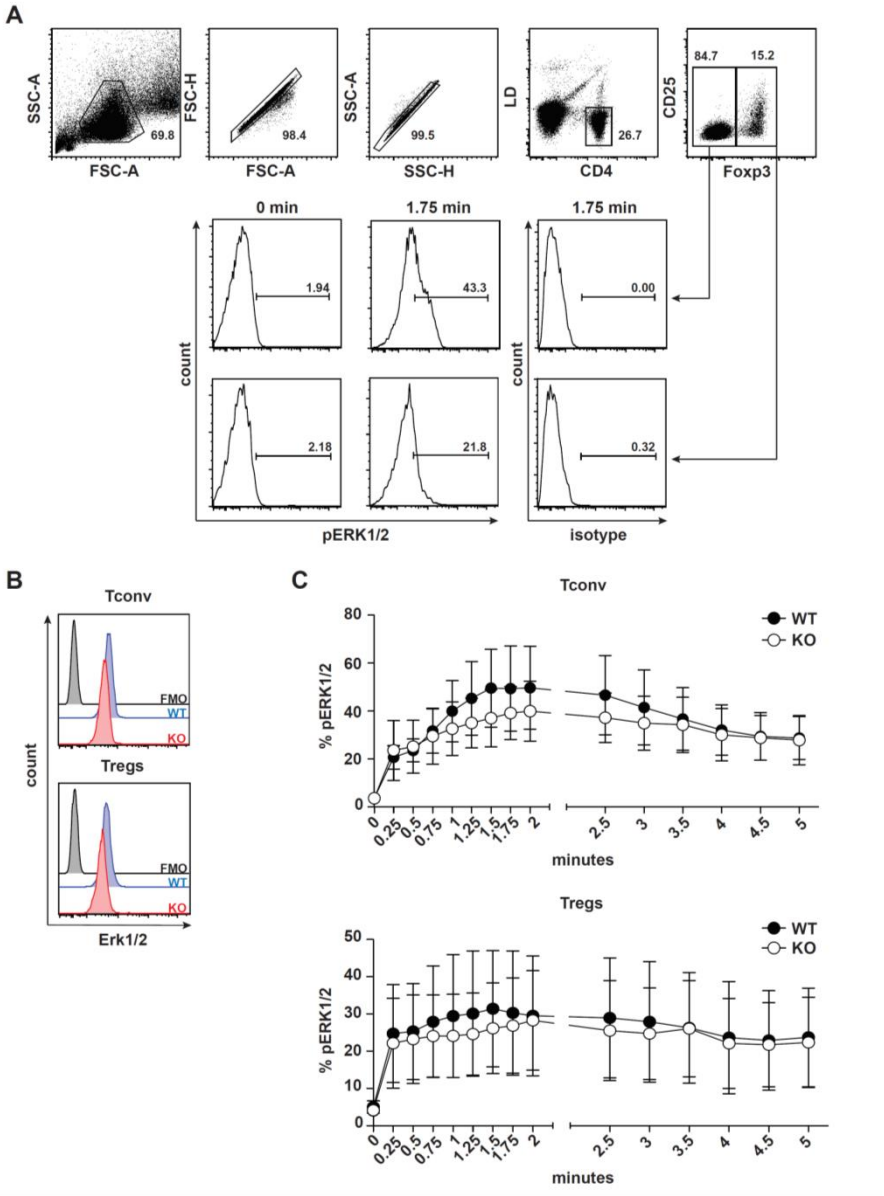

Fig. 17: Phospho-flow cytometry for pERK1/2 pT202/pY204 in Tregs and Tconv from CalDAG GEFI$^{+/+}$ and CalDAG GEFI$^{-/-}$ mice. Single cell suspensions from pooled spleen and LNs from CalDAG GEFI$^{+/+}$ (WT) and CalDAG GEFI$^{-/-}$ (KO) mice were stained for CD4 and stimulated via streptavidin-mediated crosslinking of biotinylated anti-CD3/28 antibodies. Cells were fixed at indicated time points and intracellularly stained for total ERK1/2, pERK1/2 pT202/pY204 and Foxp3. **(A)** Exemplary gating strategy depicts alive, single CD4^{+} lymphocytes of a WT mouse gated Tconv and Tregs according to Foxp3 expression (middle panel and lower panel, respectively). Gates for determination of pERK1/2^{+} cells were set according to 0 min stimulation control (middle and lower panel, left) and exemplary histogram plots depict 1.75 min of anti-CD3/28 crosslinking for pERK1/2 (middle and lower panel, center) and isotype control (middle and lower panel, right). **(B)** Gating was performed as described in **(A)** to determine total ERK1/2 expression in WT (blue) and KO (red) Tconv (upper panel) and Tregs (lower panel) with FMO (black) serving as staining control. **(C)** Summarizing kinetic of ERK1/2 phosphorylation in Tconv (upper panel) and Tregs (lower panel) from WT (closed circles) and KO (open circles) mice. Data are pooled from, respectively representative of, five independent experiments, mean±SD is depicted (n=10 mice per group).

In order to assess phosphorylation-dependent signal transduction processes globally, $CD4^+$ T cells from pooled spleen and LNs from CalDAG GEFI$^{+/+}$, CalDAG GEFI$^{+/-}$ and CalDAG GEFI$^{-/-}$ mice were MACS-enriched, stimulated and applied for total phosphotyrosine Western Blot analysis. As controls, cells were either kept on ice or incubated in medium at 37 °C for 5 minutes, whereas stimulation was carried out via streptavidin-mediated crosslinking of biotinylated anti-CD3/28, PMA/iono or pervanadate treatment for 5 minutes. As expected, nearly no phosphotyrosines were detectable from freshly *ex vivo* isolated $CD4^+$ T cells in both stimulation controls, whereas all applied stimulation conditions resulted in phosphorylation of tyrosine residues corresponding to the applied stimulus strength. However, no major differences were observed for $CD4^+$ T cells from CalDAG GEFI$^{+/+}$, CalDAG GEFI$^{+/-}$ and CalDAG GEFI$^{-/-}$ mice **(Fig. 18)**. In summary, global phosphorylation-dependent signal transduction processes and particularly ERK1/2 phosphorylation are not affected by loss of CalDAG GEFI in primary murine $CD4^+$ T cells.

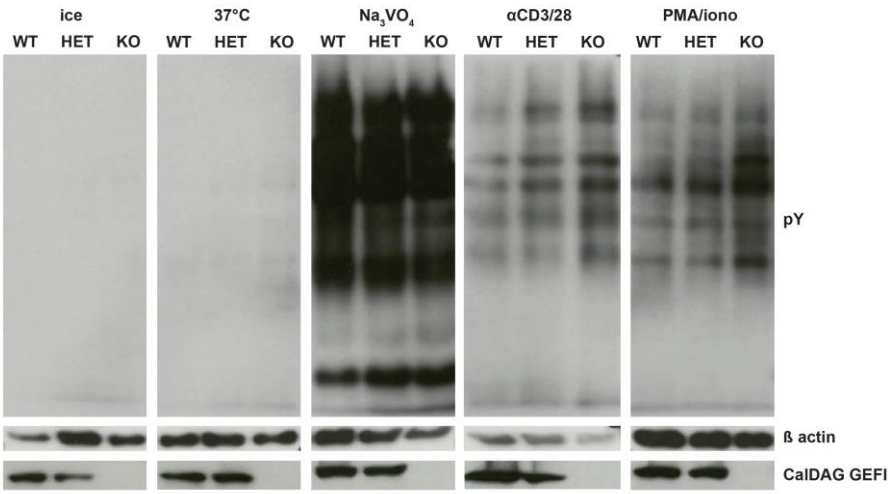

Fig. 18: Phospho-tyrosine analysis of $CD4^+$ T cells from CalDAG GEFI$^{+/+}$, CalDAG GEFI$^{+/-}$ and CalDAG GEFI$^{-/-}$ mice. $CD4^+$ T cells from pooled spleen and LNs from CalDAG GEFI$^{+/+}$ (WT), CalDAG GEFI$^{+/-}$ (HET) and CalDAG GEFI$^{-/-}$ (KO) mice were MACS-enriched and were either kept unstimulated on ice (left) or were incubated for 5 min at 37 °C (second from left) in cRPMI as negative controls. For stimulation, part of the cells were treated with sodium pervanadate (Na_3VO_4, middle), stimulated via streptavidin-mediated crosslinking of anti-CD3/28 (αCD3/28, second from right) or treated with PMA/iono (right) for 5 min at 37 °C. Subsequently, cell were lysed and total tyrosine phosphorylation (pY) was assessed via Western Blotting, with β-actin serving as loading control and detection of CalDAG GEFI as genotype control of the employed mice. Data depicted are representative of three independent experiments.

2.3.7 CalDAG GEFI$^{-/-}$ Tregs are fully functional *in vitro*

As CalDAG GEFI is differentially phosphorylated in Tregs versus Tconv, functional properties of CalDAG GEFI$^{-/-}$ Tregs were examined. *Ex vivo* isolated lymphocytes from pooled spleen and LNs of CalDAG GEFI$^{+/+}$, CalDAG GEFI$^{+/-}$ and CalDAG GEFI$^{-/-}$ mice were MACS-enriched for CD4^{+} T cells, FACS-sorted as CD4^{+}CD25^{+} Tregs and pre-activated for 72 h on plate bound anti-CD3/28 antibodies in presence of IL-2. FACS-sorted and CTV-labeled CD4^{+}CD25^{-}CD62L^{high} Tnaive were co-cultured at different ratios with pre-activated CD4^{+}CD25^{+} Tregs with T activator beads as stimulus. After four days, cells were analyzed by flow cytometry. First, the *in vitro* suppressive capacity of CalDAG GEFI$^{+/+}$, CalDAG GEFI$^{+/-}$ and CalDAG GEFI$^{-/-}$ Tregs was determined by quantification of the Geomean of CTV of the total Tnaive population **(Fig. 19A)**. Expectedly, Tnaive in absence of Tregs and T activator beads did not proliferate and sustained a high CTV signal, whereas Tnaive stimulated with T activator beads in the absence of Tregs divided and gave rise to up to five cell divisions. However, Tregs from CalDAG GEFI$^{+/+}$, CalDAG GEFI$^{+/-}$ and CalDAG GEFI$^{-/-}$ mice were equally able to suppress the proliferation of Tnaive corresponding to the ratio of co-cultured Tnaive:Tregs **(Fig. 19B and C)**. Second, the stability of Tregs was analyzed by intracellular Foxp3 staining, and frequencies of Foxp3^{+} cells amongst CD4^{+}CTV^{-} cells were determined **(Fig. 19A and D)**. Around 65 % of co-cultured Tregs from CalDAG GEFI$^{+/+}$, CalDAG GEFI$^{+/-}$ and CalDAG GEFI$^{-/-}$ mice retained stable Foxp3 expression **(Fig. 19D)**. In summary, these findings show that CalDAG GEFI expression is dispensable for suppressive capacity of Tregs *in vitro* and it is not critical for the maintenance of Foxp3 expression.

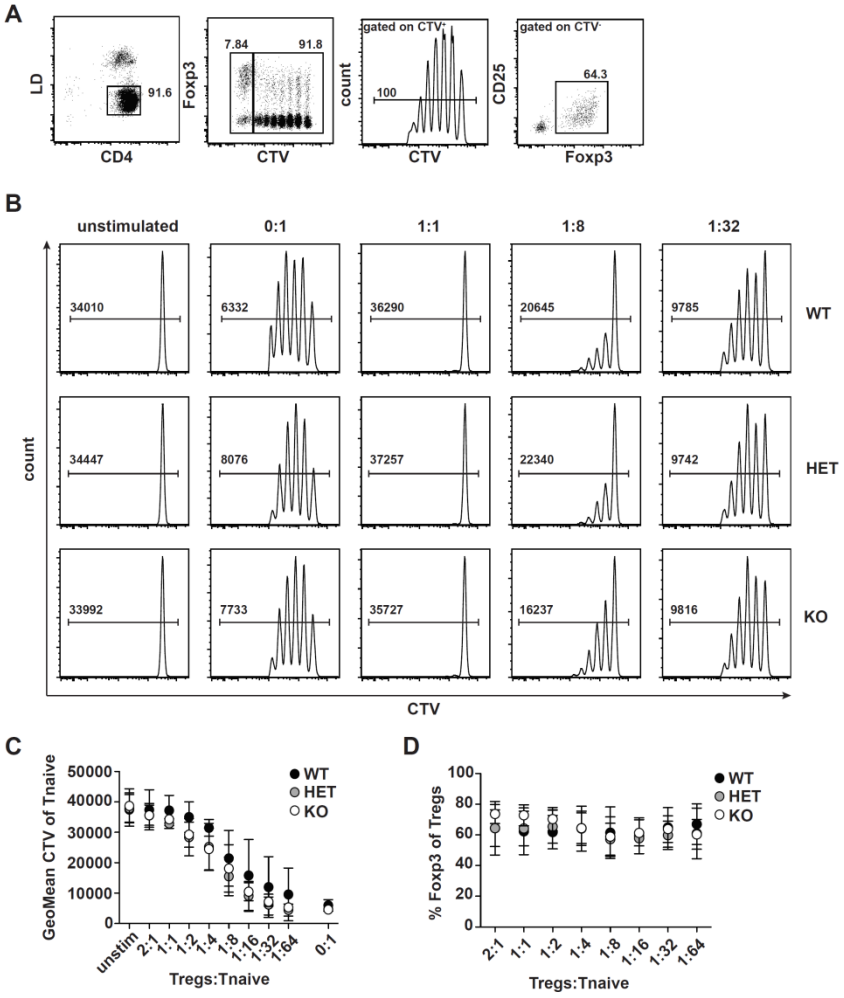

Fig. 19: *In vitro* suppression assay using Tregs from CalDAG GEFI$^{+/+}$, CalDAG GEFI$^{+/-}$ and CalDAG GEFI$^{-/-}$ mice. Tregs from CalDAG GEFI$^{+/+}$ (WT) CalDAG GEFI$^{+/-}$ (HET) and CalDAG GEFI$^{-/-}$ (KO) mice were FACS-sorted from pooled spleen and LNs as CD4^{+}CD25^{+} cells and pre-activated for 72 h on plate-bound anti-CD3/28. Freshly sorted and CTV-labeled Tnaive were co-cultured with pre-activated Tregs at indicated ratios and on day 4 proliferation-dependent CTV-dilution was analyzed via flow cytometry. **(A)** Exemplary gating strategy is depicted based on pregated lymphocyte singlets: Alive CD4^{+} T cells were gated as CTV^{-} Tregs and CTV^{+} Tnaive, to assess stability of Foxp3 expression in Tregs and to determine the Geomean of CTV of the total Tnaive population. **(B)** Exemplary histogram plots gated on Tnaive cells after four days co-culture with WT (top), HET (middle) and KO (bottom) Tregs at indicated ratios. Unstimulated Tnaive and Tnaive without addition of Tregs (0:1) served as controls. Numbers in gates represent Geomean of CTV of Tnaive. **(C)** Plot summarizes the Geomean of the CTV signal of Tnaive cells with or without co-cultured Tregs from WT (closed black circles), HET (closed gray circle) or KO (open circles) mice at indicated ratios. **(D)** Scatter plot summarizes the stability of Foxp3 expression within gated Tregs from WT (closed black circles), HET (closed gray circle) or KO (open circles) mice after four days co-culture with Tnaive at indicated ratios. Data are representative of three independent experiments and mean±SD is depicted.

2.3.8 CalDAG GEFI fine-tunes Treg suppressive ability *in vivo*

CalDAG GEFI$^{-/-}$ Tregs did not show any defect in the suppression of Tnaive proliferation *in vitro* under T activator bead stimulation. To address Treg suppressive capacity under more physiological conditions, CalDAG GEFI$^{-/-}$ Tregs were tested in an *in vivo* model of transfer colitis. Tregs were FACS-sorted as CD4^{+}CD25^{+} cells from pooled spleen and LNs from CalDAG GEFI$^{+/+}$ and CalDAG GEFI$^{-/-}$ mice, and co-transferred with CD4^{+}CD25^{-}CD62L^{high} Tnaive from CalDAG GEFI$^{+/+}$ mice at a ratio of 1:4 into Rag2$^{-/-}$ recipient mice via *intraperitoneal* injection. PBS-treated mice or mice receiving only Tnaive without Tregs served as controls. Body weight and general health status of recipient mice was monitored biweekly over ten weeks. Mice that lost >20 % of initial body weight were sacrificed. As expected, PBS recipients gained weight continuously, whereas Tnaive recipients started to lose body weight rapidly upon seven weeks after adoptive transfer. Mice receiving Tnaive together with Tregs also moderately lost weight from seven weeks onward, but did not show significant differences with respect to the source of Tregs **(Fig. 20A)**. Endpoint analyses of the experiment included a histological examination and measurement of colon length, weight and cellularity of spleen as well as flow cytometric analyses of the T cell compartment of spleen, mesenteric and peripheral LN (mLN and pLN, respectively). No variations between the two treatment groups were detected regarding colon length, spleen weight and organ cellularity **(Fig. 20B, C and D)**. Histological scores of Tnaive recipients were drastically elevated in comparison to PBS recipients, whereas Tnaive plus Treg recipient scores were intermediate to the two control groups indicating a partial suppression of colitis development under these conditions. A direct comparison of CalDAG GEFI$^{+/+}$ or CalDAG GEFI$^{-/-}$ Treg recipients did not show statistically significant differences. However, the histological score of CalDAG GEFI$^{-/-}$ Treg recipient mice was virtually identical to that of Tnaive recipients without addition of Tregs, whereas the score of CalDAG GEFI$^{+/+}$ Treg recipients scattered enormously and was also not significantly different from the score of the negative control **(Fig. 20E)**. Expectedly, exemplary photographs from H&E stained colon sections showed strong hyperplasia of the epithelium of all T cell recipients and transmural immigration of inflammatory cells, mainly lymphocytes **(Fig. 20F)**.

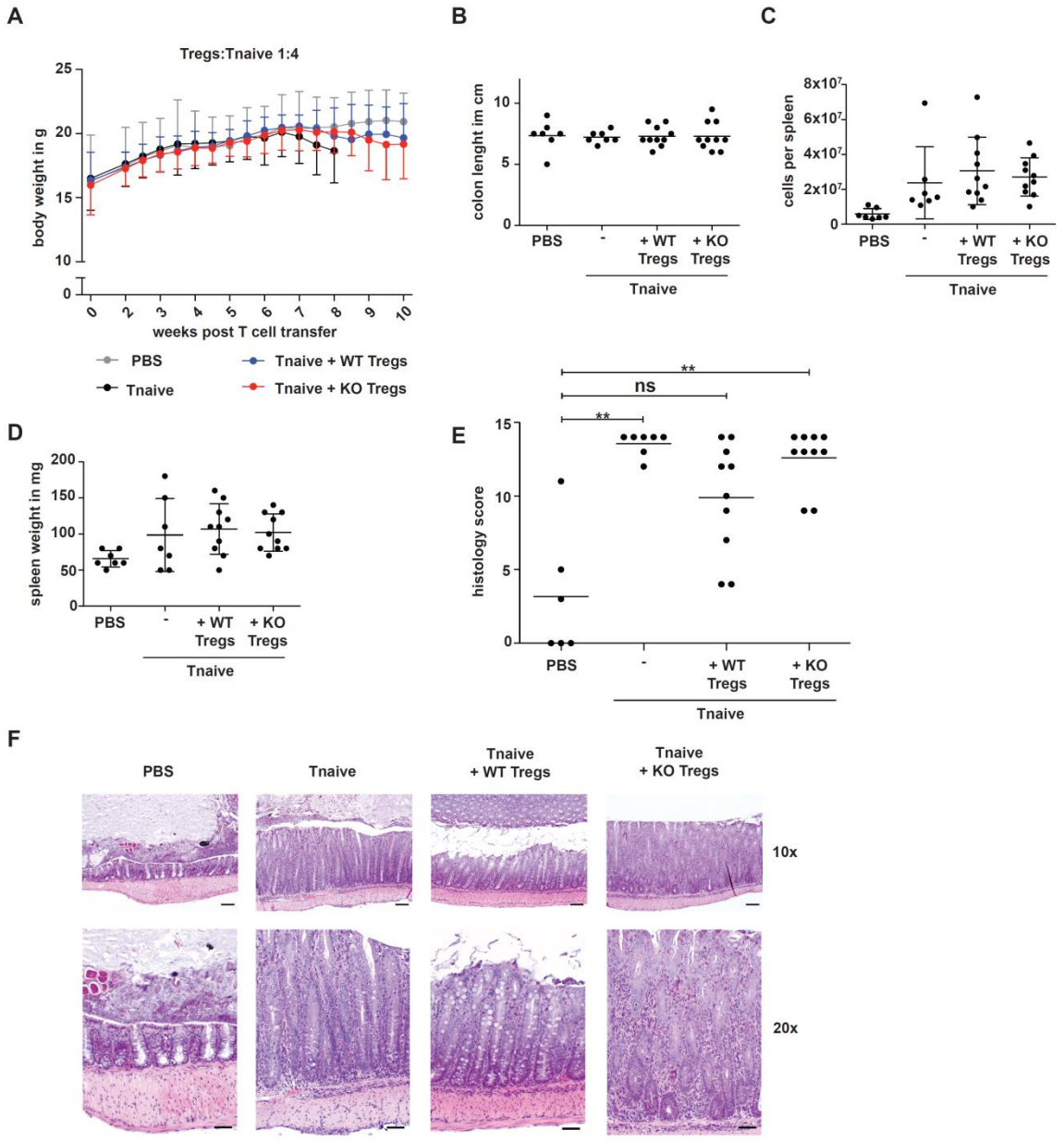

Fig. 20: *In vivo* suppression assay employing the transfer colitis model using Tregs:Tnaive at a ratio of 1:4. Tregs from pooled spleen and LNs from CalDAG GEFI$^{+/+}$ (WT) and CalDAG GEFI$^{-/-}$ (KO) mice were FACS-sorted as CD4^{+}CD25^{+} cells and co-transferred with CD4^{+}CD25^{-}CD62L^{high} Tnaive from CalDAG GEFI$^{+/+}$ mice at a ratio of 1:4 into Rag2$^{-/-}$ recipient mice via intraperitoneal injection. **(A)** Body weight of mice, which received PBS (grey), only Tnaive cells (black), Tnaive plus WT Tregs (blue) or Tnaive plus KO Tregs (red), was monitored biweekly up to ten weeks. Mean±SD is depicted. **(B)** Colon length was measured as inflammation readout as well as **(C)** weight and **(D)** cellularity of the spleen at the termination of the experiment. **(E)** Colons were analyzed via histology and scored according to severity of inflammation by Dr. Marina Pils (Mousepathology, HZI, Braunschweig). Scatter plot depicts the total histology scores with a maximum value of 16. **(F)** Exemplary photographs from H&E stained colon sections from PBS (left), Tnaive (second from left), Tnaive plus WT Tregs (second from right) or Tnaive plus KO Tregs (right) receiving mice at a magnification of 10x (upper panel) and 20x (lower panel). Scale bars represent 100 µm and 50 µm for the 10x and 20x magnification, respectively. Data are pooled from two independent experiments, scatter plots depict

mean of each group and each data point in scatter plots represents a single recipient mouse (n=6-10 mice per group).

Single cell suspensions from spleen, mLN and pLN were analyzed for frequencies and absolute numbers of $CD3^+$ and $CD3^+CD4^+$, $CD44^+CD62L^-$ memory T cells, $Foxp3^-$ Tconv, $Foxp3^+$ Tregs as well as $Foxp3^+CTLA\text{-}4^+$ and $Foxp3^+CD103^+$ amongst $CD3^+CD4^+$, and $CTLA\text{-}4^+CD103^+$ double positive amongst Tregs **(Fig. 21A)**. All examined populations appeared at comparable frequencies and absolute numbers in mice which received Tnaive in combination with either CalDAG GEFI$^{+/+}$ or CalDAG GEFI$^{-/-}$ Tregs **(Fig. 21B and Suppl. Fig. 3)**.

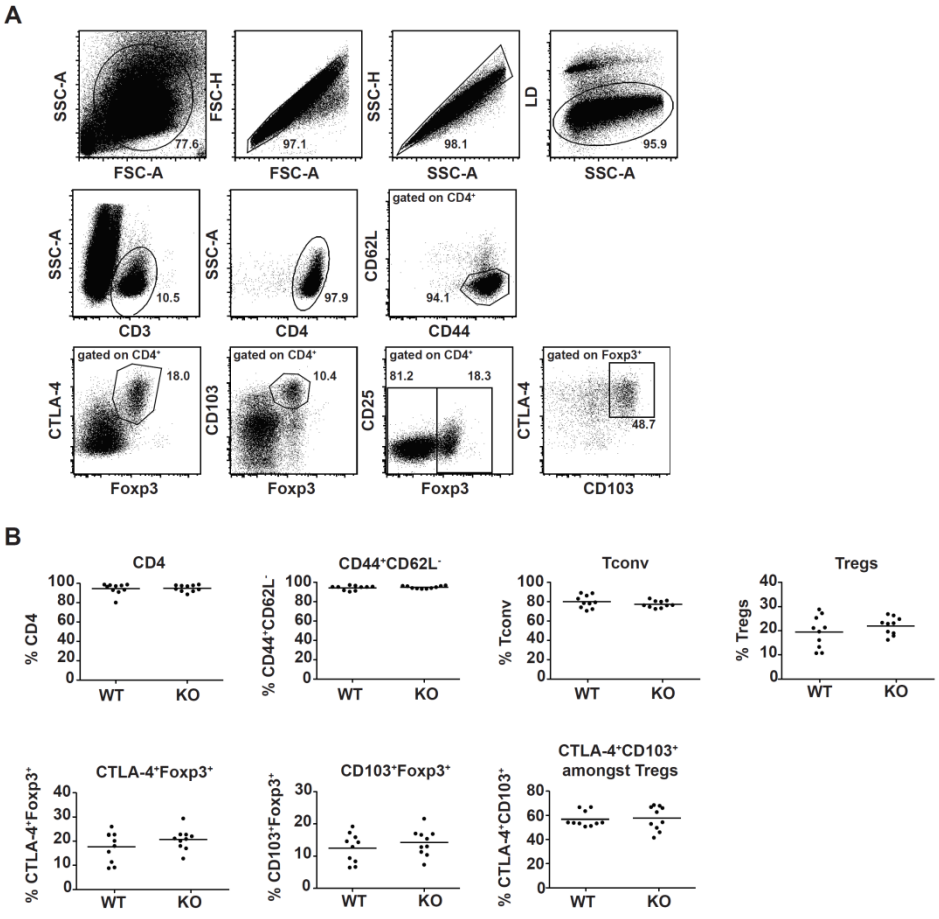

Fig. 21: Flow cytometric analysis of the splenic T cell compartment from transfer colitis experiments with Tregs:Tnaive at a ratio of 1:4. Analysis of the transfer colitis experiments included flow cytometry for the injected T cells from SLOs of Rag2$^{-/-}$ recipient mice transferred with Tnaive plus CalDAG GEFI$^{+/+}$ or plus CalDAG GEFI$^{-/-}$ Tregs. **(A)** Exemplary gating strategy for single cell suspensions from spleen. It was gated on living singlet lymphocytes and subsequently on $CD3^+$ and $CD4^+$ cells, which were analyzed for expression of Foxp3, CTLA-4, CD25 and CD103. **(B)** Scatter

plots summarize respective population frequencies of splenocytes from recipient mice transferred with Tnaive plus CalDAG GEFI$^{+/+}$ (WT) or plus CalDAG GEFI$^{-/-}$ (KO) Tregs. Data are representative of two independent experiments, mean of each group is depicted and each data point in scatter plots represents an individual mouse (n=10 mice per group).

To assess the impact of a higher proportion of Tregs on the development of colon inflammation, the ratio of injected Tnaive:Tregs was adjusted to 1:2 for the following experiments. Measurement of body weight revealed no significant differences between the two Treg-receiving groups **(Fig. 22A)**. For colon length, only a minor but expected reduction was detected for the Tnaive-receiving positive control while all other groups did not show differences **(Fig. 22B)**. This was in line with spleen cellularity and weight **(Fig. 22C and D)**. Injection of an increased number of Tregs resulted in a drop of the histology score of the CalDAG GEFI$^{-/-}$ Treg-receiving group, which now appeared largely identical to the CalDAG GEFI$^{+/+}$ Treg recipients, although still with considerable variance within the two Treg-receiving groups **(Fig. 22E)**.

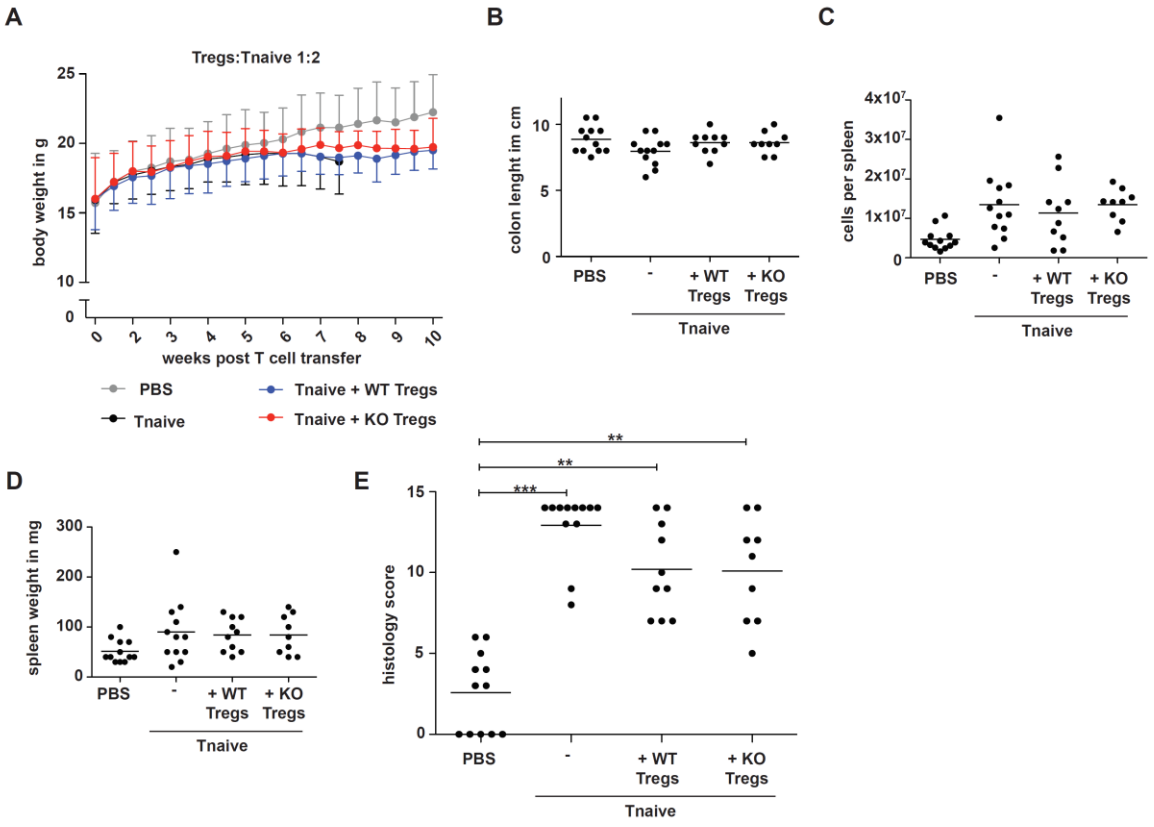

Fig. 22: *In vivo* suppression assay employing the transfer colitis model using Tregs:Tnaive at a ratio of 1:2. FACS-sorted $CD4^+CD25^+$ Tregs from pooled spleen and LNs from CalDAG $GEFI^{+/+}$ (WT) and CalDAG $GEFI^{-/-}$ (KO) mice were co-transferred with Tnaive, FACS-sorted as $CD4^+CD25^-CD62L^{high}$ from CalDAG $GEFI^{+/+}$ mice, at a ratio of 1:2 into $Rag2^{-/-}$ recipient mice via intraperitoneal injection. **(A)** Body weight of recipient mice, which received PBS (grey) as negative control, Tnaive cells (black) as positive control, Tnaive plus WT Tregs (blue) or Tnaive plus KO Tregs (red), was monitored biweekly over a maximum of ten weeks. Mean±SD is depicted. As inflammation readout at the termination of the experiment, **(B)** colon length was measured as well as **(C)** weight and **(D)** total cellularity of the spleen. **(E)** Histology scores according to severity of inflammation of colons were determined by Dr. Marina Pils (Mousepathology, HZI, Braunschweig). Scatter plot depicts the total histology scores with a maximum value of 16. Data are pooled from two independent experiments and each data point in scatter plots represents an individual recipient mouse (n=9-12 mice per group).

In line with histology scores, no differences were observed by flow cytometric analyses of the T cell compartment of spleen, mLN and pLN for the populations mentioned above **(Fig. 23 and data not shown)**.

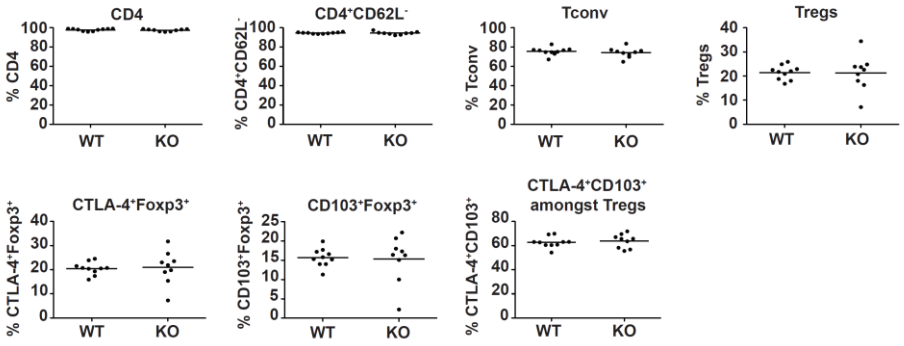

Fig. 23: Flow cytometric analysis of the splenic T cell compartment from transfer colitis experiments with Tregs:Tnaive at a ratio of 1:2. Injected T cells from spleen of $Rag2^{-/-}$ recipient mice transferred with Tnaive plus CalDAG $GEFI^{+/+}$ or plus CalDAG $GEFI^{-/-}$ Tregs were analyzed by flow cytometry for frequencies of $CD3^+$ and $CD4^+$ cells, and subsequently for expression of Foxp3, CTLA-4, CD25 and CD103. Gating was performed as shown in Fig. 21A. Scatter plots summarize respective population frequencies of splenocytes from recipient mice transferred with Tnaive plus CalDAG $GEFI^{+/+}$ (WT) or plus CalDAG $GEFI^{-/-}$ (KO) Tregs. Mean is depicted for each group and each dot in scatter plots represents an individual mouse (n=9-10 mice per group). Data are pooled from two independently performed experiments.

Additionally, small intestine lamina propria lymphocytes were isolated and analyzed via flow cytometry as introduced above. Regarding frequencies, again no significant differences were observed, although there were slight trends for elevated frequencies of $CD4^+$ T cells , memory T cells and all assessed Treg subsets for

CalDAG GEFI$^{-/-}$ Treg recipients as compared to CalDAG GEFI$^{+/+}$ Treg recipients **(Fig. 24A)**. In line with these findings, absolute numbers of all analyzed T cell populations were significantly increased in the CalDAG GEFI$^{-/-}$ Treg-receiving group **(Fig. 24B)**. In summary, CalDAG GEFI has a minor impact on Treg suppressive capacity *in vivo*, though this effect is only apparent at certain Tnaive:Treg ratios and can be overcome by sufficient Treg numbers.

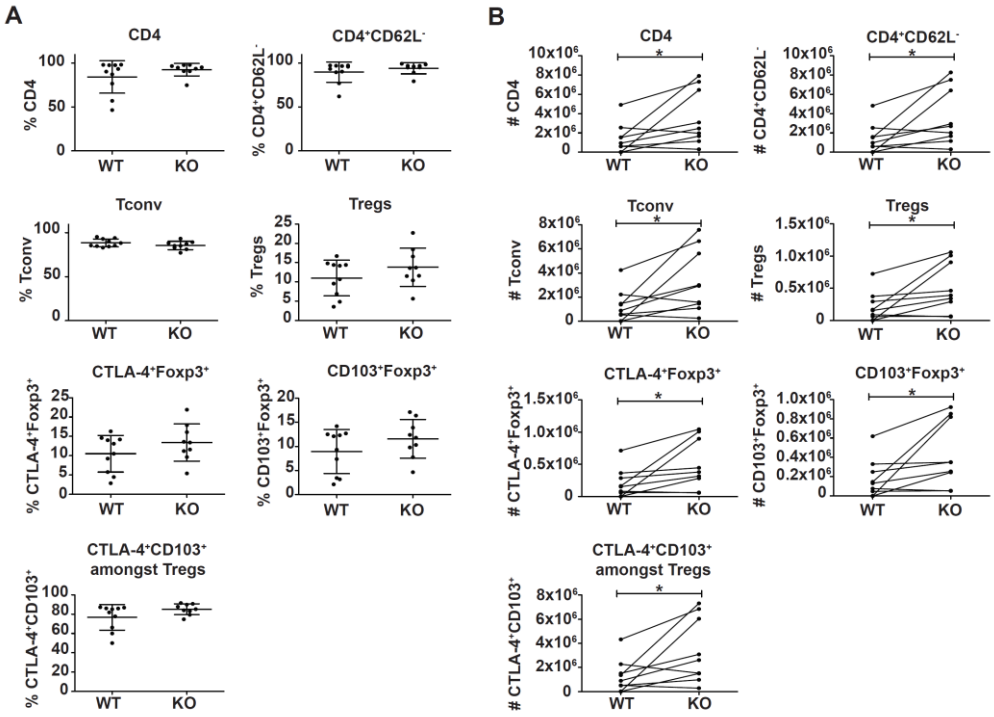

Fig. 24: Flow cytometric analysis of the T cell compartment of small intestinal lamina propria lymphocytes from transfer colitis experiments with Tregs:Tnaive at a ratio of 1:2. Lymphocytes were isolated from the small intestinal lamina propria of Rag2$^{-/-}$ recipient mice transferred with Tnaive plus CalDAG GEFI$^{+/+}$ or plus CalDAG GEFI$^{-/-}$ Tregs and analyzed via flow cytometry. Gating was performed as shown in Fig. 21A. **(A)** Scatter plots summarize indicated population frequencies of siLPLs from recipient mice transferred with Tnaive plus CalDAG GEFI$^{+/+}$ (WT) or plus CalDAG GEFI$^{-/-}$ (KO) Tregs. **(B)** Total cell count of isolated siLPLs was determined by using Accuri flow cytometer and absolute numbers of the indicated cell populations were calculated respective to their measured frequency. Mean of each group is depicted and each dot in scatter plots represents an individual mouse (n=9-10 mice per group). Data are pooled from two independent experiments.

3. Discussion

Tregs are in the spotlight of immunological research since nearly three decades and decent amount of data were collected regarding unique features and mechanisms of action of Tregs. Regarding health and disease, Tregs represent a double-edged sword as on the one side appropriate Treg function is needed to maintain self-tolerance and avoid e.g. autoimmunity and allergy, whereas on the other hand Tregs can have detrimental impact in the context of cancer or chronic infection [50-54]. Therefore, there is an urgent need to pinpoint unique proteins, signaling pathways and modes of action of Tregs to gather better understanding of this T cell subset and potentially find new targets that allow therapeutic manipulation in the one or the other direction. Only in recent years, it became evident that the protein inventory of Tregs and Tconv is predominantly comparable, and therefore, interest is switching towards identification of signaling processes which are uniquely used by Tregs and might allow for functional interference [129, 131, 132, 158-161]. “Big data” analyses from comparative screens of e.g. posttranslational modifications have permitted an educated guess for possible targets. Still it remains very demanding to unravel signaling peculiarities, especially because signal transduction pathways are usually not straight-lined but interconnected and interdependent, and current cutting edge techniques do not allow revealing these interconnections easily. However, as a fact, TCR signaling is an indispensable prerequisite for T cell function and the IS is a primary hub of TCR signal initiation. There is accumulating evidence that TCR signaling differs in Tregs and Tconv and therefore, the IS and TCR signaling serve a promising starting point to further unravel specialties of Tregs as compared to Tconv. In this study, the role of Themis and CalDAG GEFI on Treg function was examined, as both proteins represent promising candidates that might contribute to Treg-specific IS formation. Additionally, phosphorylation-specific flow cytometry as state of the art technique was employed to expand knowledge on signaling differences between Tregs and Tconv circumventing material intense screening methods.

3.1 The role of Themis in Treg development and function

Themis is one of the proteins which is differentially expressed in Tregs as compared to Tconv, and so far the functional role of this difference was not

unraveled. Several studies find Themis underrepresented in Tregs as compared to Tconv, both on mRNA and protein level [118, 132, 139]. Themis is recruited to the LAT signalosome following TCR ligation via direct interaction with GRB2 and SHP-1 [136, 137, 252]. Earlier publications reported that Themis acts as a TCR inhibitor, which adjusts the tight signal threshold at the transition of positive to negative selection in the thymus. Accordingly, Themis knockdown in Jurkat T cells or human $CD4^+$ T cells from blood results in elevated ERK1/2 phosphorylation and upregulation of activation markers such as CD25 and CD69 [137, 140, 255]. Only recently, it was identified that due to direct interaction with SHP-1, Themis actually dampens SHP-1 phosphatase activity and thereby ultimately enhances TCR signaling [138]. A possible explanation for these contradictory results is given by Choi and colleagues: It is reported that Themis affects phosphatase activity of SHP-1, but it is not known whether also Tyrosine-protein phosphatase non-receptor type 11 (PTPN11, SHP-2) is a target of Themis. SHP-2 is a known enhancer of ERK1/2 phosphorylation [256, 257], and if its activity is independent of Themis, it could be responsible for elevated T cell activation in absence of Themis [138]. Though, it is also conceivable that Themis functions contrarily during T cell development in the thymus and T cell activation in SLOs. In line with its crucial role during thymocyte maturation, Themis expression levels are elevated in thymocytes as compared to T cells from SLOs [258]. Apart from T cell development, differential expression levels of Themis in peripheral Tregs and Tconv as well as published divergent ERK1/2 activation levels in the two T cell subsets support the postulated signal-enhancing role for Themis: Themis expression is reduced specifically in Tregs as compared to Tconv, and also ERK1/2 activation and Ca^{2+} flux are attenuated in this T cell subset [118, 139, 155-157].

Hence, it was tempting to speculate that Themis impacts suppressive activity of Tregs. In the present study, Tregs were transduced in order to overexpress Themis and the suppressive capacity of these Tregs was assessed in *in vitro* suppression assays. Themis-overexpressing Tregs were found to be as suppressive as control-transduced Tregs. In conclusion, the reduced expression level of Themis specifically in Tregs has no impact on their suppressive function in the tested experimental setup. Though, these results are opposing to a recent report, which states elevated suppressive capacity of Themis-overexpressing Tregs both *in vitro*

and *in vivo* [139]. Duguet *et al*. isolated Tregs from transgenic mice expressing Themis under the control of the human CD2 promoter, which results in raised Themis expression in all T cells, including Tregs, *in vivo* [139, 259]. *In vitro*, Themis-transgenic (Themis-tg) Tregs showed a survival benefit over WT Tregs, which is not due to advanced proliferation. This corresponds to another report, which also identifies a survival-promoting role for Themis [137]. Interestingly, thymic T cell development is unaffected in Themis-tg mice, which might be due to the fact that Themis expression levels are upregulated during thymocyte development [259]. The finding that Themis-tg Tregs are more suppressive correlates with the hypothesis of Choi *et al.* of Themis as signaling enhancer. The discrepancy regarding suppressive capacity of retrovirally transduced Tregs and Themis-tg Tregs might result from the respective experimental setting. In order to transduce *ex vivo* isolated T cells, pre-activation was necessary, which might cover slight functional differences between control Tregs and Themis-overexpressing Tregs.

In conclusion, although Themis expression levels might have a minor impact on Treg suppressive capacity, this protein appears rather unsuitable for Treg-specific manipulation, but might be an interesting target in effector T cells. A blockade of Themis function would rather affect Tconv, due to reduced Themis levels in Tregs, and results in enhanced T cell activation [137, 140, 255]. As Themis expression levels are only mildly affecting Treg function, it would be interesting to investigate elevated Themis levels in effector T cells, which according to Choi *et al.* should result in augmented T cell activation [138] and might prospectively be applicable in e.g. cancer therapy. Finally, from a researcher's point of view, it remains interesting to unravel the functional reason for the lower protein expression in Tregs as compared to Tconv.

3.2 TCR signaling in Tregs versus Tconv

Our department recently performed quantitative phosphopeptide sequencing of *ex vivo* isolated murine Tregs and Tconv, both unstimulated and stimulated, to gain insights into diverging phosphorylation events at steady state and following activation in the two T cell subsets [132]. Due to large amounts of required material a single experiment was accomplished, which excluded the possibility to perform kinetics following TCR stimulation over time. Therefore, in the thesis in hand, phosphorylation

kinetics were addressed via phospho-flow cytometry, which combined the advantages of single cell-based analysis, side by side comparison of Tregs and Tconv, adequate cell material needs and unproblematic feasibility of kinetics. Poor availability of phospho-specific antibodies against molecules and sites of interest allowed thorough examination of only one of the previously identified differentially regulated phosphorylation-sites, namely CD3ζ pY142 **(Fig. 2)**. It was reported that this site shows reduced phosphorylation upon TCR ligation in Tregs as compared to Tconv [157]. Interestingly, data from the previously performed phosphoproteome in our department depicts drastically elevated phosphorylation of Y142 in resting Tregs as compared to Tconv. Upon stimulation, phosphorylation is reduced in Tregs whereas in Tconv the phosphorylation level rises **(Fig. 2)** [132]. None of these described phosphorylation phenotypes of CD3ζ pY142 could be detected from the phospho-flow cytometry kinetics performed in the study in hand. In line with these finding, no changes of phosphorylation level of Lck pY505 and ZAP70 pY319 were detected. According to literature, Lck pY505 is expected to be rapidly dephosphorylated upon TCR ligation: Lck is constitutively membrane bound and located in proximity to the phosphatase CD45 and C-terminal Src kinase *(*CSK) in resting T cells. Interaction with those two enzymes regulates switching of Lck between inactive, primed and active state, according to presence and absence of phosphogroups at Y534 and Y505. Under steady state, Lck is dephosphorylated at Y534 by CD45 and phosphorylated at Y505 by CSK, which keeps Lck in a closed conformation (inactive: Y534 pY505). Upon dephosphorylation of Y505, also mediated by CD45, Lck structure opens, and the molecule is primed (primed: Y534 Y505). Auto-transphosphorylation at Y534 by Lck itself, finally results in full activation of the kinase, which subsequently enables Lck to phosphorylate the ITAMs of the TCR/CD3 complex (active: pY534 Y505) [260]. Amongst the targets of activated Lck are the ITAMs located at CD3ζ [261, 262], which in a phosphorylated state serve as docking stations for other components of the TCR signalosome such as ZAP70 [263-267]. Following TCR engagement, ZAP70 is recruited to the plasma membrane and directly binds phosphorylated ITAMs. This interaction causes structural rearrangements within ZAP70 and phosphorylation of Y319, which in turn recruits Lck [268, 269]. By autophosphorylation and via Lck, the amino acid residues, Y492 and Y493 of ZAP70, are phosphorylated, which subsequently fully activates ZAP70 [270].

Phosphorylated Y319 therefore stabilizes the active conformation of ZAP70 indirectly through recruitment and binding of Lck. Therefore, for the analyzed phosphorylation site Y319 in ZAP70, increasing phosphorylation levels following TCR ligation were expected, but could not be detected in the present study. Possible explanations, why for none of the three examined sites, the expected phosphorylation dynamics could be observed, might be inappropriate stimulation or insufficient sensitivity of phospho-flow cytometry. Though, inadequate cell activation can be excluded as ERK1/2 was phosphorylated both in Tregs and Tconv, and the measured kinetic of ERK1/2 phosphorylation also ensures that the observed time frame included activation and slow return back to steady state. For ZAP70, differential expression levels in Tregs and Tconv following anti-CD3/28 stimulation are described, which might blur the comparison of protein phosphorylation within the two T cell subsets [64]. Therefore, total expression levels of the respective protein could be determined to normalize detected phosphorylation events to the general protein level. However, regarding the present study, perturbations of the phosphorylation kinetics by differentially regulated gene expression upon stimulation within Tregs as compared to Tconv can be excluded, as the observed time frame of 5 minutes is most probably too short to severely affect gene expression, protein synthesis or degradation.

Therefore, phospho-flow cytometry might lack sufficient sensitivity to track minor and fast changes of phosphorylation levels in primary T cells upon TCR ligation. Alternative methods to analyze early TCR downstream signaling include immunoprecipitation steps to enrich signaling complexes of interest and thereby reduce amounts of needed cell material. However, this excludes the possibility to analyze different cell subsets, such as Tregs and Tconv, side by side from the same stimulated sample [271, 272]. Another option to reduce cell amounts but enable kinetics of various phosphorylation sites in parallel is mass cytometry. Therefore, this method might be a promising alternative to expand our findings from quantitative phosphopeptide sequencing. [273]. But also here, Tregs and Tconv would need to be separately stimulated and barcode-labeled, and for both suggested methods phosphospecific antibodies are urgently required. In summary, although phospho-flow cytometry currently belongs to state of the art techniques, there are two major obstacles that prevent expansion of knowledge of TCR downstream signaling using this method: (i) More flow-suitable phospho-specific antibodies are urgently

needed and (ii) sensitivity of flow cytometers need improvement. Advancement of techniques in these regards is of utmost importance for immunological research, as evidence is accumulating that T cell subset-specific signaling serves as very promising target for the development of new therapeutic strategies.

3.3 The role of CalDAG GEFI in murine T cells

CalDAG GEFI is known for its role in integrin activation and integrins are important for formation and stability of the IS [182, 195, 209, 210]. Therefore, and additionally due to the newly identified and differentially regulated phosphorylation-site at Y523 in Tregs and Tconv [132], it appeared as promising candidate to address IS formation and stability specifically in Tregs.

3.3.1 Y523 – A novel phosphorylation site at murine CalDAG GEFI

The functional role of the novel phosphorylation site Y523 is of relevance, as it might e.g. regulate subcellular localization or enzymatic activity of CalDAG GEFI specifically in Tregs. Thus, characterization of this phosphorylation-site might enable identification of molecular targets for specific intervention with IS formation, and hence activation, in Tregs.

As Y523 locates to the C1 domain of CalDAG GEFI it was tempting to speculate that the phosphorylation status impacts phorbol ester responsiveness. It was shown before that the amino acid composition of CalDAG GEFI C1 domain does not permit DAG or PMA binding and interestingly, Johnson and colleagues hypothesized, that the inability of CalDAG GEFI to respond to phorbol esters might not solely result from the secondary protein structure of the C1 domain [244, 246]. Therefore, as Y523 is localized within the DAG binding pouch **(Fig. 4e)** and a phosphogroup impacts the local charge of the protein, we speculated that DAG responsiveness of CalDAG GEFI depends on the phosphorylation status of Y523. This hypothesis could not be confirmed by the performed membrane lipid PIP strips, at least for the given experimental setup in the present study. Although more sensitive and specific techniques could be applied to ensure that the phosphorylation status of Y523 is not affecting DAG affinity, it appears highly unlikely that CalDAG GEFI is directly interacting with phorbol esters. The functional implication of pY523 and its differential

regulation in Tregs and Tconv is presumably not related to DAG-mediated subcellular localization of CalDAG GEFI.

To address a possible impact of pY523 on enzymatic activity of CalDAG GEFI, pull-down of active Rap1 from stimulated Tregs and Tconv could be employed. Differences in Rap1 activation in the two T cell subsets might originate from varying enzymatic activity of CalDAG GEFI caused by differential phosphorylation at Y523. Of course other cell intrinsic factors influence Rap1 activation, therefore the applied experimental system would need to be planed precisely and require e.g. knockout of other RapGEFs than CalDAG GEFI to specifically draw conclusions for this molecule. It was published that protein kinase A-mediated phosphorylation of CalDAG GEFI at S116/117, located within the N-terminal RasGEF domain, interferes with Rap1 activation [274, 275]. Given the position of Y523 within the protein's domain structure, it is therefore rather unlikely that this phosphorylation-site affects enzymatic function of CalDAG GEFI.

Besides recruitment by phorbol esters and activity regulation, tyrosine phosphorylations can serve as docking sites for SH2 domain-containing proteins [276]. Therefore, it might be helpful to compare the interactome of phosphorylated and unphosphorylated CalDAG GEFI to draw conclusions for the pY523 function. Additionally, interaction partners could potentially also explain the responsiveness of CalDAG GEFI to PMA stimulation, although the protein cannot directly interact with phorbol esters. Interacting proteins could experimentally be identified by combined co-immunoprecipitations and mass spectrometry. This experimental setup might also allow the identification of the kinase and phosphatase, which are phosphorylating and dephosphorylating CalDAG GEFI at Y523, respectively. Plenty of tyrosine phosphatases are reported to contribute to TCR downstream signaling, e.g. CD45, SHP-1 and SHP-2, PTPN2 and PTPN22 just to name a few [277]. As expected some of these phosphatases were also shown to be involved in T cell adhesion processes [278, 279]. Accordingly, there are several possible tyrosine kinases which might be responsible for pY532. The TEC-family member IL-2-inducible T cell kinase (ITK) might be a promising candidate, as it was shown before that mutations in ITK affect LFA-1 recruitment following TCR stimulation [280]. Knowledge about the kinases, respectively phosphatases that modulate Y523 includes the possibility to identify

molecular targets to indirectly impact CalDAG GEFI and downstream signaling in Tregs or Tconv.

Taken together, there is reasonable evidence that CalDAG GEFI localization and function are regulated by several phosphorylation events, but the role of pY523 still needs to be clarified. To achieve that, the most promising option might be the identification of interaction partners of phosphorylated and unphosphorylated CalDAG GEFI. Generally, functional characterization of phosphorylation-sites serves a promising tool for the identification of targets to specifically interfere with signaling pathways, and might include the possibility to precisely address certain cell subsets in a particular environmental context, such as infection.

3.3.2 The role of CalDAG GEFI in adhesion and migration of Jurkat T cells

Adhesion experiments performed in the thesis in hand clearly demonstrated a function of CalDAG GEFI in cell adhesion of Jurkat T cells. This applied to fibronectin and ICAM-1, which covered β_1 integrin- and β_2 integrin-dependent adhesion processes, respectively. Regarding β_1 integrin-mediated adhesion, findings of the present study are in contrast to published results: Ghandour *et al.* postulate no role for CalDAG GEFI and Rap1 in very late antigen-4 (VLA-4) activation, the prominent fibronectin-binding integrin of T cells [249]. However, there are two major differences regarding the experimental setup of the study referred to and the thesis in hand: (i) Ghandour and colleagues inhibit Rap1 directly by overexpression of the RapGAP Spa-1, which actually bypasses CalDAG GEFI. In the present study, the utilization of knockout Jurkat T cells unequivocally showed the impact of CalDAG GEFI deficiency on T cell adhesion. (ii) Whereas in the study in hand direct TCR stimulation was employed, Ghandour *et al.* utilized SDF-1α as T cell stimulant. Therefore, differences in TCR downstream signaling and chemokine receptor-mediated signaling might also account for the observed discrepancy [249]. In summary, we conclude that CalDAG GEFI implemented both affinity- and avidity-mediated cell adhesion, facilitated by β_1 and β_2 integrins, respectively.

Migration behavior of CalDAG GEFI$^{-/-}$ T cells was not investigated so far, but it was shown that Rap1 functions in T cell locomotion [224, 281, 282]. GDP-bound Rap1 limits T cell rolling on blood vessel endothelium and thereby restrains cells from

homing to organs. GTP-bound Rap1 activates LFA-1 and induces T cell arrest on high endothelial venules (HEVs) promoting T cell LN homing [224]. In the thesis in hand, CalDAG GEFI$^{-/-}$ Jurkat T cells did not display aberrant migration behavior in *in vitro* assays towards SDF-1α. This finding corresponds to results from Ghandour *et al*. who stated no impact of CalDAG GEFI on VLA-4-dependent adhesion upon SDF-1α treatment [249]. Therefore, CalDAG GEFI might be dispensable for chemokine-induced T cell migration, but implements cell adhesion, triggered by TCR stimulation or PMA treatment. As studies regarding neutrophils were conducted under inflammatory conditions, also CalDAG GEFI$^{-/-}$ T cells might be challenged in an inflammatory or infectious environment to investigate their migration capabilities. Additionally, the function of CalDAG GEFI might not only be context- but also cell-specific and thus, CalDAG GEFI might be generally dispensable for integrin-mediated T cell migration. Another study identifies an integrin-independent impact of CalDAG GEFI on neutrophil chemotaxis, involving the actin cytoskeleton, especially F-actin distribution, and cell polarization [283]. This finding is particularly interesting as an interaction between CalDAG GEFI and F-actin was reported before [248].

In summary, several studies, including the thesis in hand, have shown a role for CalDAG GEFI in cell adhesion of various cell types. Regarding migration processes, CalDAG GEFI might be dispensable in T cells. Therefore, CalDAG GEFI might support integrin activation at the IS and the differential phosphorylation might affect this scenario divergently in Tregs and Tconv. This could e.g. lead to enhanced or faster LFA-1 activation in Tregs, resulting in a benefit over Tconv. In terms of suppressive activity this advantage would be essential for Tregs to enable e.g. down-modulation of costimulatory molecules from the APC surface before Tconv get activated. On the other side, CalDAG GEFI$^{-/-}$ Jurkat T cells did not fully abrogate cell adhesion, which is probably due to the fact that other RapGEFs compensate for the loss of CalDAG GEFI [214-220]. Thus, experimentally it would be very challenging to unequivocally show the impact of CalDAG GEFI on IS formation or stability. Simultaneous knockout or chemical blockade of redundant RapGEFs would be required, which certainly affects cell survival drastically.

3.3.3 Phenotypic characterization of murine CalDAG GEFI$^{-/-}$ T cells

The detected differential phosphorylation at Y523 of CalDAG GEFI attracted our attention to the general role of this protein in T cells, especially in Tregs. Although, CalDAG GEFI$^{-/-}$ mice were generated more than a decade ago, the T cell compartment was not analyzed yet, because Crittenden *et al.* did not detect CalDAG GEFI in murine T cells [237]. CalDAG GEFI$^{-/-}$ mice are fertile and do not display any obvious abnormalities, besides slightly extended bleeding times after injury due to delayed platelet activation [237, 243]. Flow cytometric analysis of the T cell compartment of thymi and SLOs conducted within the present study were in line with these findings and did not reveal peculiarities between CalDAG GEFI$^{+/+}$, CalDAG GEFI$^{+/-}$ and CalDAG GEFI$^{-/-}$ mice. A recent publication identifies CalDAG GEFII and CalDAG GEFIII (RasGRP1 and RasGRP3, respectively) as important molecular players for efficient migration of early thymic progenitors from the bone marrow via the blood stream into the thymus [284-286]. Double knockout mice for CalDAG GEFII and CalDAG GEFIII display significantly reduced thymocyte numbers, which is not due to bone marrow- or thymus-intrinsic aberrations of T cell development, but because of impaired CCR9-dependent migration of precursor cells from the blood into the thymus [287]. However, the authors did not analyze frequencies and absolute numbers of thymocytes after the DN stage. In the thesis in hand, CalDAG GEFI$^{-/-}$ mice displayed thymocyte frequencies at expected ratios and at unaltered numbers, which also applied to Treg precursors and different maturation levels of Tregs and Tconv according to CD24 expression. In line with these findings, all analyzed T cell subsets from pooled spleen and LNs appeared comparable in CalDAG GEFI$^{+/+}$, CalDAG GEFI$^{+/-}$ and CalDAG GEFI$^{-/-}$ mice in terms of population frequency and absolute numbers. Therefore, CalDAG GEFI expression of murine T cells is dispensable for thymic T cell development and T cell homeostasis in peripheral lymphoid organs under steady state conditions.

3.3.4 Signaling properties of murine CalDAG GEFI$^{-/-}$ T cells

Due to the fact that Rap1 and CalDAG GEFI were shown to be involved in signaling networks including ERK1/2 [216, 220, 225, 226, 232], TCR downstream signaling events were analyzed in primary murine T cells in the study in hand. Analysis of ERK1/2 phosphorylation in Tregs and Tconv from CalDAG GEFI$^{+/+}$ and

CalDAG GEFI$^{-/-}$ mice following TCR stimulation via crosslinked anti-CD3/28 antibodies did not discover aberrant ERK1/2 phosphorylation. Accordingly, global signaling events detected by total tyrosine phosphorylation were found comparable in CD4^{+} T cells from CalDAG GEFI$^{+/+}$, CalDAG GEFI$^{+/-}$ and CalDAG GEFI$^{-/-}$ mice. Therefore, the postulated role for Rap1 in ERK1/2 signaling is most probably not mediated via CalDAG GEFI but by another Rap1GEF. Furthermore, the majority of studies stating a Rap1/ERK1/2 connection are conducted in cancer cell lines such as HEK 293T cells [216, 232] and utilize dominant active mutants of Rap1 or a RapGAP [225, 226]. Taking into account the clean experimental system using primary cells from knockout and control mice and the direct stimulation of the TCR employed for pERK1/2 phospho-flow experiments, there is no evidence from the study in hand that CalDAG GEFI is involved in ERK1/2 signaling or TCR downstream signaling in general in T cells. As all experiments were performed under steady state conditions, this picture might change in an inflammatory or infectious environment. However, again the major obstacle remains RapGEFs that act in redundancy to CalDAG GEFI.

3.3.5 CalDAG GEFI fine-tunes Treg function *in vivo*

In order to further study the general role of CalDAG GEFI in Tregs we analyzed the suppressive capacity of CalDAG GEFI$^{-/-}$ Tregs *in vitro* and *in vivo*. Pre-activated Tregs from CalDAG GEFI$^{+/+}$, CalDAG GEFI$^{+/-}$ and CalDAG GEFI$^{-/-}$ Tregs displayed comparable capacity to suppress bead-stimulated proliferation of Tnaive *in vitro*. Consequentially, CalDAG GEFI might be dispensable for Treg suppressive activity or the experimental setup covers subtle differences due to the applied pre-activation. Directly *ex vivo* isolated Tregs from CalDAG GEFI$^{+/+}$, CalDAG GEFI$^{+/-}$ and CalDAG GEFI$^{-/-}$ mice were not suppressive at any tested Treg:Tnaive ratio and under various tested stimulation conditions (data not shown), which made pre-activation of the Tregs necessary. Using the *in vivo* T cell transfer model of colitis, CalDAG GEFI$^{-/-}$ Tregs displayed slightly reduced capacity to rescue inflammation severity as compared to CalDAG GEFI$^{+/+}$ Tregs. The observed phenotype was rather mild and only apparent from histology scores of the colons, and interestingly, transfer of elevated Treg numbers rescued the slight defect of CalDAG GEFI$^{-/-}$ Tregs. This reflects reduced, but not abolished suppression, which might be explained by improper IS formation between CalDAG GEFI$^{-/-}$ Tregs and APCs.

CalDAG GEFI$^{-/-}$ Tregs might display reduced Rap1 activation, resulting in impaired LFA-1 activation and loosened interaction strength between Tregs and APCs. Regarding the suppressive modes of Tregs, inappropriate IS formation might impede CTLA-4-mediated down-regulation of CD80/86 from APCs [108-111, 288] or might affect directed vesicle release from the Tregs towards the APCs [289]. Therefore, the observed rescue from colitis by a mere increase of Tregs might be explained by utilization of different mechanisms of action of the Tregs, as for example cytokine deprivation. To address these possibilities experimentally, reduced activation of Rap1 and LFA-1 in CalDAG GEFI$^{-/-}$ Tregs could be tested via pull-down of active Rap1 or microcopy of the synapse using conformation-specific antibodies against LFA-1. As migration of CalDAG GEFI$^{-/-}$ Jurkat T cells was unaffected, it is unlikely that the observed phenotype in transfer colitis experiments is due to impaired migration of CalDAG GEFI$^{-/-}$ Tregs to the gut. Furthermore, expression of CD103, which is needed for T cell retention in the gut [290], was found equivalent on CalDAG GEFI$^{-/-}$ and CalDAG GEFI$^{+/+}$ Tregs. Additionally, if diminished migration would be the leading cause, an earlier onset of colitis after co-transfer of CalDAG GEFI$^{-/-}$ Tregs as compared to CalDAG GEFI$^{+/+}$ Tregs would be expected, which was not apparent from body weight of the recipient animals. Survival and proliferation of CalDAG GEFI$^{-/-}$ Tregs as compared to CalDAG GEFI$^{+/+}$ Tregs was unaffected, as similar T cell frequencies and absolute numbers were observed in recipient mice from both experimental groups. Elevated absolute numbers of all analyzed T cells populations were observed in siLPLs from CalDAG GEFI$^{-/-}$ Treg recipients. However, as this affected effector T cells as well as Tregs, it did not influence the development of colitis as compared to CalDAG GEFI$^{+/+}$ Treg recipient mice.

In conclusion, CalDAG GEFI fine-tunes Treg functional properties in an inflammatory environment, but the molecular basis remains elusive. In line with the observed adhesion deficit, the impairment of the suppressive capacity of CalDAG GEFI$^{-/-}$ Tregs was moderate, which is most probably due to redundant RapGEFs in T cells. Finally, CalDAG GEFI certainly plays a role during IS formation of T cells, but although the differential phosphorylation at Y523 in Tregs and Tconv might lead to distinct protein recruitment or activity, this impact seems to be rather minor as knockout of the whole protein did not result in a drastic phenotype.

3.4 Concluding remarks

Undeniably the IS formed between T cells and APCs is of supreme importance for proper activation and function of Tconv as well as Tregs, and serves as the main structural feature that integrates diverse incoming stimuli and initiates TCR signaling. Therefore, and due to the increasing number of studies revealing molecular differences in Tregs and Tconv with respect to signaling processes, the IS persists in the focus of T cell research. It remains demanding to specifically address differences in signaling between Tregs and Tconv, which is due to lack of appropriate tools and clean experimental systems. Screening approaches covering transcriptomics, proteomics and phosphoproteomics gather hints for potential candidate genes, proteins and posttranslational modifications. In the present study, the role of Themis and CalDAG GEFI, both candidates identified from screening approaches, were investigated with regard to their contribution to the peculiar immunosuppressive phenotype of Tregs. For Themis, no specific functional implementation of the observed underrepresentation at protein level in Tregs could be found. Regarding CalDAG GEFI, a minor involvement in Treg suppressive capacity was identified, which probably originates from CalDAG GEFI's role during IS formation.

Besides focusing on certain candidate genes or proteins, the bigger biological context should be considered intensely to pinpoint assailable differences between Tregs and Tconv. It becomes apparent, that fundamental alterations between Tregs and Tconv are not only found at gene or protein level, but rather within specialized intracellular signaling networks and processes. Thereby, identical protein inventory allows for distinct functional features simply by differentially regulated interplay between signaling components in Tregs and Tconv. Up to date, it remains laborious to untangle signaling networks, as seen regarding phospho-flow cytometry experiments in the present study, but new methods are constantly being developed and improved, which will prospectively supply basic research as well as diagnostics with appropriate tools. Definitively, signaling processes are promising targets for T cell subset- and context-specific manipulation of T cell function.

4. Materials and Methods

4.1 Mouse strains

Foxp3^{hCD2}Thy1.1^{+} reporter mice (BALB/c, [291]), Foxp3^{hCD2}Thy1.2^{+} reporter mice (BALB/c, [292]), CalDAG GEFI$^{-/-}$ (129S4-Sv/Jae, [237]) and Rag2$^{-/-}$ (C57BL/6, [293]) mice were bred, housed and handled under specific pathogen-free conditions at the Helmholtz Centre for Infection Research (Braunschweig, Germany). Mice used in *in vivo* experiments were age- and gender-matched. Animals were handled with welfare and care according to regulations of FELASA. All efforts were made to minimize suffering and animal experiments were performed according to institutional, state, and federal guidelines.

4.2 Isolation of primary cells

Mice were euthanized by CO_2 asphyxiation and thymus, spleen and LNs (mandibular, accessory mandibular, axillary, brachial, inguinal, mesenteric, iliac) were rapidly removed and stored in PBS (Gibco) 0.2 % BSA (Sigma Aldrich). Single cell suspensions were prepared by meshing of the organs through a 100 µm cell strainer. Cells were pelleted by centrifugation at 350 g for 8 min at room temperature (RT) and erythrocytes were lysed by incubation in hypo osmotic lysis buffer (0.01 M potassium bicarbonate, 0.155 M ammonium chloride, 0.1 mM EDTA, pH 7.5) for 3 min at RT with occasional shaking. Lysis was stopped by addition of 10 fold excess of PBS 0.2 % BSA, cells were filtered again to remove fat and clumped tissue, and cells were pelleted as described above. Subsequently, cell suspensions were kept on ice, handled with pre-chilled buffers and centrifuged at 4 °C. Cell number was determined by manual counting using a Neubauer improved hemocytometer and trypan blue (Sigma Aldrich) for discrimination of dead cells, or aided by Accuri flow cytometer (BD Biosciences) and propidium iodide (PI, Sigma Aldrich) for exclusion of dead cells.

4.3 Automated magnetic-activated cell sorting (MACS)

In order to enrich primary cell suspensions from spleen and LNs for CD4^{+} T cells, cell suspensions were incubated with MACS CD4 direct beads (L3T4) (Miltenyi Biotech) at a dilution of 1:20 and, after removal of unbound beads by

washing with PBS 0.2 % BSA and centrifugation as described before, separated aided by AutoMACS Pro (Miltenyi Biotech).

4.4 Flow cytometry and fluorescence-assisted cell sorting (FACS)

For flow cytometric analysis of primary murine cells or cell lines such as HEK293T and Jurkat T cells, discrimination of dead cells was facilitated by LIVE/DEAD Fixable Dead Cell Stain (LD, Invitrogen) prior to surface and intracellular staining. For exclusion of dead cells of unfixed samples, PI was added prior to acquisition at the flow cytometer. For the sake of cell viability, LD discrimination was dispensed during cell sorting as available agents bear certain toxicity after long term incubation. Antibodies were titrated prior to experimental use in order to determine antibody concentrations with sufficient separation of positive and negative populations combined with minimal background staining. Surface staining using anti-human CD2 (RPA-2.10), anti-mouse CD3 (17A2), anti-mouse CD4 (RM4-5), anti-mouse CD8 (53-6.7), anti-mouse CD24 (M1/69), anti-mouse CD25 (PC61.5), anti-mouse CD62L (MEL-14), anti-mouse CD90.1 (Thy1.1, HIS51), anti-mouse CD103 (2E7), anti-mouse CD304 (Neuropilin-1, 3E12), anti-mouse CD357 (GITR, DTA-1), anti-human CD3 (OKT3), anti-human CD11a (HI111) or anti-human CXCR4 (12G5), purchased from BioLegend, eBioscience or BD Biosciences, was performed in PBS 0.2 % BSA for 15 min on ice protected from light, and unspecific antibody binding was prevented by co-incubation with anti-mouse CD16/32 (2.4G2, BioXcell). Intracellular staining for anti-mouse Foxp3 (FJK-16S) and anti-mouse CD152 (CTLA-4, UC10-4B9) (both eBioscience) was carried out employing Foxp3 staining kit (eBioscience) according to the manufacturer's protocol. Unspecific antigens were blocked by co-incubation with RatIgG (Dianova) as used intracellular antibodies were purified from rat. Data acquisition was performed using LSRII SORP or LSR Fortessa equipped with Diva software (BD Biosciences). Cell sorting was performed in the Cell Sorting Facility of the HZI on Aria II SORP (BD Biosciences), Aria Ilu (BD Biosciences) or MoFlo XDP (Beckman Coulter) with the help of Lothar Gröbe, Maria Höxter and Petra Hagendorff. For data analysis FlowJo software (TreeStar) was used.

4.5 Phospho-flow cytometry (BD Biosciences)

Cells were isolated from pooled from spleen and LNs and were stained for dead cells and subsequently for surface markers CD4 and CD25 or Foxp3^{hCD2}, if reporter mice were used, as described. Next, cells were coated with 10 µg/ml biotinylated anti-CD3 (145-2C11, BD Biosciences) and 5 µg/ml biotinylated anti-CD28 (37.51, BD Biosciences) for 15 min on ice. After removal of unbound antibodies, cells were pre-warmed to 37 °C and stimulation was initiated by addition of 10 µg/ml streptavidin (Dianova) in Roswell Park Memorial Institute medium (RMPI, Gibco Glutamax) complemented with 10 % FCS, 50 U/ml Penicillin, 50 U/ml streptomycin, 25 mM HEPES, 1mM sodium pyruvate (all Biochrom AG) and 50 µM β-mercaptoethanol (Gibco) (cRPMI). After indicated time points, cells were fixed (Phosflow Lyse/Fix, BD Biosciences) and permeabilized (Phosflow Perm Buffer III, BD Biosciences) according to the manufacturer's protocol. Cells were stained intracellularly for total ERK1/2, ERK1/2 pT202/pY204, CD3zeta pY142, Lck pY505, ZAP70 pY319 or isotype control (all BD Biosciences Phosflow) and Foxp3, if mice were not Foxp3^{hCD2} reporter, at 4 °C overnight. Extensive washing removed excess antibodies the following day and samples were acquired in PBS 0.2 % BSA.

4.6 Pre-activation of Tregs

Tregs were sorted as CD4$^+$CD25$^+$ from pooled spleen and LNs as described above and sorted cells were cultured for 72 h on plate-bound anti-CD3/CD28. For antibody coating, wells were incubated overnight at 4 °C with 50 µg/ml goat fraction to hamster IgG (MP Biomedicals), washed with PBS and subsequently incubated for 1 h at 4 °C with 1 µg/ml anti-CD3 (145-2C11, BioLegend) and 3 µg/ml anti-CD28 (37.51, BioLegend). Sorted cells were cultured in cRPMI supplemented with 40 ng/ml IL-2 (R&D).

4.7 Transduction of Tregs

As described before, CD4$^+$ T cells were enriched via MACS and cultured on plate-bound anti-CD3/CD28 (plate coating as described before) for 40 h. For transduction, cells were kept on the stimulus, medium was carefully removed and replaced by retrovirus. Cells were spin-infected for 60 min at 400 g and 35 °C and additionally incubated 5 h at 37 °C, 95 % humidity and 5 % CO_2. Afterwards, virus

was carefully aspirated and cRPMI was added instead. 72 h after transduction, cells were harvested and transduced Tregs were resorted as $CD4^{+}Foxp3^{hCD2+}Thy1.1^{+}$, where Thy1.1 served as reporter for successful transduction.

4.8 *In vitro* suppression assay

Tnaive were sorted as $CD4^{+}CD25^{-}CD62L^{high}$ and PBS washed for Cell Trace™ Violet (CTV, Invitrogen) labeling. CTV was utilized at a final concentration of 2 µM and cells were stained for 15 min at 37 °C, staining was stopped by 10 fold excess of cRPMI. CTV-labeled Tnaive were co-cultured with pre-activated or transduced Tregs at indicated ratios in presence of T activator Beads (Life Technologies) at a ratio of one bead to two cells. On day 4, proliferation-dependent CTV dilution was determined in living Tnaive by flow cytometry.

4.9 Transfer colitis

Tregs were sorted as $CD4^{+}CD25^{+}$ cells and Tnaive as $CD4^{+}CD25^{-}CD62L^{high}$ cells from pooled spleen and LNs as described above. Subsequent to sorting, cells were washed in PBS and a total of $4x10^{5}$ cells was injected intraperitoneally into $Rag2^{-/-}$ recipient mice in a ratio of 1:2 or 1:4 (Tregs:Tnaive). General health status and body weight of recipient mice was monitored biweekly over maximal ten weeks, and mice that lost >20 % of initial body weight were sacrificed. Final analysis included measurement of colon length, colon histology, spleen weight, total cell count of spleen, mLN and pLN (axial, brachial, inguinal) and FACS analysis of lymphocytes from spleen, mLN, pLN and small intestine lamina propria (only performed for experiments with 1:2 Tregs:Tnaive). Histology analysis was performed by the Mousepathology platform at the HZI and the scoring system was developed by Dr. Marina Pils. Briefly, colons were rolled into a “Swiss roll”, fixed in 4 % neutrally buffered formaldehyde and embedded in paraffin. Approximately 3 µm thick sections were stained with hematoxylin/eosin (H&E) according to standard laboratory procedures. Slides were evaluated in a randomized and blinded manner and a semi-quantitative score was applied for the marker’s severity, lymphocytic invasion, epithelial hyperplasia, single cell apoptosis and area involved. Each marker was graded from 0-3 and grades for these markers were added up for a total score of 0-15.

4.10 Isolation of small intestine lamina propria lymphocytes (siLPLs)

Small intestines were taken from stomach exit to origin of the cecum and feces were removed. Guts were cut open lengthwise and intensely washed in PBS 2 mM EDTA 0.2 % BSA to remove mucus and intraepithelial lymphocytes. Afterwards, guts were rinsed in HBSS 0.2 % BSA to completely remove EDTA and organs were cut into small pieces. Pieces were digested for 30 min at 37 °C in HBSS 10 % FCS, 50 U/ml Penicillin, 50 U/ml streptomycin, 25 mM HEPES, 1 mM sodium pyruvate, 50 µM β-mercaptoethanol supplemented with 0.1 mg/ml DNAseI, 1 mg/ml Collagenase D and 0.1 U/ml Dispase (all Roche Diagnostics). The resulting cell suspension was filtered through a 100 µm cell strainer and the isolated cells were separated via Percoll (Biochrom AG) gradient. Lymphocytes accumulating at the interphase were harvested, washed two more times in PBS 0.2 % BSA, counted and stained for flow cytometry.

4.11 Phosphotyrosine analysis

$CD4^+$ T cells were MACS-enriched from pooled spleen and LNs of CalDAG $GEFI^{-/-}$, CalDAG $GEFI^{+/-}$ and CalDAG $GEFI^{+/+}$ mice as described before. $1x10^6$ cells were stimulated in cRPMI supplemented with either 20 ng/ml PMA and 1 µg/ml ionomycin (iono) or 35 µM sodium pervanadate (all Sigma Aldrich) for 5 min at 37 °C. For anti-CD3/CD28 stimulation, cells were stained with 20 µg/ml biotinylated anti-CD3 (145-2C11, BD Biosciences) and 10 µg/ml biotinylated anti-CD28 (37.51, BD Biosciences), subsequently crosslinking was allowed for 5 min by addition of 10 µg/ml streptavidin (Dianova) in cRPMI. As stimulation controls, cells were either left on ice or incubated at 37 °C for 5 min in cRPMI. To stop stimulation, cells were washed once in ice-cold PBS and cell pellets were lysed for Western Blot analysis.

4.12 Cell lines

HEK293T cells (DSMZ ACC 635) were cultured in Dulbecco's Modified Eagle Medium (DMEM, Gibco) supplemented with 10 % FCS, 50 U/ml Penicillin, 50 U/ml streptomycin, 25 mM HEPES and 1 mM sodium pyruvate (all Biochrom AG) at 37 °C, 95 % humidity and 5 % CO_2. In order to passage or seed cells, cells were carefully rinsed with PBS and treated with 0.5 % Trypsin-EDTA (Gibco) for up to 5 min at

37 °C. Detachment of cells was stopped by 10 fold excess of cDMEM. Jurkat T cells (clone JE6, gift from Dr. Stefanie Kliche, OvGU, Magdeburg) were cultured in RPMI complemented with 10 % FCS at 37 °C, 95 % humidity and 5 % CO_2. Cells were counted using a Neubauer improved hemocytometer and trypan blue for live/dead discrimination.

4.13 Production of lentiviral and retroviral particles

Retroviral and lentiviral particles were produced using HEK293T cells seeded in 19 cm^2 culture dishes with $1x10^6$ cells/dish in 3 ml cDMEM. The following day, cells were transfected utilizing calcium chloride precipitation. For retrovirus production, 3 µg of the empty expression vector MSCV_Thy1.1 or MSCV_Thy1.1 containing murine Themis (Addgene plasmid #17442, [294]) and 3 µg pCL Eco helper plasmid (encoding gag, pol and env, Addgene plasmid #12371, [295]) were used. For lentiviral production 5 µg pRRL.PPT.SF.newMCS.i2.EGFP (empty vector or vector containing human CalDAG GEFI, modified from pRRL.PPT.SF.IRES.EGFP.PRE, [296]), 12 µg pcDNA3.HIV1GP, 5 µg pRSV Rev and 1.5 µg pMD2G plasmid (all plasmids were gifted from Dr. Melanie Galla, MHH, Hannover) were utilized. Respective plasmids were mixed with 30 µl 2 M $CaCl_2$ and filled to 250 µl with sterile water. This mixture was dripped into 250 µl 2x HBS buffer (280 mM sodium chloride, 50 mM HEPES, 12 mM D-glucose, 10 mM potassium chloride, 1.5 mM disodium phosphate, pH 7.05) or 2x phosphate buffer (280 mM sodium chloride, 50 mM HEPES, 1.5 mM disodium hydrogen phosphate), for retrovirus and lentivirus production respectively, under vigorous mixing. 500 µl of this transfection solution was added immediately to each dish in a drop-wise manner. Cells were incubated with transfection solution for 16 h, then medium was exchanged and virus production was allowed. Virus supernatant (VSN) was collected the following day and filtered through a 0.45 µm strainer to remove detached HEK293T cells. VSN was concentrated by overnight centrifugation at 2755 g and 4 °C, and subsequently VSN volume was carefully reduced according to the experimental need.

4.14 CRISPR/Cas9-mediated gene knock-out in Jurkat T cells

SgRNAs targeting CalDAG GEFI in Jurkat T cells were generated utilizing the online tool http://crispr.mit.edu/ (Zhang Lab, MIT, 2015). Selected sgRNAs (see

Table 1, page 79) were cloned into pX458 (pSpCas9(BB)-2A-GFP, Addgene plasmid #48138, [297]) via *Bbs*I restriction site. Jurkat T cells were electroporated employing the Amaxa Cell Line Nucleofector V Kit and the Amaxa Nucleofector device using program X-005 according to the manufacturer's protocol. 48 h after nucleofection, single Jurkat T cells were sorted into 96-well round bottom plates according to GFP expression using BD FACS Aria II SORP. Single cell clones were expanded and tested for CalDAG GEFI expression via Western Blot and a second round of single cell sorting was applied to promising clones. Both clones examined in this study, namely 1E8_2D5 (clone #1) and 1E8_3D6 (clone #2), were derived from sgRNA#1 and clone 1E8 generated by the first single cell sorting. Successful knockout of CalDAG GEFI was confirmed by repetitive Western Blot analysis and sequencing of the genomic DNA of exon 1, subcloned into pCR^{TM}4-TOPO® (Thermo Fisher Scientific).

4.15 Transduction of Jurkat T cells

Re-expression of CalDAG GEFI in CalDAG GEFI$^{-/-}$ Jurkat T cell clones was facilitated by lentiviral transduction utilizing pRRL.PPT.SF.IRES.EGFP.newMCS (primer for subcloning see Table 1, page 79). Lentivirus particles were produced employing HEK293T cells as described in section 4.13. For transduction, 2x10^6 Jurkat T cells were resuspended in 2 ml of concentrated VSN and spin-infected for 30 min at 800 g. VSN was aspirated and Jurkat T cells were cultured for 72 h in RPMI with 10 % FCS before functional assays were performed. Efficiency of HEK293T cell transfection and Jurkat T cell transduction was determined via GFP expression of HEK293T and Jurkat T cells, respectively.

4.16 Adhesion and migration assays

One day prior to the experiment, WT or CalDAG GEFI$^{-/-}$ Jurkat T cells were adjusted to 1x10^5 cells/ml in RPMI with 10 % FCS. Cell adhesion was assessed by cell stimulation with 5 µg/ml anti-CD3 (OKT3, BD Biosciences), 50 ng/ml PMA (Calbiochem), or 1 mM $MnCl_2$ (Sigma Aldrich) for 30 min at 37 °C. Adhesion on Fc-ICAM-1-coated (0.5 µg/well, R&D system) or Fibronectin-coated (1 µg/well, Roche) 96-well flat-bottom plates was allowed for 30 min at 37 °C and unbound cells were removed by gently washing three times with HBSS (Biochrom AG). The bound

cell fraction was determined by counting using an ocular reticle and bound cells were calculated as ‚% of input' in duplicates ($2x10^5$ cells seeded initially). Migration behavior was analyzed using 5 µm polycarbonate filter transwells (Costar) coated with 20 µg/ml fibronectin (1 h at 37 °C, Roche). The lower transwell chamber contained either migration assay medium (RPMI, 1 % bovine serum albumin fraction V, 10 mM HEPES pH 7.4) or migration assay medium supplemented with 200 ng/ml human SDF-1α (BioLegend). $2x10^5$ cells in 200 µl migration assay medium were transferred to the upper chamber and after 2.5 h at 37 °C the number of migrated cells into the lower chamber was counted. Adhesion and migration assays were performed by Dr. Stefanie Kliche (OvGU, Magdeburg).

4.17 Western Blot

Primary T cells or Jurkat T cells were lysed in RIPA lysis buffer (50 mM Tris-HCl pH 8.0, 150 mM NaCl, 0.5 % sodium deoxycholate, 1 % NP40, 0.1 mM PMSF, Roche Complete Mini Protease Inhibitor) and BCA assay (Thermo Fisher Scientific) was utilized according to the manufacturer's instructions to determine total protein concentration. Proteins were denatured by incubation in reducing sample buffer (50 mM Tris pH 6.8, 50 % v/v glycerol, 10 % w/v SDS, 25 % v/v β-mercaptoethanol, 0.25 mg/ml bromphenol blue) for 5 min at 95 °C and subsequently separated according to protein size using 12 % SDS gels. Proteins were transferred to polyvinylidene difluoride (PVDF) membranes employing a "Criterion" blotter (BioRad) and transfer buffer (25 mM Tris pH 8.0, 192 mM glycerol, 20 % v/v methanol). After protein transfer, PVDF membranes were blocked using blotting-grade milk powder, 5 % in TBST (137 mM sodium chloride, 2.68 mM potassium chloride, 24.76 mM Tris, 0.1 % v/v Tween20, pH 7.8), and specific protein bands were detected via anti-Rasgrp2 (GTX108616, Genetex), anti-β-actin (AC-74, Sigma) or anti-phosphotyrosine (4G10, Upstate) with secondary antibodies anti-rabbit IgG-HRP, anti-mouse IgG2a-HRP or anti-mouse IgG2b-HRP (all Southern Biotech). Western Blots were developed using Super Signal West Dura Extended Duration Substrate (Thermo Fisher Scientific) and Amersham Hyperfilm™ ECL (GE Healthcare).

4.18 Protein expression, purification and lipid binding assay

The coding sequence of the C1 domain of murine CalDAG GEFI (corresponding to amino acids 495-553) was amplified by Phusion Flash II DNA polymerase (Thermo Fisher Scientific) and the PCR product was digested with *Eco*RI/*Xho*I and subcloned into pGEX-4T-1 (Amersham Bioscience), which concomitantly enabled fusion to a GST-tag (primer see Table 1, page 79). The final construct was verified by sequencing. Phosphomutant C1 domain constructs were generated employing the Q5® Site-Directed Mutagenesis Kit (NEB) following the manufacturer's protocol (primer see Table 1, page 79). For recombinant expression, the respective plasmids were transformed into *E. coli* BL21 and expression was induced using 1 mM isopropylthio-β-galactoside at an optical density of 0.7 - 0.9 at 600 nm. Bacteria were lysed, recombinant proteins were purified using GSH-columns and dialyzed against PBS or PBS supplemented with 100 µM $ZnCl_2$. Expression and purification of recombinant proteins was performed at the Free University Berlin in the laboratory of Prof. Christian Freund (FU Berlin). To ensure equal protein input to lipid binding assays, recombinant protein concentration was determined via BCA assay, and 0.5 µg/ml of each protein was applied to membrane lipid PIP Strips (Echelon) following the manufacturer's instructions.

4.19 Statistical analysis

Graphs and statistics were generated utilizing Prism software (GraphPad). Each data point in scatter plots of *in vivo* experiments represents an individual mouse. If not stated otherwise, data are represented as mean±SD. Statistical significance was determined via Mann-Whitney test or One-way ANOVA (Bonferroni's multiple comparisons test or Kruskal-Wallis with Dunn's test for multiple comparisons). * $p < 0.05$ was considered significant with * $p < 0.05$, ** $p < 0.01$, *** $p < 0.001$.

Table 1: Oligonucleotides and primer

Name	Direction	Restriction site	Sequence 5'→ 3'	Purpose
sg_hRasgrp2_1_f	forward	*Bbs*I	CACCGGGGTTCGGTCCGAGCCCGGT	sgRNA#1 targeting human CalDAG GEFI
sg_hRasgrp2_1_r	reverse	*Bbs*I	AAACACCGGGCTCGGACCGAACCC	sgRNA#1 targeting human CalDAG GEFI

Name	Direction	Restriction site	Sequence 5'→ 3'	Purpose
sg_hRasgrp2_2_f	forward	*Bbs*I	CACCGTGTACCAGGGGTG CATCATG	sgRNA#2 targeting human CalDAG GEFI
sg_hRasgrp2_2_r	reverse	*Bbs*I	AAACCATGATGCACCCCTG GTACA	sgRNA#2 targeting human CalDAG GEFI
sg_hRasgrp2_3_f	forward	*Bbs*I	CACCGAGTTGTCCTTCCGG GATTGT	sgRNA#3 targeting human CalDAG GEFI
sg_hRasgrp2_3_r	reverse	*Bbs*I	AAACACAATCCCGGAAGGA CAACT	sgRNA#3 targeting human CalDAG GEFI
sg_hRasgrp2_4_f	forward	*Bbs*I	CACCGGCAGGTGAAAACG TGCCACC	sgRNA#4 targeting human CalDAG GEFI
sg_hRasgrp2_4_r	reverse	*Bbs*I	AAACGGTGGCACGTTTTCA CCTGC	sgRNA#4 targeting human CalDAG GEFI
sg_hRasgrp2_5_f	forward	*Bbs*I	CACCGGGGTTCAAGTCAAA CTCCGC	sgRNA#5 targeting human CalDAG GEFI
sg_hRasgrp2_5_r	reverse	*Bbs*I	AAACGCGGAGTTTGACTTG AACCC	sgRNA#5 targeting human CalDAG GEFI
seq_pX458_U6_fwd	forward	none	GAGGGCCTATTTCCCATGA TTCC	Sequencing of pX458
Gen_J_sg1b_fwd	forward	*Hind*III	AAGCTTCAGGACGCCTGG GTTCTC	Amplify exon 1 of human CalDAG GEFI for sequencing
Gen_J_sg1b_rev	reverse	*Xho*I	CTCGAGGGCTAGAGAAGG GAAACCTCATC	Amplify exon 1 of human CalDAG GEFI for sequencing
T7 primer	forward	none	TAATACGACTCACTATAGG G	Sequencing of pCR™4-TOPO®
mRasgrp_C1_fwd	forward	*EcoR*I	GAATTCATGGGCTTCGTAC ACAACTTC	Cloning of murine CalDAG GEFI C1 domain into pGEX-4T-1
mRasgrp_C1_rev	reverse	*Xho*I	CTCGAGCTGGGCCCTGCG GCGACA	Cloning of murine CalDAG GEFI C1 domain into pGEX-4T-1
SDM_Y523F_fwd	forward	none	CTGGGCATCTTCAAGCAGG GC	Site directed mutagenesis of murine CalDAG GEFI C1 domain Y523F
SDM_Y523F_rev	reverse	none	GATCAGAGCTTTGCAGTGG	Site directed mutagenesis of murine CalDAG GEFI C1 domain Y523F
SDM_Y523D_fwd	forward	none	CCTGGGCATCGACAAGCA GGG	Site directed mutagenesis of murine CalDAG GEFI C1 domain Y523D
SDM_Y523D_rev	reverse	none	ATCAGAGCTTTGCAGTGGC	Site directed mutagenesis of murine CalDAG GEFI C1 domain Y523D
seq_pGEX4_fwd	forward	none	CGACTCGAGCGGCCGCAT C	Sequencing of pGEX-4T-1
seq_pGEX4_rev	reverse	none	CCGGGAGCTGCATGTGTC AGAGG	Sequencing of pGEX-4T-1
cpRRL_hGRP2_fwd	forward	*Asc*I	GGCGCGCCCATGGCAGGC ACCCTG	Cloning of human CalDAG GEFI into pRRL.PPT.SF.newMCS.i2.EGFP
cpRRL_hGRP2_rev	reverse	*Xba*I	GGCGCGCCCATGGCAGGC ACCCTG	Cloning of human CalDAG GEFI into pRRL.PPT.SF.newMCS.i2.EGFP

Supplementary Information

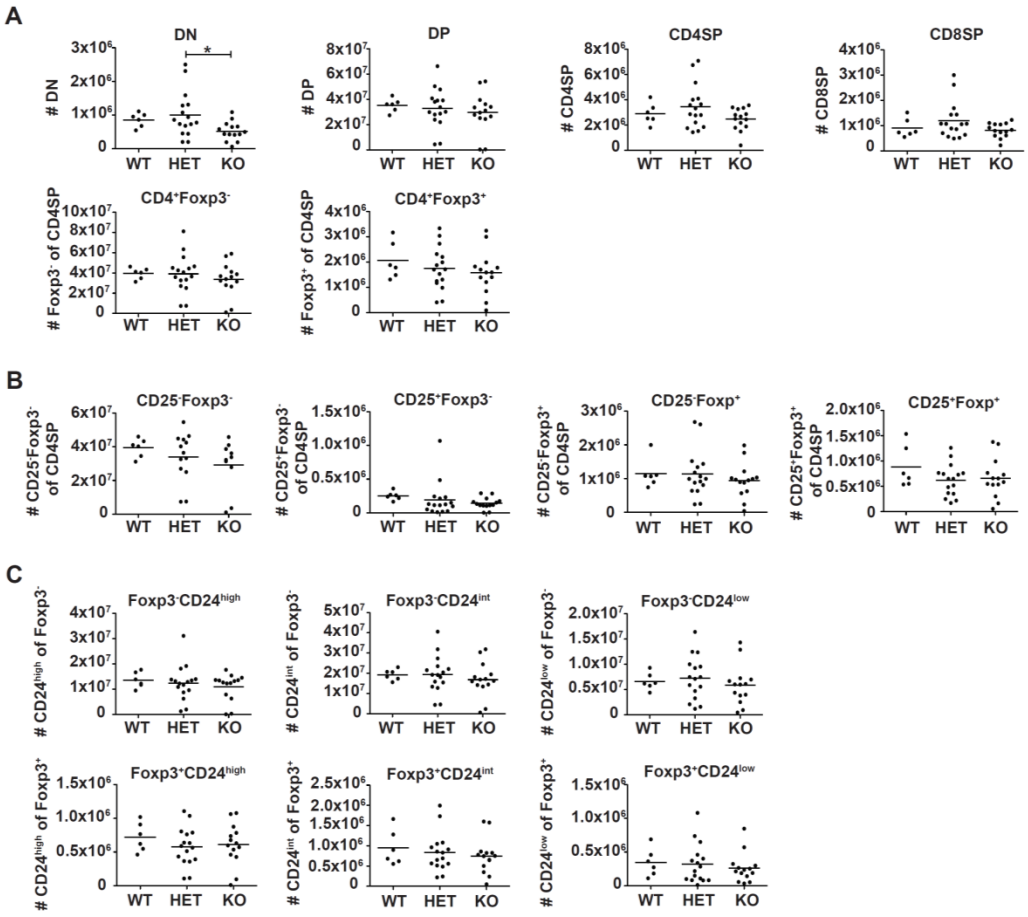

Suppl. Fig. 1: Absolute numbers of thymic T cell subsets from CalDAG GEFI$^{+/+}$, CalDAG GEFI$^{+/-}$ and CalDAG GEFI$^{-/-}$ mice. Single cell suspensions from thymi from CalDAG GEFI$^{+/+}$ (WT) CalDAG GEFI$^{+/-}$ (HET) and CalDAG GEFI$^{-/-}$ (KO) mice were counted using Accuri flow cytometer and analyzed for the depicted markers by flow cytometry (see Fig. 15). Absolute numbers of the indicated populations were calculated according to total cell count and population frequency. **(A)** Thymic T cell development was addressed via staining for CD4, CD8 and Foxp3 amongst CD4SP thymocytes. **(B)** The CD4SP compartment was analyzed for CD25$^-$Foxp3$^-$ Tconv, the Treg precursors CD25$^+$Foxp3$^-$ and CD25$^-$Foxp3$^+$ as well as CD25$^+$Foxp3$^+$ Tregs. **(C)** Maturation stages of Foxp3$^-$ (upper panel) and Foxp3$^+$ (lower panel) were examined according to CD24 expression. Mean of each group is depicted and each data point represents an individual mouse (n=6-16). Data are pooled from ten independent experiments.

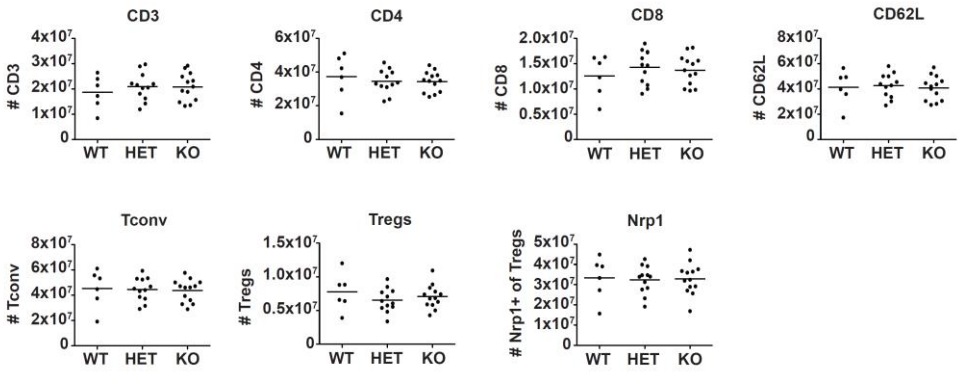

Suppl. Fig. 2: Absolute numbers of splenic T cell subsets from CalDAG GEFI$^{+/+}$, CalDAG GEFI$^{+/-}$ and CalDAG GEFI$^{-/-}$ mice. Single cell suspensions from spleens from CalDAG GEFI$^{+/+}$ (WT) CalDAG GEFI$^{+/-}$ (HET) and CalDAG GEFI$^{-/-}$ (KO) mice were counted using Accuri flow cytometer and analyzed for the depicted markers by flow cytometry (see Fig. 16). Absolute cell numbers of the indicated populations were calculated according to total cell count and population frequency. Mean is depicted per group and each data point represents an individual mouse (n=6-13 mice per group). Data are pooled from ten independent experiments.

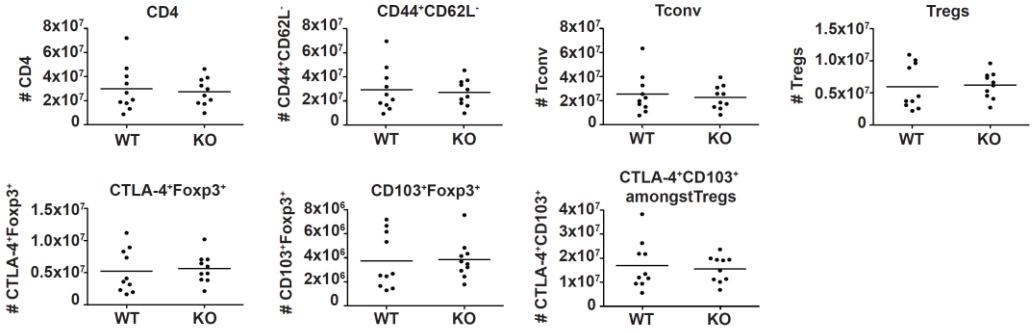

Suppl. Fig. 3: Absolute numbers of splenic T cell subsets from transfer colitis experiments with Tregs:Tnaive at a ratio of 1:4. Single cell suspensions from spleens from Rag2$^{-/-}$ recipient mice transferred with Tnaive plus CalDAG GEFI$^{+/+}$ (WT) or plus CalDAG GEFI$^{-/-}$ (KO) Tregs were counted using Accuri flow cytometer and analyzed for the indicated markers by flow cytometry (see Fig. 21). Absolute cell numbers of the indicated populations were calculated according to total cell count and population frequency. Data are pooled from two independent experiments, mean is depicted per group and each data point represents an individual mouse (n=10 mice per group).

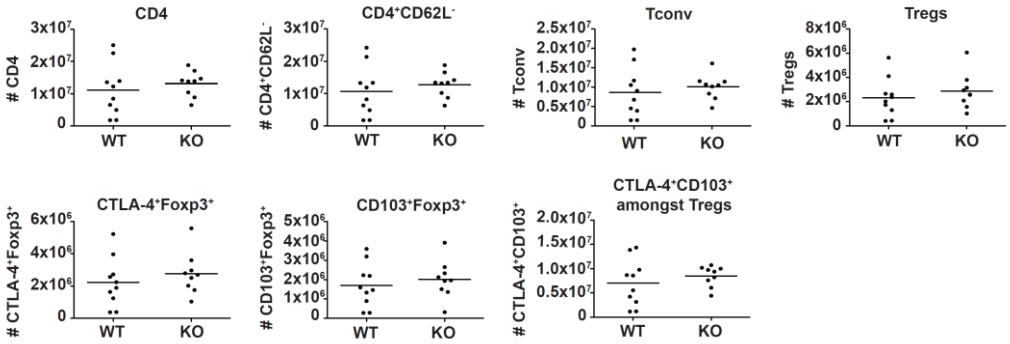

Suppl. Fig. 4: Absolute numbers of splenic T cell subsets from transfer colitis experiments with Tregs:Tnaive at a ratio of 1:2. Single cell suspensions from spleens from Rag2$^{-/-}$ recipient mice transferred with Tnaive plus CalDAG GEFI$^{+/+}$ (WT) or plus CalDAG GEFI$^{-/-}$ (KO) Tregs were counted using Accuri flow cytometer and analyzed for the indicated markers by flow cytometry (see Fig. 23). Absolute cell numbers of the indicated populations were calculated according to total cell count and population frequency. Data are pooled from two independent experiments, mean is depicted for each group and each data point represents an individual mouse (n=9-10 mice per group).

References

1. Janeway, C.A., Jr., *Approaching the asymptote? Evolution and revolution in immunology.* Cold Spring Harb Symp Quant Biol, 1989. **54 Pt 1**: p. 1-13.

2. Kawai, T. and S. Akira, *The role of pattern-recognition receptors in innate immunity: update on Toll-like receptors.* Nat Immunol, 2010. **11**(5): p. 373-84.

3. Owen, R.D., *Immunogenetic Consequences of Vascular Anastomoses between Bovine Twins.* Science, 1945. **102**(2651): p. 400-1.

4. Billingham, R.E., L. Brent, and P.B. Medawar, *Actively acquired tolerance of foreign cells.* Nature, 1953. **172**(4379): p. 603-6.

5. Steinman, R.M. and Z.A. Cohn, *Identification of a novel cell type in peripheral lymphoid organs of mice. I. Morphology, quantitation, tissue distribution.* J Exp Med, 1973. **137**(5): p. 1142-62.

6. Kapsenberg, M.L., et al., *Antigen-presenting cell function of dendritic cells and macrophages in proliferative T cell responses to soluble and particulate antigens.* Eur J Immunol, 1986. **16**(4): p. 345-50.

7. Zinkernagel, R.M. and P.C. Doherty, *The discovery of MHC restriction.* Immunol Today, 1997. **18**(1): p. 14-7.

8. Meuer, S.C., et al., *Surface structures involved in target recognition by human cytotoxic T lymphocytes.* Science, 1982. **218**(4571): p. 471-3.

9. Marrack, P., et al., *Antigen-specific, major histocompatibility complex-restricted T cell receptors.* Immunol Rev, 1983. **76**: p. 131-45.

10. Silverstein, A.M., *Paul Ehrlich's passion: the origins of his receptor immunology.* Cell Immunol, 1999. **194**(2): p. 213-21.

11. Chesnut, R.W., R.O. Endres, and H.M. Grey, *Antigen recognition by T cells and B cells: recognition of cross-reactivity between native and denatured forms of globular antigens.* Clin Immunol Immunopathol, 1980. **15**(3): p. 397-408.

12. Hozumi, N. and S. Tonegawa, *Evidence for somatic rearrangement of immunoglobulin genes coding for variable and constant regions.* Proc Natl Acad Sci U S A, 1976. **73**(10): p. 3628-32.

13. Yanagi, Y., et al., *A human T cell-specific cDNA clone encodes a protein having extensive homology to immunoglobulin chains.* Nature, 1984. **308**(5955): p. 145-9.

14. Hedrick, S.M., et al., *Isolation of cDNA clones encoding T cell-specific membrane-associated proteins.* Nature, 1984. **308**(5955): p. 149-53.

15. Starr, T.K., S.C. Jameson, and K.A. Hogquist, *Positive and negative selection of T cells.* Annu Rev Immunol, 2003. **21**: p. 139-76.

16. Kyewski, B. and J. Derbinski, *Self-representation in the thymus: an extended view.* Nat Rev Immunol, 2004. **4**(9): p. 688-98.

17. Metzger, T.C. and M.S. Anderson, *Control of central and peripheral tolerance by Aire.* Immunol Rev, 2011. **241**(1): p. 89-103.

18. Jenkins, M.K. and R.H. Schwartz, *Antigen presentation by chemically modified splenocytes induces antigen-specific T cell unresponsiveness in vitro and in vivo.* J Exp Med, 1987. **165**(2): p. 302-19.

19. Wood, K.J., A. Bushell, and J. Hester, *Regulatory immune cells in transplantation.* Nat Rev Immunol, 2012. **12**(6): p. 417-30.

20. Papp, G., et al., *Regulatory immune cells and functions in autoimmunity and transplantation immunology.* Autoimmun Rev, 2017. **16**(5): p. 435-444.

21. Carpenter, A.C. and R. Bosselut, *Decision checkpoints in the thymus.* Nat Immunol, 2010. **11**(8): p. 666-73.

22. Burnet, F.M., *A modification of Jerne's theory of antibody production using the concept of clonal selection.* CA Cancer J Clin, 1976. **26**(2): p. 119-21.

23. Meuer, S.C., S.F. Schlossman, and E.L. Reinherz, *Clonal analysis of human cytotoxic T lymphocytes: $T4^+$ and $T8^+$ effector T cells recognize products of different major histocompatibility complex regions.* Proc Natl Acad Sci U S A, 1982. **79**(14): p. 4395-9.

24. Reinherz, E.L., et al., *Antibody directed at a surface structure inhibits cytolytic but not suppressor function of human T lymphocytes.* Nature, 1981. **294**(5837): p. 168-70.

25. Evans, R.L., et al., *Thymus-dependent membrane antigens in man: inhibition of cell-mediated lympholysis by monoclonal antibodies to TH2 antigen.* Proc Natl Acad Sci U S A, 1981. **78**(1): p. 544-8.

26. Flynn, J.L., et al., *Major histocompatibility complex class I-restricted T cells are required for resistance to Mycobacterium tuberculosis infection.* Proc Natl Acad Sci U S A, 1992. **89**(24): p. 12013-7.

27. Van Pel, A. and T. Boon, *Protection against a nonimmunogenic mouse leukemia by an immunogenic variant obtained by mutagenesis.* Proc Natl Acad Sci U S A, 1982. **79**(15): p. 4718-22.

28. Castelli, C., et al., *T-cell recognition of melanoma-associated antigens.* J Cell Physiol, 2000. **182**(3): p. 323-31.

29. Assenmacher, M., et al., *Specific expression of surface interferon-g on interferon-g producing T cells from mouse and man.* Eur. J. Immunol., 1996. **26**: p. 263-267.

30. Szabo, S.J., et al., *A novel transcription factor, T-bet, directs Th1 lineage commitment.* Cell, 2000. **100**(6): p. 655-69.

31. Zheng, W. and R.A. Flavell, *The transcription factor GATA-3 is necessary and sufficient for Th2 cytokine gene expression in CD4 T cells.* Cell, 1997. **89**(4): p. 587-96.

32. Le Gros, G., et al., *Generation of interleukin 4 (IL-4)-producing cells in vivo and in vitro: IL-2 and IL-4 are required for in vitro generation of IL-4-producing cells.* J Exp Med, 1990. **172**(3): p. 921-9.

33. Swain, S.L., et al., *IL-4 directs the development of Th2-like helper effectors.* J. Immunol., 1990. **145**(11): p. 3796-3806.

34. Aggarwal, S., et al., *Interleukin-23 promotes a distinct CD4 T cell activation state characterized by the production of interleukin-17.* J Biol Chem, 2003. **278**(3): p. 1910-4.

35. Ivanov, II, et al., *The orphan nuclear receptor RORgammat directs the differentiation program of proinflammatory IL-17$^+$ T helper cells.* Cell, 2006. **126**(6): p. 1121-33.

36. MacLeod, M.K., J.W. Kappler, and P. Marrack, *Memory CD4 T cells: generation, reactivation and re-assignment.* Immunology, 2010. **130**(1): p. 10-5.

37. Sakaguchi, S., et al., *Organ-specific autoimmune diseases induced in mice by elimination of T cell subset. I. Evidence for the active participation of T cells in natural self-tolerance; deficit of a T cell subset as a possible cause of autoimmune disease.* J Exp Med, 1985. **161**(1): p. 72-87.

38. Sakaguchi, S., et al., *Immunologic self-tolerance maintained by activated T cells expressing IL-2 receptor alpha-chains (CD25). Breakdown of a single mechanism of self-tolerance causes various autoimmune diseases.* J Immunol, 1995. **155**(3): p. 1151-64.

39. Morgan, M.E., et al., *Expression of FOXP3 mRNA is not confined to CD4$^+$CD25$^+$ T regulatory cells in humans.* Hum Immunol, 2005. **66**(1): p. 13-20.

40. Roncador, G., et al., *Analysis of FOXP3 protein expression in human CD4$^+$CD25$^+$ regulatory T cells at the single-cell level.* Eur J Immunol, 2005. **35**(6): p. 1681-1691.

41. Allan, S.E., et al., *Activation-induced FOXP3 in human T effector cells does not suppress proliferation or cytokine production.* Int Immunol, 2007. **19**(4): p. 345-54.

42. Wang, J., et al., *Transient expression of FOXP3 in human activated nonregulatory CD4$^+$ T cells.* Eur J Immunol, 2007. **37**(1): p. 129-38.

43. Hori, S., T. Nomura, and S. Sakaguchi, *Control of regulatory T cell development by the transcription factor Foxp3.* Science, 2003. **299**(5609): p. 1057-61.

44. Khattri, R., et al., *An essential role for Scurfin in $CD4^+CD25^+$ T regulatory cells.* Nat Immunol, 2003. **4**(4): p. 337-42.

45. Fontenot, J.D., M.A. Gavin, and A.Y. Rudensky, *Foxp3 programs the development and function of $CD4^+CD25^+$ regulatory T cells.* Nat Immunol, 2003. **4**(4): p. 330-6.

46. Annacker, O., et al., *$CD25^+$ $CD4^+$ T cells regulate the expansion of peripheral CD4 T cells through the production of IL-10.* J Immunol, 2001. **166**(5): p. 3008-18.

47. Stephens, L.A. and D. Mason, *CD25 is a marker for $CD4^+$ thymocytes that prevent autoimmune diabetes in rats, but peripheral T cells with this function are found in both $CD25^+$ and $CD25^-$ subpopulations.* J Immunol, 2000. **165**(6): p. 3105-10.

48. Brunkow, M.E., et al., *Disruption of a new forkhead/winged-helix protein, scurfin, results in the fatal lymphoproliferative disorder of the scurfy mouse.* Nat Genet, 2001. **27**(1): p. 68-73.

49. Bennett, C.L., et al., *The immune dysregulation, polyendocrinopathy, enteropathy, X-linked syndrome (IPEX) is caused by mutations of FOXP3.* Nat Genet, 2001. **27**(1): p. 20-1.

50. Woo, E.Y., et al., *Regulatory $CD4^+CD25^+$ T cells in tumors from patients with early-stage non-small cell lung cancer and late-stage ovarian cancer.* Cancer Res, 2001. **61**(12): p. 4766-72.

51. Belkaid, Y. and K. Tarbell, *Regulatory T cells in the control of host-microorganism interactions (*).* Annu Rev Immunol, 2009. **27**: p. 551-89.

52. Curiel, T.J., et al., *Specific recruitment of regulatory T cells in ovarian carcinoma fosters immune privilege and predicts reduced survival.* Nat Med, 2004. **10**(9): p. 942-9.

53. Mills, K.H., *Regulatory T cells: friend or foe in immunity to infection?* Nat Rev Immunol, 2004. **4**(11): p. 841-55.

54. Belkaid, Y. and B.T. Rouse, *Natural regulatory T cells in infectious disease.* Nat Immunol, 2005. **6**(4): p. 353-60.

55. Hori, S., T. Takahashi, and S. Sakaguchi, *Control of autoimmunity by naturally arising regulatory $CD4^+$ T cells.* Adv Immunol, 2003. **81**: p. 331-71.

56. Fontenot, J.D., et al., *Regulatory T cell lineage specification by the forkhead transcription factor foxp3.* Immunity, 2005. **22**(3): p. 329-41.

57. Gavin, M.A., et al., *Foxp3-dependent programme of regulatory T-cell differentiation.* Nature, 2007. **445**(7129): p. 771-5.

58. Wan, Y.Y. and R.A. Flavell, *Regulatory T-cell functions are subverted and converted owing to attenuated Foxp3 expression.* Nature, 2007. **445**(7129): p. 766-70.

59. Williams, L.M. and A.Y. Rudensky, *Maintenance of the Foxp3-dependent developmental program in mature regulatory T cells requires continued expression of Foxp3.* Nat Immunol, 2007. **8**(3): p. 277-84.

60. Shimizu, J., et al., *Stimulation of $CD25^{(+)}CD4^{(+)}$ regulatory T cells through GITR breaks immunological self-tolerance.* Nat Immunol, 2002. **3**(2): p. 135-42.

61. Takahashi, T., et al., *Immunologic self-tolerance maintained by $CD25^{(+)}CD4^{(+)}$ regulatory T cells constitutively expressing cytotoxic T lymphocyte-associated antigen 4.* J Exp Med, 2000. **192**(2): p. 303-10.

62. Read, S., V. Malmstrom, and F. Powrie, *Cytotoxic T lymphocyte-associated antigen 4 plays an essential role in the function of $CD25^{(+)}CD4^{(+)}$ regulatory cells that control intestinal inflammation.* J Exp Med, 2000. **192**(2): p. 295-302.

63. Floess, S., et al., *Epigenetic control of the foxp3 locus in regulatory T cells.* PLoS Biol, 2007. **5**(2): p. e38.

64. Ohkura, N., et al., *T cell receptor stimulation-induced epigenetic changes and Foxp3 expression are independent and complementary events required for Treg cell development.* Immunity, 2012. **37**(5): p. 785-99.

65. Jordan, M.S., et al., *Thymic selection of $CD4^{+}CD25^{+}$ regulatory T cells induced by an agonist self-peptide.* Nat Immunol, 2001. **2**(4): p. 301-6.

66. Wirnsberger, G., M. Hinterberger, and L. Klein, *Regulatory T-cell differentiation versus clonal deletion of autoreactive thymocytes.* Immunol Cell Biol, 2011. **89**(1): p. 45-53.

67. Lio, C.W. and C.S. Hsieh, *A two-step process for thymic regulatory T cell development.* Immunity, 2008. **28**(1): p. 100-11.

68. Tai, X., et al., *Foxp3 transcription factor is proapoptotic and lethal to developing regulatory T cells unless counterbalanced by cytokine survival signals.* Immunity, 2013. **38**(6): p. 1116-28.

69. Hsieh, C.S., H.M. Lee, and C.W. Lio, *Selection of regulatory T cells in the thymus.* Nat Rev Immunol, 2012. **12**(3): p. 157-67.

70. Chen, W., et al., *Conversion of peripheral $CD4^{+}CD25^{-}$ naive T cells to $CD4^{+}CD25^{+}$ regulatory T cells by TGF-beta induction of transcription factor Foxp3.* J Exp Med, 2003. **198**(12): p. 1875-86.

71. Apostolou, I. and H. von Boehmer, *In vivo instruction of suppressor commitment in naive T cells.* J Exp Med, 2004. **199**(10): p. 1401-8.

72. Kretschmer, K., et al., *Inducing and expanding regulatory T cell populations by foreign antigen.* Nature Immunology, 2005. **12**: p. 1219-27.

73. Atarashi, K., et al., *Induction of colonic regulatory T cells by indigenous Clostridium species.* Science, 2011. **331**(6015): p. 337-41.

74. Lathrop, S.K., et al., *Peripheral education of the immune system by colonic commensal microbiota.* Nature, 2011. **478**(7368): p. 250-4.

75. Kim, K.S., et al., *Dietary antigens limit mucosal immunity by inducing regulatory T cells in the small intestine.* Science, 2016.

76. Milpied, P., et al., *Neuropilin-1 is not a marker of human Foxp3$^+$ Treg.* Eur J Immunol, 2009. **39**(6): p. 1466-71.

77. Thornton, A.M., et al., *Expression of Helios, an Ikaros transcription factor family member, differentiates thymic-derived from peripherally induced Foxp3$^+$ T regulatory cells.* J Immunol, 2010. **184**(7): p. 3433-41.

78. Akimova, T., et al., *Helios expression is a marker of T cell activation and proliferation.* PLoS One, 2011. **6**(8): p. e24226.

79. Serre, K., et al., *Helios is associated with CD4 T cells differentiating to T helper 2 and follicular helper T cells in vivo independently of Foxp3 expression.* PLoS One, 2011. **6**(6): p. e20731.

80. Weiss, J.M., et al., *Neuropilin-1 is expressed on thymus-derived natural regulatory T cells, but not mucosa-generated induced Foxp3$^+$ Treg cells.* J Exp Med, 2012. **209**(10): p. 1723-1742.

81. Yadav, M., et al., *Neuropilin-1 distinguishes natural and inducible regulatory T cells among regulatory T cell subsets in vivo.* J Exp Med, 2012. **209**(10): p. 1713-22.

82. Singh, K., et al., *Concomitant analysis of Helios and Neuropilin-1 as a marker to detect thymic derived regulatory T cells in naive mice.* Sci Rep, 2015. **5**: p. 7767.

83. Zhou, X., et al., *Instability of the transcription factor Foxp3 leads to the generation of pathogenic memory T cells in vivo.* Nat Immunol, 2009. **10**(9): p. 1000-7.

84. Wang, J., T.W. Huizinga, and R.E. Toes, *De novo generation and enhanced suppression of human CD4$^+$CD25$^+$ regulatory T cells by retinoic acid.* J Immunol, 2009. **183**(6): p. 4119-26.

85. Sasidharan Nair, V., M.H. Song, and K.I. Oh, *Vitamin C Facilitates Demethylation of the Foxp3 Enhancer in a Tet-Dependent Manner.* J Immunol, 2016. **196**(5): p. 2119-31.

86. Yue, X., et al., *Control of Foxp3 stability through modulation of TET activity.* J Exp Med, 2016. **213**(3): p. 377-97.

87. Lu, L., et al., *Characterization of protective human CD4CD25 FOXP3 regulatory T cells generated with IL-2, TGF-beta and retinoic acid.* PLoS One, 2010. **5**(12): p. e15150.

88. Golovina, T.N., et al., *Retinoic acid and rapamycin differentially affect and synergistically promote the ex vivo expansion of natural human T regulatory cells.* PLoS One, 2011. **6**(1): p. e15868.

89. Vignali, D.A., L.W. Collison, and C.J. Workman, *How regulatory T cells work.* Nat Rev Immunol, 2008. **8**(7): p. 523-32.

90. Annacker, O., et al., *Interleukin-10 in the regulation of T cell-induced colitis.* J Autoimmun, 2003. **20**(4): p. 277-9.

91. Asseman, C., et al., *An essential role for interleukin 10 in the function of regulatory T cells that inhibit intestinal inflammation.* J Exp Med, 1999. **190**(7): p. 995-1004.

92. Joetham, A., et al., *Naturally occurring lung $CD4^{(+)}CD25^{(+)}$ T cell regulation of airway allergic responses depends on IL-10 induction of TGF-beta.* J Immunol, 2007. **178**(3): p. 1433-42.

93. Nakamura, K., A. Kitani, and W. Strober, *Cell contact-dependent immunosuppression by $CD4^{(+)}CD25^{(+)}$ regulatory T cells is mediated by cell surface-bound transforming growth factor beta.* J Exp Med, 2001. **194**(5): p. 629-44.

94. Green, E.A., et al., *$CD4^+CD25^+$ T regulatory cells control anti-islet $CD8^+$ T cells through TGF-beta-TGF-beta receptor interactions in type 1 diabetes.* Proc Natl Acad Sci U S A, 2003. **100**(19): p. 10878-83.

95. Collison, L.W., et al., *The inhibitory cytokine IL-35 contributes to regulatory T-cell function.* Nature, 2007. **450**(7169): p. 566-9.

96. Kearley, J., et al., *Resolution of airway inflammation and hyperreactivity after in vivo transfer of $CD4^+CD25^+$ regulatory T cells is interleukin 10 dependent.* J Exp Med, 2005. **202**(11): p. 1539-47.

97. Grossman, W.J., et al., *Human T regulatory cells can use the perforin pathway to cause autologous target cell death.* Immunity, 2004. **21**(4): p. 589-601.

98. Grossman, W.J., et al., *Differential expression of granzymes A and B in human cytotoxic lymphocyte subsets and T regulatory cells.* Blood, 2004. **104**(9): p. 2840-8.

99. Herman, A.E., et al., *$CD4^+CD25^+$ T regulatory cells dependent on ICOS promote regulation of effector cells in the prediabetic lesion.* J Exp Med, 2004. **199**(11): p. 1479-89.

100. Gondek, D.C., et al., *Cutting edge: contact-mediated suppression by $CD4^+CD25^+$ regulatory cells involves a granzyme B-dependent, perforin-independent mechanism.* J Immunol, 2005. **174**(4): p. 1783-6.

101. Cao, X., et al., *Granzyme B and perforin are important for regulatory T cell-mediated suppression of tumor clearance.* Immunity, 2007. **27**(4): p. 635-46.

102. Thornton, A.M. and E.M. Shevach, *$CD4^+CD25^+$ immunoregulatory T cells suppress polyclonal T cell activation in vitro by inhibiting interleukin 2 production.* J Exp Med, 1998. **188**(2): p. 287-96.

103. De La Rosa, M., et al., *Interleukin-2 is essential for $CD4^+CD25^+$ regulatory T cell function.* Eur J Immunol, 2004. **34**(9): p. 2480-8.

104. Pandiyan, P., et al., *$CD4^+CD25^+Foxp3^+$ regulatory T cells induce cytokine deprivation-mediated apoptosis of effector $CD4^+$ T cells.* Nat Immunol, 2007. **8**(12): p. 1353-62.

105. Deaglio, S., et al., *Adenosine generation catalyzed by CD39 and CD73 expressed on regulatory T cells mediates immune suppression.* J Exp Med, 2007. **204**(6): p. 1257-65.

106. Borsellino, G., et al., *Expression of ectonucleotidase CD39 by $Foxp3^+$ Treg cells: hydrolysis of extracellular ATP and immune suppression.* Blood, 2007. **110**(4): p. 1225-32.

107. Kobie, J.J., et al., *T regulatory and primed uncommitted CD4 T cells express CD73, which suppresses effector CD4 T cells by converting 5'-adenosine monophosphate to adenosine.* J Immunol, 2006. **177**(10): p. 6780-6.

108. Qureshi, O.S., et al., *Trans-endocytosis of CD80 and CD86: a molecular basis for the cell-extrinsic function of CTLA-4.* Science, 2011. **332**(6029): p. 600-3.

109. Qureshi, O.S., et al., *Constitutive clathrin-mediated endocytosis of CTLA-4 persists during T cell activation.* J Biol Chem, 2012. **287**(12): p. 9429-40.

110. Linsley, P.S., et al., *CTLA-4 is a second receptor for the B cell activation antigen B7.* J Exp Med, 1991. **174**(3): p. 561-9.

111. Gu, P., et al., *Trogocytosis of CD80 and CD86 by induced regulatory T cells.* Cell Mol Immunol, 2012. **9**(2): p. 136-46.

112. Fallarino, F., et al., *Modulation of tryptophan catabolism by regulatory T cells.* Nat Immunol, 2003. **4**(12): p. 1206-12.

113. Oderup, C., et al., *Cytotoxic T lymphocyte antigen-4-dependent down-modulation of costimulatory molecules on dendritic cells in $CD4^+$ $CD25^+$ regulatory T-cell-mediated suppression.* Immunology, 2006. **118**(2): p. 240-9.

114. Huang, C.T., et al., *Role of LAG-3 in regulatory T cells.* Immunity, 2004. **21**(4): p. 503-13.

115. Liang, B., et al., *Regulatory T cells inhibit dendritic cells by lymphocyte activation gene-3 engagement of MHC class II.* J Immunol, 2008. **180**(9): p. 5916-26.

116. Okamura, T., et al., *$CD4^+CD25^-LAG3^+$ regulatory T cells controlled by the transcription factor Egr-2.* Proc Natl Acad Sci U S A, 2009. **106**(33): p. 13974-9.

117. Sugimoto, N., et al., *Foxp3-dependent and -independent molecules specific for $CD25^+CD4^+$ natural regulatory T cells revealed by DNA microarray analysis.* Int Immunol, 2006. **18**(8): p. 1197-209.

118. Marson, A., et al., *Foxp3 occupancy and regulation of key target genes during T-cell stimulation.* Nature, 2007. **445**(7130): p. 931-5.

119. Zheng, Y., et al., *Genome-wide analysis of Foxp3 target genes in developing and mature regulatory T cells.* Nature, 2007. **445**(7130): p. 936-40.

120. Hill, J.A., et al., *Foxp3 transcription-factor-dependent and -independent regulation of the regulatory T cell transcriptional signature.* Immunity, 2007. **27**(5): p. 786-800.

121. Birzele, F., et al., *Next-generation insights into regulatory T cells: expression profiling and FoxP3 occupancy in Human.* Nucleic Acids Res, 2011. **39**(18): p. 7946-60.

122. Feuerer, M., et al., *Genomic definition of multiple ex vivo regulatory T cell subphenotypes.* Proc Natl Acad Sci U S A, 2010. **107**(13): p. 5919-24.

123. Burzyn, D., C. Benoist, and D. Mathis, *Regulatory T cells in nonlymphoid tissues.* Nat Immunol, 2013. **14**(10): p. 1007-13.

124. Burzyn, D., et al., *A special population of regulatory T cells potentiates muscle repair.* Cell, 2013. **155**(6): p. 1282-95.

125. Levine, A.G., et al., *Continuous requirement for the TCR in regulatory T cell function.* Nat Immunol, 2014. **15**(11): p. 1070-8.

126. Vahl, J.C., et al., *Continuous T cell receptor signals maintain a functional regulatory T cell pool.* Immunity, 2014. **41**(5): p. 722-36.

127. Kubach, J., et al., *Human $CD4^+CD25^+$ regulatory T cells: proteome analysis identifies galectin-10 as a novel marker essential for their anergy and suppressive function.* Blood, 2007. **110**(5): p. 1550-8.

128. Solstad, T., et al., *CD147 (Basigin/Emmprin) identifies $FoxP3^+CD45RO^+CTLA4^+$-activated human regulatory T cells.* Blood, 2011. **118**(19): p. 5141-51.

129. Procaccini, C., et al., *The Proteomic Landscape of Human Ex Vivo Regulatory and Conventional T Cells Reveals Specific Metabolic Requirements.* Immunity, 2016. **44**(2): p. 406-21.

130. Tan, H., et al., *Integrative Proteomics and Phosphoproteomics Profiling Reveals Dynamic Signaling Networks and Bioenergetics Pathways Underlying T Cell Activation.* Immunity, 2017. **46**(3): p. 488-503.

131. Barra, M.M., et al., *Transcription Factor 7 Limits Regulatory T Cell Generation in the Thymus.* J Immunol, 2015. **195**(7): p. 3058-70.

132. van Ham, M., et al., *TCR signalling network organization at the immunological synapses of murine regulatory T cells.* Eur J Immunol, 2017.

133. Donato, R., *Intracellular and extracellular roles of S100 proteins.* Microsc Res Tech, 2003. **60**(6): p. 540-51.

134. Scheiter, M., et al., *Proteome analysis of distinct developmental stages of human natural killer (NK) cells.* Mol Cell Proteomics, 2013. **12**(5): p. 1099-114.

135. Brisslert, M., et al., *S100A4 regulates the Src-tyrosine kinase dependent differentiation of Th17 cells in rheumatoid arthritis.* Biochim Biophys Acta, 2014. **1842**(11): p. 2049-59.

136. Paster, W., et al., *GRB2-mediated recruitment of THEMIS to LAT is essential for thymocyte development.* J Immunol, 2013. **190**(7): p. 3749-56.

137. Paster, W., et al., *A THEMIS:SHP1 complex promotes T-cell survival.* EMBO J, 2015. **34**(3): p. 393-409.

138. Choi, S., et al., *THEMIS enhances TCR signaling and enables positive selection by selective inhibition of the phosphatase SHP-1.* Nat Immunol, 2017. **18**(4): p. 433-441.

139. Duguet, F., et al., *Proteomic analysis of regulatory T cells reveals the importance of Themis1 in the control of their suppressive function.* Mol Cell Proteomics, 2017.

140. Fu, G., et al., *Themis controls thymocyte selection through regulation of T cell antigen receptor-mediated signaling.* Nat Immunol, 2009. **10**(8): p. 848-56.

141. Morris, G.P. and P.M. Allen, *How the TCR balances sensitivity and specificity for the recognition of self and pathogens.* Nat Immunol, 2012. **13**(2): p. 121-8.

142. Schmidt, A.M., et al., *Regulatory T cells require TCR signaling for their suppressive function.* J Immunol, 2015. **194**(9): p. 4362-70.

143. Brownlie, R.J. and R. Zamoyska, *T cell receptor signalling networks: branched, diversified and bounded.* Nat Rev Immunol, 2013. **13**(4): p. 257-69.

144. Thauland, T.J., et al., *CD28-CD80 interactions control regulatory T cell motility and immunological synapse formation.* J Immunol, 2014. **193**(12): p. 5894-903.

145. Harding, F.A., et al., *CD28-mediated signalling co-stimulates murine T cells and prevents induction of anergy in T-cell clones.* Nature, 1992. **356**(6370): p. 607-9.

146. Yoshinaga, S.K., et al., *T-cell co-stimulation through B7RP-1 and ICOS.* Nature, 1999. **402**(6763): p. 827-32.

147. Wang, S., et al., *Costimulation of T cells by B7-H2, a B7-like molecule that binds ICOS.* Blood, 2000. **96**(8): p. 2808-13.

148. Ronchetti, S., et al., *GITR, a member of the TNF receptor superfamily, is costimulatory to mouse T lymphocyte subpopulations.* Eur J Immunol, 2004. **34**(3): p. 613-22.

149. Sierro, S., P. Romero, and D.E. Speiser, *The CD4-like molecule LAG-3, biology and therapeutic applications.* Expert Opin Ther Targets, 2011. **15**(1): p. 91-101.

150. Ishida, Y., et al., *Induced expression of PD-1, a novel member of the immunoglobulin gene superfamily, upon programmed cell death.* EMBO J, 1992. **11**(11): p. 3887-95.

151. Tone, M., et al., *Mouse glucocorticoid-induced tumor necrosis factor receptor ligand is costimulatory for T cells.* Proc Natl Acad Sci U S A, 2003. **100**(25): p. 15059-64.

152. Yan, D., et al., *Imbalanced signal transduction in regulatory T cells expressing the transcription factor FoxP3.* Proc Natl Acad Sci U S A, 2015. **112**(48): p. 14942-7.

153. Crellin, N.K., R.V. Garcia, and M.K. Levings, *Altered activation of AKT is required for the suppressive function of human $CD4^+CD25^+$ T regulatory cells.* Blood, 2007. **109**(5): p. 2014-22.

154. Park, Y., et al., *SHARPIN controls regulatory T cells by negatively modulating the T cell antigen receptor complex.* Nat Immunol, 2016. **17**(3): p. 286-96.

155. Gavin, M.A., et al., *Homeostasis and anergy of $CD4^+CD25^+$ suppressor T cells in vivo.* Nat Immunol, 2002. **3**(1): p. 33-41.

156. Hickman, S.P., et al., *Defective activation of protein kinase C and Ras-ERK pathways limits IL-2 production and proliferation by $CD4^+CD25^+$ regulatory T cells.* J Immunol, 2006. **177**(4): p. 2186-94.

157. Tsang, J.Y., et al., *Altered proximal T cell receptor (TCR) signaling in human $CD4^+CD25^+$ regulatory T cells.* J Leukoc Biol, 2006. **80**(1): p. 145-51.

158. Zanin-Zhorov, A., et al., *Protein kinase C-theta mediates negative feedback on regulatory T cell function.* Science, 2010. **328**(5976): p. 372-6.

159. Zanin-Zhorov, A., et al., *Scaffold protein Disc large homolog 1 is required for T-cell receptor-induced activation of regulatory T-cell function.* Proc Natl Acad Sci U S A, 2012. **109**(5): p. 1625-30.

160. Konig, S., et al., *Kinome analysis of receptor-induced phosphorylation in human natural killer cells.* PLoS One, 2012. **7**(1): p. e29672.

161. Ulges, A., et al., *Protein kinase CK2 enables regulatory T cells to suppress excessive TH2 responses in vivo.* Nat Immunol, 2015. **16**(3): p. 267-75.

162. Tuettenberg, A., et al., *Kinome Profiling of Regulatory T Cells: A Closer Look into a Complex Intracellular Network.* PLoS One, 2016. **11**(2): p. e0149193.

163. Monks, C.R., et al., *Three-dimensional segregation of supramolecular activation clusters in T cells.* Nature, 1998. **395**(6697): p. 82-6.

164. Grakoui, A., et al., *The immunological synapse: a molecular machine controlling T cell activation.* Science, 1999. **285**(5425): p. 221-7.

165. Davis, S.J. and P.A. van der Merwe, *The kinetic-segregation model: TCR triggering and beyond.* Nat Immunol, 2006. **7**(8): p. 803-9.

166. Bunnell, S.C., et al., *Dynamic actin polymerization drives T cell receptor-induced spreading: a role for the signal transduction adaptor LAT.* Immunity, 2001. **14**(3): p. 315-29.

167. Campi, G., R. Varma, and M.L. Dustin, *Actin and agonist MHC-peptide complex-dependent T cell receptor microclusters as scaffolds for signaling.* J Exp Med, 2005. **202**(8): p. 1031-6.

168. Yokosuka, T., et al., *Newly generated T cell receptor microclusters initiate and sustain T cell activation by recruitment of Zap70 and SLP-76.* Nat Immunol, 2005. **6**(12): p. 1253-62.

169. Bunnell, S.C., et al., *T cell receptor ligation induces the formation of dynamically regulated signaling assemblies.* J Cell Biol, 2002. **158**(7): p. 1263-75.

170. Vardhana, S., et al., *Essential role of ubiquitin and TSG101 protein in formation and function of the central supramolecular activation cluster.* Immunity, 2010. **32**(4): p. 531-40.

171. Varma, R., et al., *T cell receptor-proximal signals are sustained in peripheral microclusters and terminated in the central supramolecular activation cluster.* Immunity, 2006. **25**(1): p. 117-27.

172. Stinchcombe, J.C., et al., *The immunological synapse of CTL contains a secretory domain and membrane bridges.* Immunity, 2001. **15**(5): p. 751-61.

173. Stinchcombe, J.C., et al., *Centrosome polarization delivers secretory granules to the immunological synapse.* Nature, 2006. **443**(7110): p. 462-5.

174. Kupfer, A., T.R. Mosmann, and H. Kupfer, *Polarized expression of cytokines in cell conjugates of helper T cells and splenic B cells.* Proc Natl Acad Sci U S A, 1991. **88**(3): p. 775-9.

175. Poo, W.J., L. Conrad, and C.A. Janeway, Jr., *Receptor-directed focusing of lymphokine release by helper T cells.* Nature, 1988. **332**(6162): p. 378-80.

176. Choudhuri, K., et al., *Polarized release of T-cell-receptor-enriched microvesicles at the immunological synapse.* Nature, 2014. **507**(7490): p. 118-23.

177. Das, V., et al., *Activation-induced polarized recycling targets T cell antigen receptors to the immunological synapse; involvement of SNARE complexes.* Immunity, 2004. **20**(5): p. 577-88.

178. Finetti, F., et al., *Intraflagellar transport is required for polarized recycling of the TCR/CD3 complex to the immune synapse.* Nat Cell Biol, 2009. **11**(11): p. 1332-9.

179. Martinez-Martin, N., et al., *T cell receptor internalization from the immunological synapse is mediated by TC21 and RhoG GTPase-dependent phagocytosis.* Immunity, 2011. **35**(2): p. 208-22.

180. Huppa, J.B. and M.M. Davis, *T-cell-antigen recognition and the immunological synapse.* Nat Rev Immunol, 2003. **3**(12): p. 973-83.

181. Shattil, S.J., C. Kim, and M.H. Ginsberg, *The final steps of integrin activation: the end game.* Nat Rev Mol Cell Biol, 2010. **11**(4): p. 288-300.

182. Evans, R., et al., *Integrins in immunity.* J Cell Sci, 2009. **122**(Pt 2): p. 215-25.

183. Kinashi, T., *Integrin regulation of lymphocyte trafficking: lessons from structural and signaling studies.* Adv Immunol, 2007. **93**: p. 185-227.

184. Hogg, N., I. Patzak, and F. Willenbrock, *The insider's guide to leukocyte integrin signalling and function.* Nat Rev Immunol, 2011. **11**(6): p. 416-26.

185. Van Seventer, G.A., et al., *The LFA-1 ligand ICAM-1 provides an important costimulatory signal for T cell receptor-mediated activation of resting T cells.* J. Immunol., 1990. **144**(12): p. 4579-86.

186. Peterson, E.J., et al., *Coupling of the TCR to integrin activation by Slap-130/Fyb.* Science, 2001. **293**(5538): p. 2263-5.

187. Griffiths, E.K., et al., *Positive regulation of T cell activation and integrin adhesion by the adapter Fyb/Slap.* Science, 2001. **293**(5538): p. 2260-3.

188. Griffiths, E.K. and J.M. Penninger, *Communication between the TCR and integrins: role of the molecular adapter ADAP/Fyb/Slap.* Curr Opin Immunol, 2002. **14**(3): p. 317-22.

189. Wang, H., et al., *SKAP-55 regulates integrin adhesion and formation of T cell-APC conjugates.* Nat Immunol, 2003. **4**(4): p. 366-74.

190. Han, J., et al., *Reconstructing and deconstructing agonist-induced activation of integrin alphaIIbbeta3.* Curr Biol, 2006. **16**(18): p. 1796-806.

191. Menasche, G., et al., *RIAM links the ADAP/SKAP-55 signaling module to Rap1, facilitating T-cell-receptor-mediated integrin activation.* Mol Cell Biol, 2007. **27**(11): p. 4070-81.

192. Wegener, K.L., et al., *Structural basis of integrin activation by talin.* Cell, 2007. **128**(1): p. 171-82.

193. Kasirer-Friede, A., et al., *ADAP interactions with talin and kindlin promote platelet integrin alphaIIbbeta3 activation and stable fibrinogen binding.* Blood, 2014. **123**(20): p. 3156-65.

194. Moser, M., et al., *Kindlin-3 is essential for integrin activation and platelet aggregation.* Nat Med, 2008. **14**(3): p. 325-30.

195. Katagiri, K., et al., *RAPL, a Rap1-binding molecule that mediates Rap1-induced adhesion through spatial regulation of LFA-1.* Nat Immunol, 2003. **4**(8): p. 741-8.

196. Kim, M., et al., *The primacy of affinity over clustering in regulation of adhesiveness of the integrin {alpha}L{beta}2.* J Cell Biol, 2004. **167**(6): p. 1241-53.

197. Lafuente, E.M., et al., *RIAM, an Ena/VASP and Profilin ligand, interacts with Rap1-GTP and mediates Rap1-induced adhesion.* Dev Cell, 2004. **7**(4): p. 585-95.

198. Lee, H.S., et al., *RIAM activates integrins by linking talin to ras GTPase membrane-targeting sequences.* J Biol Chem, 2009. **284**(8): p. 5119-27.

199. Sampath, R., P.J. Gallagher, and F.M. Pavalko, *Cytoskeletal interactions with the leukocyte integrin beta2 cytoplasmic tail. Activation-dependent regulation of associations with talin and alpha-actinin.* J Biol Chem, 1998. **273**(50): p. 33588-94.

200. Feigelson, S.W., et al., *Occupancy of lymphocyte LFA-1 by surface-immobilized ICAM-1 is critical for TCR- but not for chemokine-triggered LFA-1 conversion to an open headpiece high-affinity state.* J Immunol, 2010. **185**(12): p. 7394-404.

201. de Bruyn, K.M., et al., *The small GTPase Rap1 is required for $Mn^{(2+)}$- and antibody-induced LFA-1- and VLA-4-mediated cell adhesion.* J Biol Chem, 2002. **277**(33): p. 29468-76.

202. Bianchi, E., et al., *Integrin LFA-1 interacts with the transcriptional co-activator JAB1 to modulate AP-1 activity.* Nature, 2000. **404**(6778): p. 617-21.

203. Perez, O.D., et al., *Leukocyte functional antigen 1 lowers T cell activation thresholds and signaling through cytohesin-1 and Jun-activating binding protein 1.* Nat Immunol, 2003. **4**(11): p. 1083-92.

204. Cherry, L.K., et al., *RhoH is required to maintain the integrin LFA-1 in a nonadhesive state on lymphocytes.* Nat Immunol, 2004. **5**(9): p. 961-7.

205. Svensson, L., et al., *Calpain 2 controls turnover of LFA-1 adhesions on migrating T lymphocytes.* PLoS One, 2010. **5**(11): p. e15090.

206. Wernimont, S.A., et al., *PIPKI gamma 90 negatively regulates LFA-1-mediated adhesion and activation in antigen-induced $CD4^{+}$ T cells.* J Immunol, 2010. **185**(8): p. 4714-23.

207. Anthis, N.J., et al., *Beta integrin tyrosine phosphorylation is a conserved mechanism for regulating talin-induced integrin activation.* J Biol Chem, 2009. **284**(52): p. 36700-10.

208. Guittard, G., et al., *Cutting edge: Dok-1 and Dok-2 adaptor molecules are regulated by phosphatidylinositol 5-phosphate production in T cells.* J Immunol, 2009. **182**(7): p. 3974-8.

209. Kitayama, H., et al., *A ras-related gene with transformation suppressor activity.* Cell, 1989. **56**(1): p. 77-84.

210. Henning, S.W. and D.A. Cantrell, *GTPases in antigen receptor signalling.* Curr Opin Immunol, 1998. **10**(3): p. 322-9.

211. Bivona, T.G., et al., *Rap1 up-regulation and activation on plasma membrane regulates T cell adhesion.* J Cell Biol, 2004. **164**(3): p. 461-70.

212. Dustin, M.L., T.G. Bivona, and M.R. Philips, *Membranes as messengers in T cell adhesion signaling.* Nat Immunol, 2004. **5**(4): p. 363-72.

213. Bourne, H.R., D.A. Sanders, and F. McCormick, *The GTPase superfamily: a conserved switch for diverse cell functions.* Nature, 1990. **348**(6297): p. 125-32.

214. Yajnik, V., et al., *DOCK4, a GTPase activator, is disrupted during tumorigenesis.* Cell, 2003. **112**(5): p. 673-84.

215. de Rooij, J., et al., *Epac is a Rap1 guanine-nucleotide-exchange factor directly activated by cyclic AMP.* Nature, 1998. **396**(6710): p. 474-7.

216. Kawasaki, H., et al., *A Rap guanine nucleotide exchange factor enriched highly in the basal ganglia.* Proc Natl Acad Sci U S A, 1998. **95**(22): p. 13278-83.

217. Gotoh, T., et al., *Identification of Rap1 as a target for the Crk SH3 domain-binding guanine nucleotide-releasing factor C3G.* Mol Cell Biol, 1995. **15**(12): p. 6746-53.

218. Ebinu, J.O., et al., *RasGRP, a Ras guanyl nucleotide- releasing protein with calcium- and diacylglycerol-binding motifs.* Science, 1998. **280**(5366): p. 1082-6.

219. Ohtsuka, T., et al., *nRap GEP: a novel neural GDP/GTP exchange protein for rap1 small G protein that interacts with synaptic scaffolding molecule (S-SCAM).* Biochem Biophys Res Commun, 1999. **265**(1): p. 38-44.

220. Hattori, M. and N. Minato, *Rap1 GTPase: functions, regulation, and malignancy.* J Biochem, 2003. **134**(4): p. 479-84.

221. Kawasaki, H., et al., *A family of cAMP-binding proteins that directly activate Rap1.* Science, 1998. **282**(5397): p. 2275-9.

222. Mochizuki, N., et al., *Activation of the ERK/MAPK pathway by an isoform of rap1GAP associated with G alpha(i).* Nature, 1999. **400**(6747): p. 891-4.

223. Liu, L., et al., *The GTPase Rap1 regulates phorbol 12-myristate 13-acetate-stimulated but not ligand-induced beta 1 integrin-dependent leukocyte adhesion.* J Biol Chem, 2002. **277**(43): p. 40893-900.

224. Ishihara, S., et al., *Dual functions of Rap1 are crucial for T-cell homeostasis and prevention of spontaneous colitis.* Nat Commun, 2015. **6**: p. 8982.

225. Katagiri, K., et al., *Rap1 functions as a key regulator of T-cell and antigen-presenting cell interactions and modulates T-cell responses.* Mol Cell Biol, 2002. **22**(4): p. 1001-15.

226. Dillon, T.J., et al., *Regulation of the small GTPase Rap1 and extracellular signal-regulated kinases by the costimulatory molecule CTLA-4.* Mol Cell Biol, 2005. **25**(10): p. 4117-28.

227. Boussiotis, V.A., et al., *Maintenance of human T cell anergy: blocking of IL-2 gene transcription by activated Rap1.* Science, 1997. **278**(5335): p. 124-8.

228. Carey, K.D., et al., *CD28 and the tyrosine kinase lck stimulate mitogen-activated protein kinase activity in T cells via inhibition of the small G protein Rap1.* Mol Cell Biol, 2000. **20**(22): p. 8409-19.

229. Calvo, C.R., D. Amsen, and A.M. Kruisbeek, *Cytotoxic T lymphocyte antigen 4 (CTLA-4) interferes with extracellular signal-regulated kinase (ERK) and Jun NH2-terminal kinase (JNK) activation, but does not affect phosphorylation of T cell receptor zeta and ZAP70.* J Exp Med, 1997. **186**(10): p. 1645-53.

230. Vossler, M.R., et al., *cAMP activates MAP kinase and Elk-1 through a B-Raf- and Rap1-dependent pathway.* Cell, 1997. **89**(1): p. 73-82.

231. York, R.D., et al., *Rap1 mediates sustained MAP kinase activation induced by nerve growth factor.* Nature, 1998. **392**(6676): p. 622-6.

232. Ren, J., et al., *A negative-feedback loop regulating ERK1/2 activation and mediated by RasGPR2 phosphorylation.* Biochem Biophys Res Commun, 2016. **474**(1): p. 193-8.

233. Okada, T., et al., *The strength of interaction at the Raf cysteine-rich domain is a critical determinant of response of Raf to Ras family small GTPases.* Mol Cell Biol, 1999. **19**(9): p. 6057-64.

234. Bos, J.L., J. de Rooij, and K.A. Reedquist, *Rap1 signalling: adhering to new models.* Nat Rev Mol Cell Biol, 2001. **2**(5): p. 369-77.

235. Li, L., et al., *Rap1-GTP is a negative regulator of Th cell function and promotes the generation of $CD4^{+}CD103^{+}$ regulatory T cells in vivo.* J Immunol, 2005. **175**(5): p. 3133-9.

236. Li, L., J. Kim, and V.A. Boussiotis, *Rap1A regulates generation of T regulatory cells via LFA-1-dependent and LFA-1-independent mechanisms.* Cell Immunol, 2010. **266**(1): p. 7-13.

237. Crittenden, J.R., et al., *CalDAG-GEFI integrates signaling for platelet aggregation and thrombus formation.* Nat Med, 2004. **10**(9): p. 982-6.

238. Ebinu, J.O., et al., *RasGRP links T-cell receptor signaling to Ras.* Blood, 2000. **95**(10): p. 3199-203.

239. Yamashita, S., et al., *CalDAG-GEFIII activation of Ras, R-ras, and Rap1.* J Biol Chem, 2000. **275**(33): p. 25488-93.

240. Teixeira, C., et al., *Integration of DAG signaling systems mediated by PKC-dependent phosphorylation of RasGRP3.* Blood, 2003. **102**(4): p. 1414-20.

241. Yang, Y., et al., *RasGRP4, a new mast cell-restricted Ras guanine nucleotide-releasing protein with calcium- and diacylglycerol-binding motifs. Identification of defective variants of this signaling protein in asthma, mastocytosis, and mast cell leukemia patients and demonstration of the importance of RasGRP4 in mast cell development and function.* J Biol Chem, 2002. **277**(28): p. 25756-74.

242. Crittenden, J.R., et al., *CalDAG-GEFI down-regulation in the striatum as a neuroprotective change in Huntington's disease.* Hum Mol Genet, 2010. **19**(9): p. 1756-65.

243. Bergmeier, W., et al., *Mice lacking the signaling molecule CalDAG-GEFI represent a model for leukocyte adhesion deficiency type III.* J Clin Invest, 2007. **117**(6): p. 1699-707.

244. Johnson, J.E., et al., *Differential membrane binding and diacylglycerol recognition by C1 domains of RasGRPs.* Biochem J, 2007. **406**(2): p. 223-36.

245. Irie, K., et al., *Tumor promoter binding of the protein kinase C C1 homology domain peptides of RasGRPs, chimaerins, and Unc13s.* Bioorg Med Chem, 2004. **12**(17): p. 4575-83.

246. Czikora, A., et al., *Structural Basis for the Failure of the C1 Domain of Ras Guanine Nucleotide Releasing Protein 2 (RasGRP2) to Bind Phorbol Ester with High Affinity.* J Biol Chem, 2016. **291**(21): p. 11133-47.

247. Clyde-Smith, J., et al., *Characterization of RasGRP2, a plasma membrane-targeted, dual specificity Ras/Rap exchange factor.* J Biol Chem, 2000. **275**(41): p. 32260-7.

248. Caloca, M.J., et al., *F-actin-dependent translocation of the Rap1 GDP/GTP exchange factor RasGRP2.* J Biol Chem, 2004. **279**(19): p. 20435-46.

249. Ghandour, H., et al., *Essential role for Rap1 GTPase and its guanine exchange factor CalDAG-GEFI in LFA-1 but not VLA-4 integrin mediated human T-cell adhesion.* Blood, 2007. **110**(10): p. 3682-90.

250. Cifuni, S.M., D.D. Wagner, and W. Bergmeier, *CalDAG-GEFI and protein kinase C represent alternative pathways leading to activation of integrin alphaIIbbeta3 in platelets.* Blood, 2008. **112**(5): p. 1696-703.

251. Svensson, L., et al., *Leukocyte adhesion deficiency-III is caused by mutations in KINDLIN3 affecting integrin activation.* Nat Med, 2009. **15**(3): p. 306-12.

252. Brockmeyer, C., et al., *T cell receptor (TCR)-induced tyrosine phosphorylation dynamics identifies THEMIS as a new TCR signalosome component.* J Biol Chem, 2011. **286**(9): p. 7535-47.

253. Castagna, M., et al., *Direct activation of calcium-activated, phospholipid-dependent protein kinase by tumor-promoting phorbol esters.* J Biol Chem, 1982. **257**(13): p. 7847-51.

254. van Kooyk, Y. and C.G. Figdor, *Avidity regulation of integrins: the driving force in leukocyte adhesion.* Curr Opin Cell Biol, 2000. **12**(5): p. 542-7.

255. Kakugawa, K., et al., *A novel gene essential for the development of single positive thymocytes.* Mol Cell Biol, 2009. **29**(18): p. 5128-35.

256. Milarski, K.L. and A.R. Saltiel, *Expression of catalytically inactive Syp phosphatase in 3T3 cells blocks stimulation of mitogen-activated protein kinase by insulin.* J Biol Chem, 1994. **269**(33): p. 21239-43.

257. Noguchi, T., et al., *Role of SH-PTP2, a protein-tyrosine phosphatase with Src homology 2 domains, in insulin-stimulated Ras activation.* Mol Cell Biol, 1994. **14**(10): p. 6674-82.

258. Lesourne, R., et al., *Themis, a T cell-specific protein important for late thymocyte development.* Nat Immunol, 2009. **10**(8): p. 840-7.

259. Lesourne, R., et al., *Interchangeability of Themis1 and Themis2 in thymocyte development reveals two related proteins with conserved molecular function.* J Immunol, 2012. **189**(3): p. 1154-61.

260. Davis, S.J. and P.A. van der Merwe, *Lck and the nature of the T cell receptor trigger.* Trends Immunol, 2011. **32**(1): p. 1-5.

261. Weiss, A. and D.R. Littman, *Signal transduction by lymphocyte antigen receptors.* Cell, 1994. **76**(2): p. 263-74.

262. Latour, S. and A. Veillette, *Proximal protein tyrosine kinases in immunoreceptor signaling.* Curr Opin Immunol, 2001. **13**(3): p. 299-306.

263. Irving, B.A. and A. Weiss, *The cytoplasmic domain of the T cell receptor zeta chain is sufficient to couple to receptor-associated signal transduction pathways.* Cell, 1991. **64**(5): p. 891-901.

264. Romeo, C., M. Amiot, and B. Seed, *Sequence requirements for induction of cytolysis by the T cell antigen/Fc receptor zeta chain.* Cell, 1992. **68**(5): p. 889-97.

265. Chan, A.C., et al., *ZAP-70: a 70 kd protein-tyrosine kinase that associates with the TCR zeta chain.* Cell, 1992. **71**(4): p. 649-62.

266. Irving, B.A., A.C. Chan, and A. Weiss, *Functional characterization of a signal transducing motif present in the T cell antigen receptor zeta chain.* J Exp Med, 1993. **177**(4): p. 1093-103.

267. van Oers, N.S., N. Killeen, and A. Weiss, *ZAP-70 is constitutively associated with tyrosine-phosphorylated TCR zeta in murine thymocytes and lymph node T cells.* Immunity, 1994. **1**(8): p. 675-85.

268. Di Bartolo, V., et al., *Tyrosine 319, a newly identified phosphorylation site of ZAP-70, plays a critical role in T cell antigen receptor signaling.* J Biol Chem, 1999. **274**(10): p. 6285-94.

269. Williams, B.L., et al., *Phosphorylation of Tyr319 in ZAP-70 is required for T-cell antigen receptor-dependent phospholipase C-gamma1 and Ras activation.* EMBO J, 1999. **18**(7): p. 1832-44.

270. Chan, A.C., et al., *Activation of ZAP-70 kinase activity by phosphorylation of tyrosine 493 is required for lymphocyte antigen receptor function.* EMBO J, 1995. **14**(11): p. 2499-508.

271. Deswal, S., et al., *Quantitative analysis of protein phosphorylations and interactions by multi-colour IP-FCM as an input for kinetic modelling of signalling networks.* PLoS One, 2011. **6**(7): p. e22928.

272. Roncagalli, R., et al., *Quantitative proteomics analysis of signalosome dynamics in primary T cells identifies the surface receptor CD6 as a Lat adaptor-independent TCR signaling hub.* Nat Immunol, 2014. **15**(4): p. 384-92.

273. Spitzer, M.H. and G.P. Nolan, *Mass Cytometry: Single Cells, Many Features.* Cell, 2016. **165**(4): p. 780-91.

274. Subramanian, H., et al., *Phosphorylation of CalDAG-GEFI by protein kinase A prevents Rap1b activation.* J Thromb Haemost, 2013. **11**(8): p. 1574-82.

275. Guidetti, G.F., et al., *Phosphorylation of the guanine-nucleotide-exchange factor CalDAG-GEFI by protein kinase A regulates $Ca^{(2+)}$-dependent activation of platelet Rap1b GTPase.* Biochem J, 2013. **453**(1): p. 115-23.

276. Songyang, Z., et al., *SH2 domains recognize specific phosphopeptide sequences.* Cell, 1993. **72**(5): p. 767-78.

277. Stanford, S.M., N. Rapini, and N. Bottini, *Regulation of TCR signalling by tyrosine phosphatases: from immune homeostasis to autoimmunity.* Immunology, 2012. **137**(1): p. 1-19.

278. Kwon, J., et al., *Receptor-stimulated oxidation of SHP-2 promotes T-cell adhesion through SLP-76-ADAP.* EMBO J, 2005. **24**(13): p. 2331-41.

279. Sauer, M.G., et al., *SHP-1 Acts as a Key Regulator of Alloresponses by Modulating LFA-1-Mediated Adhesion in Primary Murine T Cells.* Mol Cell Biol, 2016. **36**(24): p. 3113-3127.

280. Woods, M.L., et al., *A novel function for the Tec family tyrosine kinase Itk in activation of beta 1 integrins by the T-cell receptor.* EMBO J, 2001. **20**(6): p. 1232-44.

281. McLeod, S.J., et al., *The Rap GTPases regulate B cell migration toward the chemokine stromal cell-derived factor-1 (CXCL12): potential role for Rap2 in promoting B cell migration.* J Immunol, 2002. **169**(3): p. 1365-71.

282. Shimonaka, M., et al., *Rap1 translates chemokine signals to integrin activation, cell polarization, and motility across vascular endothelium under flow.* J Cell Biol, 2003. **161**(2): p. 417-27.

283. Carbo, C., et al., *Integrin-independent role of CalDAG-GEFI in neutrophil chemotaxis.* J Leukoc Biol, 2010. **88**(2): p. 313-9.

284. Rossi, F.M., et al., *Recruitment of adult thymic progenitors is regulated by P-selectin and its ligand PSGL-1.* Nat Immunol, 2005. **6**(6): p. 626-34.

285. Zlotoff, D.A., et al., *CCR7 and CCR9 together recruit hematopoietic progenitors to the adult thymus.* Blood, 2010. **115**(10): p. 1897-905.

286. Krueger, A., et al., *CC chemokine receptor 7 and 9 double-deficient hematopoietic progenitors are severely impaired in seeding the adult thymus.* Blood, 2010. **115**(10): p. 1906-12.

287. Golec, D.P., L.M. Henao Caviedes, and T.A. Baldwin, *RasGRP1 and RasGRP3 Are Required for Efficient Generation of Early Thymic Progenitors.* J Immunol, 2016. **197**(5): p. 1743-53.

288. Yokosuka, T., et al., *Spatiotemporal basis of CTLA-4 costimulatory molecule-mediated negative regulation of T cell activation.* Immunity, 2010. **33**(3): p. 326-39.

289. Okoye, I.S., et al., *MicroRNA-containing T-regulatory-cell-derived exosomes suppress pathogenic T helper 1 cells.* Immunity, 2014. **41**(1): p. 89-103.

290. Schon, M.P., et al., *Mucosal T lymphocyte numbers are selectively reduced in integrin alpha E (CD103)-deficient mice.* J Immunol, 1999. **162**(11): p. 6641-9.

291. Miyao, T., et al., *Plasticity of Foxp3$^+$ T cells reflects promiscuous Foxp3 expression in conventional T cells but not reprogramming of regulatory T cells.* Immunity, 2012. **36**(2): p. 262-75.

292. Komatsu, N., et al., *Heterogeneity of natural Foxp3$^+$ T cells: a committed regulatory T-cell lineage and an uncommitted minor population retaining plasticity.* Proc Natl Acad Sci U S A, 2009. **106**(6): p. 1903-8.

293. Shinkai, Y., et al., *RAG-2-deficient mice lack mature lymphocytes owing to inability to initiate V(D)J rearrangement.* Cell, 1992. **68**(5): p. 855-67.

294. Wu, Y., et al., *FOXP3 controls regulatory T cell function through cooperation with NFAT.* Cell, 2006. **126**(2): p. 375-87.

295. Naviaux, R.K., et al., *The pCL vector system: rapid production of helper-free, high-titer, recombinant retroviruses.* J Virol, 1996. **70**(8): p. 5701-5.

296. Müller, L.U.W., et al., *Rapid Lentiviral Transduction Preserves the Engraftment Potential of Fanca$^{-/-}$ Hematopoietic Stem Cells.* Molecular Therapy, 2008. **16**(6): p. 1154-1160.

297. Ran, F.A., et al., *Genome engineering using the CRISPR-Cas9 system.* Nat Protoc, 2013. **8**(11): p. 2281-308.

Abbreviations

129S4-Sv/Jae	Steel group of 129 substrains, (inbred mouse strain)
ADAP	Adhesion and degranulation promoting adaptor protein
Aire	Autoimmune regulator
AKT	Protein kinase B
AP-1	Activator protein 1
APC	Antigen presenting cell
BALB/c	Bagg albino (inbred mouse strain)
BCA	Bicinchoninic acid
BCR	B cell receptor
Breg	Regulatory B cell
BSA	Bovine serum albumin
C1	conserved region 1
C3G	CRK-SH3 domain binding GEF
C57BL/6	inbred mouse strain, black fur
CABIT	Cysteine-containing all beta in Themis
CalDAG GEFI	Ca^{2+} and DAG regulated guanine nucleotide exchange factor I, GRP2
cAMP	Cyclic adenosine monophosphate
Cas9	CRISPR-associated protein 9 (nuclease)
CCR	C-C chemokine receptor
CD	Cluster of differentiation
CD11a	Integrin α_L
CD18	Integrin β_2
CD103	Integrin α_E
CD4SP	CD4 single positive ($CD4^+CD8^-$)
CD8SP	CD8 single positive ($CD4^-CD8^+$)
Cdc25	Cell division control protein 25
Cdc42	Cell division control protein 42
CDM	C. elegans Ced-5, mammalian Dock180 and D. melanogaster myoblast city
Clone #1/#2	CalDAG $GEFI^{-/-}$ Jurkat T cell clones, 1E8_2D5 and 1E8_3D6
CNS	Conserved non-coding sequence
CRISPR	Clustered regularly interspaced short palindromic repeats
CSK	C-terminal Src kinase
cSMAC	Central SMAC
CTL	Cytotoxic T lymphocyte
CTLA-4	Cytotoxic T lymphocyte-associated antigen-4, CD152
CTV	Cell Trace™ Violet
CXCR4	C-X-C chemokine receptor type 4
DAG	Diacylglycerol
DC	Dendritic cell
Dlgh1	Disc large homologue 1
DMEM	Dulbecco's modified Eagles medium
DN	Double negative ($CD4^-CD8^-$)
DNase	Deoxyribonuclease

Dock4	Dedicator of cytokinesis protein 4
DP	Double positive ($CD4^+CD8^+$)
dSMAC	Distal SMAC
ECL	Enhanced chemiluminescence
E. coli	Escherichia coli
EDTA	Ethylenediaminetetraacetic acid
EF-hand	Ca^{2+}-binding motif composed of two helices (E and F) joined by a loop
Elk1	Ets-domain-containing protein
Epac	Exchange factor directly activated by cAMP
ERK	Extracellular signal-regulated kinase
F-actin	Filamentous actin
FACS	Fluorescence-activated cell sorting
Fc	Fragment constant
FCS	Fetal calf serum
FMO	Fluorescence minus one
Foxp3	Forkhead box protein 3
GAP	GTPase activating protein
Gata-3	Trans-acting T cell-specific transcription factor
GDP	Guanosine diphosphate
GEF	Guanine exchange factor
Geomean	Geometric mean fluorescence intensity
GFP	Green fluorescent protein
GITR	Glucocorticoid-induced TNFR-related protein, CD357
GRB2	Growth factor receptor bound protein 2
GST	Glutathion-S-transferase
GTP	Guanosine triphosphate
GTPase	Guanosine triphosphatase
GzmA	Granzyme A
GzmB	Granzyme B
HBS	HEPES buffered saline
HBSS	Hank's buffered saline solution
hCD	Human CD
H&E	Hematoxylin & Eosin
HEK293T	Human embryonic kidney cells
HEPES	N-2-hydroxyethylpiperazine-N'-2-ethanesulfonic acid
HEV	High endothelial venules
HSC	hematopoietic stem cell
HRP	Horse radish peroxidase
ICAM-1	Intercellular adhesion molecule-1
ICOS	Inducible costimulator
IDO	Indoleamine (2,3)-dioxygenase 1
IFNγ	Interferon gamma
IgG	Immunoglobulin G
IL	Interleukin
Iono	Ionomycin

IP3	Inositol (1,4,5)-trisphosphate
IPEX	Immunodysregulation polyendocrinopathy enteropathy X-linked syndrome
IS	Immunological synapse
ITAM	Immune-receptor tyrosine-based activation motif
ITK	IL-2 inducible T cell kinase
iTRAQ	Isobaric tags for relative and absolute quantitation
JE6	Jurkat clone E6
kDa	kilo Dalton
KO	Knockout
LADIII	Leukocyte adhesion deficiency type III
LAG-3	Lymphocyte activation gene 3
LAT	Linker for activation of T cells
LC-MS/MS	Liquid chromatography–mass spectrometry/ mass spectrometry
Lck	Lymphocyte cell-specific protein tyrosine kinase
LD	Live/Dead
LFA-1	Lymphocyte function-associated antigen-1
LN	Lymph node
MACS	Magnetic-activated cell sorting
MDSC	Myeloid-derived suppressor cell
MELC	Multi epitope ligand cartography
MEK	Mitogen-activated protein ERK kinase
MHC	Major histocompatibility complex
mLN	Mesenteric LN
NFAT	Nuclear factor of activated T cells
NFκB	Nuclear factor „kappa-light-chain-enhancer“ of activated B cells
NK cell	Natural killer cell
Nrp1	Neuropilin-1, CD304
ns	not significant
PAMP	Pathogen-associated molecular pattern
PBS	Phosphate buffered saline
PCR	Polymerase chain reaction
PD-1	Programmed death-1, CD279
PDZ	PSD-95, DLG and ZO-1
PI	Propidium iodide
pERK	Phosphorylated ERK
PIP3	Phosphatidylinositol (3,4,5)-triphosphate
PKCθ	Protein kinase C theta
pLN	Peripheral LN
PLCγ1	Phospholipase C gamma 1
PMA	Phorbol 12-myristate 13-acetate
pMHC	Peptide-loaded major histocompatibility complex
PRR	Pattern recognition receptor
pS	Phosphorylated serine
pSMAC	Peripheral SMAC
pT	Phosphorylated threonine

pTregs	Peripherally-induced Tregs
PVDF	Polyvinylidene difluoride
pY	Phosphorylated tyrosine
Raf	Rat fibrosarcoma
Rag	Recombination activating gene
Rap1	Ras-related protein 1
RapL	Regulator for cell adhesion and polarization enriched in lymphoid tissues
Ras	Rat sarcoma
REM	Ras exchange motif
RhoH	Rho-related GTP-binding protein H
RIAM	Rap1-GTP-interacting adapter protein
RIPA	Radioimmunoprecipitation assay
RORγt	RAR-related orphan receptor gamma
ROS	Reactive oxygen species
RPMI	Roswell Park Memorial Institute
RT	Room temperature
SD	Standard deviation
SDF-1α	Stromal cell-derived factor-1, CXCL12
SDS	Sodium dodecyl sulfate
SFFV	Spleen Focus Forming Virus
sgRNA	Single guide RNA
SH2	Src homology 2
SHARPIN	SHANK-associated RH domain interactor
SHP-1	Tyrosine-protein phosphatase non-receptor type 6, PTPN6
SHP-2	Tyrosine-protein phosphatase non-receptor type 11, PTPN11
siLPL	Small intestine lamina propria lymphocyte
siRNA	Small interfering RNA
SKAP-55	Scr kinase-associated phosphoprotein of 55 kDa
SLO	Secondary lymphoid organ
SLP-76	SH2 domain-containing leukocyte protein of 76 kDa
SMAC	Supramolecular activation cluster
SOS1	Son of sevenless homologue 1
Spa-1	Signal-induced proliferation-associated protein 1
T-bet	T-box transcription factor 21, TBX21
TBST	Tris buffered saline supplemented with Tween 20
TCF7	Transcription factor 7
Tconv	Conventional T cells
TCR	T cell receptor
TEC	Transient erythroblastopenia of childhood
TGF-β	Transforming growth factor beta
Th	Helper T cell
Themis	Thymocyte-expressed molecule involved in selection
Themis-tg	Transgenic mice expressing Themis under the control of the hCD2 promoter
Thy1.1	Thymus cell antigen 1, CD90.1
Tnaive	Naïve T cell

Tregs	Regulatory T cells
TSDR	Treg-specific demethylated region
tTregs	Thymic-induced Tregs
unstim	unstimulated
VLA-4	Very late antigen-4
VSN	Virus supernatant
WT	Wild type
ZAP70	70 kDA zeta-chain associated protein

Acknowledgment

First and foremost, I thank Prof. Jochen Hühn, who is an outstanding scientist and person, for superb supervision, guidance and scientific education during the past four years. Furthermore, I would like to thank Prof. Martin Korte for his support as mentor and member of my thesis committee. I am thankful to Prof. Stefan Dübel for the acceptance of the chairmanship of the examination board, and Prof. Ingo Schmitz for advice during my thesis committees. I would like to thank all collaborators who contributed to this thesis: Dr. Stefanie Kliche for performance of adhesion and migration assays, Prof. Christian Freund, Eliot Morrison and Annika Manns for preparation of recombinant proteins, Dr. Jill R Crittenden and Prof. Ann M Graybiel for provision of the CalDAG GEFI$^{-/-}$ mice, as well as all colleagues from SIME for support with Western Blots and Dr. Marina C Pils for performance of histology. I am grateful to Dr. Lothar Gröbe, Petra Hagendorff and Maria Höxter for continuous help with cell sorting. Special thanks also to Prof. Lothar Jänsch, Dr. Marco van Ham and Nicole Amsberg for fruitful discussions. I would like to thank the CRC854 for financial support and the Graduate Schools of HZI and CRC854 for various training possibilities.

A warm thank you goes to all current and former EXIMs who made the time in the lab not only working hours but a joyful journey through various countries and cultures. I cannot thank Susi and Thies and especially Beate and Maria enough for their excellent technical assistance. Very special thanks go to Frauke, for discussions, encouragement, being a solid shoulder and a mental balance in times of need. Thanks for inspiration, criticism and craziness to Jörn, Agnes and Philippe. I am deeply grateful to have Eirini as honest companion and true friend at my side during this adventurous period. “Ευχαριστώ” for sharing offices, hotel rooms, meals, sweets and coffees as well as ideas, doubts, tears and laughter. I really do not know how students pass a PhD without having such great friends.

I would like to thank my “non-scientific” friends for real interest and mental support and I could not be more grateful to my parents for their encouragement and understanding. Last but not least, I want to thank my husband Jens for pushing me as well as taking care of my work-life balance at exactly the right time. Thank you from the bottom of my heart!

Publications (other)

2017 Van Ham M, Teich R, Philipsen L, **Niemz J**, Amsberg N, Wissing J, Nimtz M, Gröbe L, Kliche S, Thiel N, Klawonn F, Hubo M, Jonuleit H, Reichardt P, Müller AJ, Huehn J, Jänsch L. TCR signalling network organization at the immunological synapses of murine regulatory T cells. European Journal of Immunology, 2017 Aug 17. doi: 10.1002/eji.201747041. [Epub ahead of print]

2017 Ranjan S, Goihl A, Kohli S, Gadi I, Pierau M, Shahzad K, Gupta D, Bock F, Wang H, Shaikh H, Kähne T, Reinhold D, Bank U, Zenclussen AC, **Niemz J**, Schnöder TM, Brunner-Weinzierl M, Fischer T, Kalinski T, Schraven B, Luft T, Huehn J, Naumann M, Heidel FH, Isermann B. Activated protein C protects from GvHD *via* PAR2/PAR3 signalling in regulatory T-cells. Nature Communications, 2017 Aug 21; 8(1):311.

2017 Pasztoi M, Bonifacius A, Pezoldt J, Kulkarni D, **Niemz J**, Yang J, Teich R, Hajek J, Pisano F, Rohde M, Dersch P, Huehn J. Yersinia pseudotuberculosis supports Th17 differentiation and limits de novo regulatory T cell induction by directly interfering with T cell receptor signaling. Cellular and Molecular Life Sciences, 2017 Apr 4.

2012 Eckhardt FS, Gehring PS, Bartel L, Bellmann J, Beuker J, Hahne D, Korte J, Knittel V, Mensch M, Nagel D, Pohl M, Rostosky C, Vierath V, Wilms V, **Zenk J**, Vences M. Assessing sexual dimorphism in a species of Malagasy chameleon (*Calumma boettgeri*) with a newly defined set of morphometric and meristic measurements. Herpetology Notes, Volume 5, 335-344, 2012.